جامعة سيدي محمد بن عبد الله بفاس
ⵜⴰⵙⴷⴰⵡⵉⵜ ⵙⵉⴷⵉ ⵎⵓⵃⵎⵎⴰⴷ ⴱⵏ ⵄⴱⴷⵍⵍⴰⵀ ⵏ ⴼⴰⵙ
UNIVERSITÉ SIDI MOHAMED BEN ABDELLAH DE FES

كلية العلوم والتقنيات فاس
ⵜⴰⵖⵉⵡⴰⵏⵜ ⵏ ⵜⵎⴰⵙⵙⴰⵏⵉⵏ ⴷ ⵜⵙⵏⵉⴳⵉⵜⵉⵏ
FACULTÉ DES SCIENCES ET TECHNIQUES DE FÈS

**Centre d'Etudes Doctorales : Sciences et Techniques de l'Ingénieur**

*N° d'ordre 36 /2020*

# THESE DE DOCTORAT

Présentée par

**Mr : ERROUHA Mustapha**

Spécialité : **Génie électrique**

**Sujet de la thèse** : Modélisation, Commande et Optimisation d'un système de pompage photovoltaïque

**Thèse présentée et soutenue le 24/09/2020 devant le jury composé de :**

| Nom Prénom | Titre | Etablissement | |
|---|---|---|---|
| Pr. Mohammed KARIM | PES | Faculté des Sciences Dhar El Mahraz - Fès | Président |
| Pr. Abdessalam AIT MADI | PH | Ecole Nationale des Sciences Appliquées - Kénitra | Rapporteur |
| Pr. Chakib EL BEKKALI | PES | Faculté des Sciences Dhar El Mahraz - Fès | Rapporteur |
| Pr. Ahmed LAGRIOUI | PH | École Nationale Supérieure d'Arts et Métiers de Meknès | Rapporteur |
| Pr. Badre BOSSOUFI | PH | Faculté des Sciences Dhar El Mahraz - Fès | Examinateur |
| Pr. Abdelaziz EL GHZIZAL | PES | Ecole Supérieure de Technologie - Fès | Examinateur |
| Pr. Aziz DEROUICH | PH | Ecole Supérieure de Technologie - Fès | Directeur de thèse |

**Laboratoire d'accueil** : Technologies et Services Industriels (TSI)

**Etablissement** : Ecole Supérieure de Technologie de Fès

# Acknowledgments

This project has been elaborated at ***"Ecole Supérieure de Technologie ,FES", Sidi Mohamed Ben Abdellah University***. It was an unforgettable period in which I have made very precious relationships with several inspired, supportive and kindly persons. Without their precious support it would have not been possible to conduct this research.

First, I would like to take this opportunity to express my deepest gratitude and thanks to my project supervisor, Prof. Dr.***Aziz DEROUICH*** for its constant guidance and assistance and support as well as all the knowledge shared during the course of this research.

I would also like to thank Mr. ***Mohammed KARIM***, Professor of Faculty of Sciences of Fez for accepting to be the president of the reading committee of my thesis. You honored me with your presence at my defense.

My deepest gratitude is also addressed to the reading committee members : Professor ***Abdessalam AIT MADI***, Professor ***Chakib EL BEKKALI***, Professor ***Ahmed LAGRIOU***, Professor ***Abdelaziz EL GHZIZAL*** and Professor ***Badre BOSSOUFI*** for their insightful comments and suggestions. I thank you for examining my manuscript so thoroughly.

My sincere thanks also go to Pr. ***Babak NAHID-MOBARAKEH*** member of GREEN laboratory of Lorraine University, for providing the appropriate environment for research and experimental work in the laboratory. Thank you for the

continuous support of my Ph.D, for the patience and immense knowledge. Your guidance helped me during this thesis. I could not have imagined having a better mentor for my Ph.D.

Very special thanks to Professor ***Saad MOTAHHIR*** and Dr. ***Quentin COMBE*** who blessed me with their support. Many thanks also go to my best friends : ***Mohamed BENSLIMANE***, ***Anas ELHAFIDI***, ***Saadeddine HAFDI IDRISSI*** , ***Amine ZEKRAOUI*** and ***Mohammed BOUSSETTA***, for their precious advices and moral support.

From the laboratory director, to the administration staff, to the persons who were once or have always been part of the research team. I thank you all.

Last but not the least ; my biggest gratitude goes to my family.

My parents, ***Malika*** and ***Mohamed*** , without whom none of this would have ever been possible, their continuous support and unconditional love kept me going in times of despair. Mom and Dad your sacrifices, your selflessness, your wisdom, your achievements, have marked me for life. You will always be my role models.

To my sisters ***Jihane*** and ***Ibtissam*** whose support means the world to me. There isn't a day that goes by that I do not grow prouder of the women that you have become. You gave me faith in myself and my research. You have successfully pushed me to give the best of myself. During the course of the past years, I got to welcome a new member to our family. ***Imane*** , thank you for your lovely spirit.

For all the members of my larger family, I thank you all.

# Abstract

With the increasing the use of the electricity and cost diesel, finding a promising alternative to power a pumping system is required. Water pumping systems based on photovoltaic technology are good solutions for rural areas where the connection to the grid power can be difficult and expensive. Thus, these systems are more reliable than those based on diesel pumps, because they require less maintenance.

The control of PV water pumping system (PVWPS) is very much important so as to ensure accuracy and optimal operation of the PV system. In this context, the purpose is to improve the control of a photovoltaic pumping system-based on induction motor.

First, a proposed method based on Fuzzy Logic Control (FLC) is introduced and investigated to improve the conventional Direct Torque Control(DTC). The validation of the control strategy is ensured by reducing the high torque, stator flux ripples and current harmonics in induction machine and increasing pumped water flow. The results of the discussed aspects have been achieved by numerical simulation using Matlab/Simulink software.

Then, we have presented a technique based on an indirect field-oriented control (IFOC) which consists of operating the motor at optimum flux by minimizing the induction motor losses.

Furthermore, an experimental validation in GREEN laboratory of Lorraine university equipped with dSpace 1005 is conducted. The experimental results have been

depicted in order to validate the proposed approach

**Keywords** : Photovoltaic water pumping system, Induction motor, Loss minimization, Indirect field-oriented control ; Direct torque control (DTC) , Fuzzy logic control (FLC), Optimization

# Résumé

De nos jours, des efforts considérables ont été consacrés à la recherche des sources de production d'énergie électrique propres et non polluantes. Le solaire photovoltaïque (PV) est l'une des sources d'énergie renouvelable qui peut être considérée comme la meilleure solution pour produire une énergie électrique propre. Le système de pompage d'eau PV est considéré comme l'une des applications les plus populaires des systèmes d'alimentation PV, en particulier dans les régions reculées.

Dans ce contexte, les objectifs de cette thèse sont principalement liés à l'amélioration des performances d'un système de pompage photovoltaïque d'eau en développant des stratégies de commande du moteur asynchrone triphasé entrainant la pompe centrifuge du système étudié. Nos activités de recherche dans le cadre de cette thèse sont résumées dans les contributions suivantes :

Une amélioration des performances du moteur asynchrone contrôlé par la Commande Directe du Couple (DTC) à base des techniques de l'intelligence artificielle est réalisée. Cette première contribution consiste à réduire les ondulations élevées du couple, du flux et du taux de distorsion harmonique des courants de la machine asynchrone et permet d'augmenter ainsi la quantité d'eau pompée. La solution proposée est évaluée en se basant sur des données climatiques réelles pour les différentes saisons de l'année à l'aide du logiciel Matlab/Simulink.

Une technique associée à la commande vectorielle indirecte est proposée et étudiée pour améliorer le rendement du système PV de pompage d'eau. Ensuite, une

implémentation en temps réel de cette deuxième contribution est réalisée dans le laboratoire « Groupe de Recherche en Energie Electrique de Nancy, GREEN » de l'Université de Lorraine - France dans la cadre d'un stage de recherche du doctorant, en utilisant un banc d'essai équipé d'une carte dSpace 1005. Les résultats expérimentaux obtenus montrent une réduction du courant absorbé par le moteur asynchrone ce qui mène à une minimisation des pertes joules et la réduction de la puissance absorbée. Par conséquent, le rendement du système PV de pompage d'eau est amélioré. Ces résultats satisfaisants peuvent faire l'objet d'une industrialisation dans le domaine des systèmes de pompage photovoltaïques.

**Mots-clés** : Système de pompage d'eau photovoltaïque, Moteur à induction, Minimisation des pertes, commande vectorielle indirecte (IFOC) ; commande direct du couple (DTC), logique floue (FLC), optimisation

# Contents

Acknowledgments . . . . . i
Abstract . . . . . iii
Résumé . . . . . v
Contents . . . . . xi
List of Figures . . . . . xiv
List of Tables . . . . . xv
Notations . . . . . xvi
Introduction . . . . . 1

**Chapter 1 State of the art of different renewable energy sources for water pumping system**

1.1 Introduction . . . . . 4
1.2 Solar thermal water pumping system . . . . . 4
1.3 Wind energy water pumping system . . . . . 5
1.4 Gas or biogas dual fuel engine pumps . . . . . 5
1.4.1 Biomass gasifier water pumping system . . . . . 5
1.4.2 Biogas water pumping system . . . . . 6
1.5 Hybrid renewable energy water pumping system . . . . . 6
1.6 Photovoltaic water pumpig system . . . . . 6
1.6.1 On the basis of energy storage . . . . . 7
1.6.1.1 Battery-coupled . . . . . 8

1.6.1.2 Direct driven . . . . . 8
1.6.2 On the basis of type of motor . . . . . 9
1.6.2.1 DC Motors . . . . . 9
1.6.2.2 AC Motors . . . . . 10
1.6.3 Basis of categories of pumps . . . . . 12
1.6.3.1 Basis of types of pumps . . . . . 12
Submersible pump . . . . . 12
Surface pump . . . . . 12
Floating pump . . . . . 12
1.6.3.2 Basis of applications of pumps . . . . . 13
Dynamic pumps . . . . . 13
Positive displacement pumps (volumetric pumps) . . . . . 13
1.6.4 Basis of tracking of power source . . . . . 13
1.6.4.1 Fixed PV panels . . . . . 14
1.6.4.2 Tracking PV panels . . . . . 14
1.7 Literature review of control strategies applied to PVWPS system . . 14
1.8 Performance of PVWPS . . . . . 21
1.9 MPPT algorithms . . . . . 21
1.9.1 Variable step size perturb and observe . . . . . 22
1.9.2 Variable step size incremental conductance . . . . . 23

**Chapter 2 Modeling of the PV water pumping system**

2.1 Introduction . . . . . 26
2.2 PV array . . . . . 26
2.2.1 Modeling of PV cell . . . . . 27
2.2.2 Model of the PV panel . . . . . 28
2.2.3 MATLAB/Simulink Based Modelling of Photovoltaic Panel . . 28
2.2.3.1 Extract the lacked parameters of a PV panel . . . . 28

2.2.3.2 Simulink model of PV panel . . . . . 29
Effect of solar radiation variation . . . . . 30
Effect of temperature variation . . . . . 31
Effect of series resistance variation . . . . . 31
Effect of shunt resistance variation . . . . . 32
Effect of diode saturation current variation . . . . . 32
2.3 Boost converter . . . . . 33
2.3.1 Operation . . . . . 33
2.4 Voltage source inverter . . . . . 35
2.5 Machine model . . . . . 36
2.5.1 Model of Induction Motor in a (d, q) frame . . . . . 36
2.5.2 Model of Induction Motor in $(\alpha,\beta)$ frame . . . . . 37
2.6 Centrifugal pump . . . . . 38

**Chapter 3 Optimization and control of water pumping PV systems using fuzzy logic controller**

3.1 Introduction . . . . . 40
3.2 Direct torque control of induction motor . . . . . 42
3.2.1 Control of stator flux and electromagnetic torque . . . . . 42
3.2.1.1 Control of stator flux . . . . . 42
3.2.1.2 Control of electromagnetic torque . . . . . 44
3.2.2 Estimation of stator flux and electromagnetic torque . . . . . 45
3.2.2.1 Estimation of stator flux . . . . . 46
3.2.2.2 Estimation of electromagnetic torque . . . . . 46
3.2.3 Switching table construction . . . . . 47
3.2.3.1 Six sector switching table . . . . . 47
3.2.3.2 Twelve sectors switching table . . . . . 48
3.2.4 Global scheme of conventional direct torque control . . . . . 49

3.3 Fuzzy logic control . . . . . 49
3.3.1 Components of FLC . . . . . 51
3.3.1.1 Fuzzification . . . . . 51
3.3.1.2 Inference System . . . . . 51
Rule Base . . . . . 51
Database . . . . . 52
Reasoning Mechanism . . . . . 52
3.3.1.3 Defuzzification . . . . . 52
3.3.2 Advantages of Fuzzy Logic for System Control . . . . . 53
3.4 DTC base on Fuzzy logic controller . . . . . 53
3.5 Simulation Results . . . . . 60
3.6 Conclusion . . . . . 69

**Chapter 4 Improvement control of photovoltaic based water pumping system without energy storage**

4.1 Introduction . . . . . 70
4.2 Indirect field oriented control . . . . . 72
4.2.1 Estimation of $w_s$ and $\theta_s$ . . . . . 74
4.2.2 Electromagnetic torque . . . . . 74
4.2.3 Decoupling controller . . . . . 75
4.3 Global scheme of indirect field-oriented control . . . . . 76
4.4 Pulse Width Modulation *(PWM)* . . . . . 77
4.4.1 The 3-phase Inverter . . . . . 77
4.4.2 Sinusoidal PWM (SPWM) . . . . . 79
4.4.3 Space Vector Pulse Width Modulation (SVPWM) . . . . . 80
4.4.3.1 Determination of : $V_d$, $V_q$, $V_{ref}$ and angle ($\alpha$) . . . . . 81
4.4.3.2 Determination of time duration $T_0$, $T_1$, $T_2$ . . . . . 82

4.4.3.3 Determine the switching time of each transistor (S1 to S6) . . . . . 84
4.5 Proposed technique . . . . . 85
4.6 Results and discussions . . . . . 89
4.6.1 Test under varying conditions . . . . . 93
4.6.2 Test under reduced daily profile . . . . . 93
4.7 Conclusion . . . . . 94
**Conclusions and future work** . . . . . 96
Conclusions . . . . . 96
Future work . . . . . 98
**Publications arising from the Thesis** . . . . . 100
Publications arising from the Thesis . . . . . 100
**References** . . . . . 103
**Appendices** . . . . . 121
A.1 Dynamic modeling of Induction machine . . . . . 121
A.2 PI controller's gains calculation . . . . . 127
A.3 Induction motor characteristics . . . . . 129

# List of Figures


1.1 Block diagram of PVWPS with battery storage . . . . . 8
1.2 Block diagram of a direct coupled PVWPS system . . . . . 9
1.3 Block diagram of PV DC water pumping system . . . . . 10
1.4 Block diagram of PV AC water pumping system . . . . . 11
1.5 Methodology to locate the Maximum Power Point using the Power versus Voltage curve . . . . . 23
1.6 Variable step size P&O . . . . . 24
1.7 Variable step size incremental conductance . . . . . 25

2.1 Equivalent model of a PV cell . . . . . 27
2.2 Mathworks PV tool . . . . . 29
2.3 Simulink model of PV panel . . . . . 30
2.4 I-V and P-V curves of CSUN235-60P PV panel . . . . . 30
2.5 (a)I-V curves for different solar radiation and (b) P-V curves for different solar radiation . . . . . 31
2.6 (a)I-V curve for different temperature values and (b) P-V curves for different temperature values . . . . . 31
2.7 (a)I-V curves for different values of $R_s$ and (b) P-V curves for different values of $R_s$ . . . . . 32
2.8 (a)I-V curves for different values of $R_{sh}$ and (b) P-V curves for different values of $R_{sh}$ . . . . . 33

2.9 (a)I-V curves for different saturation current values and (b) P-V curves for different saturation current values . . . . . 33
2.10 Boost converter topology . . . . . 34
2.11 Boost converter configuration switch turned ON . . . . . 34
2.12 Boost converter configuration switch turned OFF . . . . . 35
2.13 Schema of the three-phase inverter . . . . . 35
2.14 Space vector diagram of two-level inverter . . . . . 36

3.1 Evolution of stator flux vector in the complex plan . . . . . 43
3.2 Two-level hysteresis comparator for stator flux control . . . . . 44
3.3 Three level hysteresis comparator for electromagnetic torque control . 45
3.4 Partition of the complex plan in six angular sectors . . . . . 47
3.5 Voltage space vector in 12 sectors cases . . . . . 49
3.6 Global control scheme of basic direct torque control . . . . . 50
3.7 Block diagram of Fuzzy controller . . . . . 54
3.8 The fuzzy membership functions of $\varepsilon_\phi$ . . . . . 55
3.9 The fuzzy membership functions of $\varepsilon$ $T_{em}$ . . . . . 55
3.10 (a)The fuzzy membership functions of $\theta_s$ (b) The fuzzy membership functions of the output . . . . . 56
3.11 Photovoltaic water pumping system based on Conventional DTC . . . 58
3.12 Photovoltaic water pumping system based on FLC - DTC . . . . . 59
3.13 Characteristics of PV water pumping system in June . . . . . 62
3.14 Characteristics of PV water pumping system in March . . . . . 64
3.15 Characteristics of PV water pumping system in December . . . . . 66
3.16 Water volume comparison . . . . . 67

4.1 Vector diagram in stationary and rotating reference frame . . . . . 73
4.2 The obtained controls . . . . . 76
4.3 Reconstruction of $V_{sd}$ and $V_{sq}$ . . . . . 76

4.4 The global control scheme of indirect field oriented . . . . . 77
4.5 Two level VSI . . . . . 78
4.6 The eight inverter voltage vectors (V0 to V7) . . . . . 78
4.7 PWM illustration by the sine-triangle comparison method (a) sine-triangle comparison (b) switching pulses . . . . . 80
4.8 SPWM technique . . . . . 80
4.9 Basic switching vectors and sectors . . . . . 81
4.10 The relationship of abc reference frame and stationary dq reference frame . . . . . 82
4.11 Reference vector as a combination of adjacent vectors at sector 1 . . . 83
4.12 Space Vector PWM switching patterns at each sector . . . . . 84
4.13 The overview of the developed experimental prototype system . . . . 88
4.14 Model block with total losses . . . . . 89
4.15 irradiation Profile . . . . . 90
4.16 Performances of PVWPS under a reduced daily profile . . . . . 91
4.17 Performances of PVWPS under sudden change in irradiance . . . . . 92
A.1 Induction motor equivalent structure . . . . . 122
A.2 block scheme of the speed control loop . . . . . 127
A.3 block scheme of the current control loop . . . . . 128

# List of Tables


2.1 Electrical characteristics of the csun235-60p photovoltaic module . . . 29

3.1 Switching Table . . . . . 48
3.2 Look up switching table with twelve sectors . . . . . 48
3.3 Voltage vector fuzzy control table . . . . . 57
3.4 Design of parameters of the system . . . . . 60
3.5 Pump flow using the Conventional and FLC-DTC Methods . . . . . 67
3.6 Torque, flux ripples and THD of the CDTC and FDTC . . . . . 68

4.1 Switching vectors, phase voltages and output line to line voltages . . 79
4.2 Switching Time Calculation at Each Sector . . . . . 85
4.3 Design of parameters of the system . . . . . 93
4.4 Comparison between our proposal and conventional control strategy . 94
A.1 Parameters of induction machine . . . . . 129
A.2 Parameters of induction machine . . . . . 129

# Notations

## Symbols

| | |
|---|---|
| a | Diode's ideality factor |
| G | Solar irradiation $[W/m^2]$ |
| I | Panel output current [A] |
| $I_0$ | Diode saturation current [A] |
| $I_{ph}$ | Panel photocurrent [A] |
| $I_r$ | Rotor current [A] |
| $I_s$ | Stator current [A] |
| K | Boltzmann constant $[J.K^{-1}]$ |
| $K_v$ | Temperature coefficient of open circuit voltage $[V/^{\circ}C]$ |
| $K_i$ | Temperature coefficient of short circuit current $[A/^{\circ}C]$ |
| $K_p$ | Pump constant |
| $l_r$ | Rotor inductance [H] |
| $l_s$ | Stator inductance [H] |
| M | Mutual inductance [H] |
| $N_s$ | Number of cells connected in series |
| q | Electron charge [C] |
| $R_r$ | Rotor resistance [Ω] |
| $R_s$ | Series resistance [Ω] |

| | |
|---|---|
| $R_{sh}$ | Shunt resistance [Ω] |
| $R_{sm}$ | Stator resistance [Ω] |
| Sa,Sb,Sc | Switching states |
| T | Junction temperature [K] |
| $T_r$ | Rotor time constant |
| V | Panel output voltage [V] |
| $w_s, w_r$ | Stator and rotor pulsations |

## Greek Letters

| | |
|---|---|
| $\alpha$ | Duty cycle |
| $\sigma$ | Dispersion coefficient |
| $\theta_s$ | Position of stator flux |
| Ω | Mechanical speed |

# Abbreviations

| | |
|---|---|
| CDTC | Conventional direct torque control |
| DTC | Direct torque control |
| FDTC | Fuzzy direct torque control |
| FFT | Fast Fourier Transforme |
| IFOC | Indirect field-oriented control |
| IM | Induction machine |
| MPPT | Maximum Power Point Tracking |
| P&O | Perturb and observe |
| PV | Photovoltaic |
| PVWPS | Photovoltaic Water Pumping System |
| STC | Standard Test Conditions |
| STWPS | Solar Thermal Water Pumping System |

# Introduction

Nowadays, considerable effort has been devoted to finding a source of production of electrical energy without yielding CO2 emissions to the environment[1].The renewable energy based water pumps present alternative solution, because it produces electricity without harming the environment, and they are mostly used due to high distribution costs/non-availability of grid-power[2][3].

Solar photovoltaic (PV) is one of the well-known sources of renewable energy which can be considered the best solution to produce clean electrical energy[4]. PV water pumping system is considered one of the most popular applications of PV power systems, particularly in remote area. Water pumping based on PV technology is a promising alternative to conventional pumping systems based diesel because there is no carbon emission or noise generation and it has a low maintenance cost. Thus, frequent repairs and maintenance of diesel pumps are generally 2-4 times more than photovoltaic pumps[3].

The induction motor is the principal element of the pumping systems[5]. Different types of motors are used with PV based water pumping system in order to drive the pump, the choice depends on the efficiency, the availability, the price and the reliability. DC motors are used for water pumping applications because they are easy to operate[6]. However, this kind of motors needs regular maintenance due to brushes and commutator[7]. To surmount this weakness, Brushless DC motors have been proposed, these motors are characterized by a simple control, high reliability and ruggedness[8][9]. PV pumping systems based on AC motors, particularly induc-

tion motors (IM) are also used, these engines are rugged, they have high efficiency, maintenance free and low cost[10].

The control of the PV water pumping system is essential so as to guarantee optimal operation and accuracy of the PVWPS. The PV system which adapts optimal control strategy of IM can reduce the count of PV panels for the designated power requirement which leads to reduce capital cost, improve the efficiency, increase the pumped water and pump life, sucking water either at low or high motor speeds, ensure good steady state, transient performance. Moreover, an optimal control strategy could avoid the motor pump from running dry and protects it against mechanical overload.

This thesis deals with the modeling, control and optimization of a photovoltaic water pumping system. The first objective of the thesis is to introduce artificial intelligence techniques to improve the performance of an induction motor drive controlled by Direct Torque Control (DTC).This research work is addressing the following principal points : firstly, the reduce of the high torque, stator flux ripples and current harmonics in induction machine and increasing pumped water flow. Fuzzy logic controller (FLC) is adapted to the nonlinear control command and not based on the model of the induction machine and the use of this type of controller allows to achieve the goal. The proposed model is evaluated based on meteorological data for the target area in the different seasons of the year using Malab/Simulink software. The second objective of the thesis is to improve the efficiency of the PV water pumping system based on loss minimization of the induction motor. Moreover, an experimental implementation is conducted in GREEN laboratory of Lorraine university to validate the proposed technique based on real-time interface using dSpace 1005 board.

The main body of the thesis is structured as follows :

- The first chapter summarizes a background about different renewable energy sources used for water pumping system. Then, the most used MPPT algorithms which are perturb and observe (P&O) and incremental conductance (INC) based on variable step size will be presented.
- The second chapter deals with the modeling of the PV water pumping system components.
- The third chapter presents the DTC control strategy using fuzzy logic controller (FLC) in order to get more robust control scheme and improve the performance of PV water pumping system.
- In the fourth chapter, a proposed approach associated to an indirect field-oriented control strategy with loss minimization of induction machine (IM) drive for the PV water pumping systems is presented.
- Finally, the conclusion of this thesis and the scope of the future work are presented.

# Chapter 1

# State of the art of different renewable energy sources for water pumping system

## 1.1 Introduction

The diesel engine pumps are used for agriculture in remote area, since they are simple to install, but these types of systems cause environmental problems because they work with the fossil fuels[11].Moreover, the increasing the use of the electricity and cost diesel, finding a promising alternative to power a pumping system is required. The renewable energy-based water pumps present alternative solution, because it produces electricity without harming the environment, and they are mostly used due to high distribution costs/non-availability of grid-power[1][2]. In this chapter, different renewable energy sources such as solar photovoltaic, solar thermal, wind, biomass and hybrid forms of energy used for water pumping and MPPT algorithms will be discussed.

## 1.2 Solar thermal water pumping system

The STWPS consists of converting the sun into mechanical energy[12][13]. The flat plate solar collectors and concentrators are used to pressurize the fluid.

In the pressurization process, the pressure and the temperature of the fluid en-

hance. The high pressure can be used by a secondary working fluid or in thermodynamic cycles in order to convert it into mechanical energy which can be used to operate the pump. This type of configuration is low cost and free of maintenance. However, it needs more land space to track the irradiance and is not appropriate for high water pumping quantity under high heads. In addition, some used liquids are environmentally unsafe and this water pumping system takes more time to reach the steady state.

## 1.3 Wind energy water pumping system

The water pumping based on wind powered system is also used[14]. The wind powered rotor is associated to a synchronous generator with permanent magnets to converter the wind energy into electrical power energy. The synchronous generators are typically used for large wind turbines, the charging of storage batteries and are associated to a common induction motor in order to drive the pump.

This water pumping system is flexible over other mechanical systems and the spare electricity can be exploited for other applications, but it's located in agriculture lands and the performance is affected by the velocity of the wind. The water pumping system based on wind powered system is more expensive and less efficient than PV water pumping system. The maintenance of mechanical components must be carried out. The installation of wind turbines is complex due to wake effect.

## 1.4 Gas or biogas dual fuel engine pumps

### 1.4.1 Biomass gasifier water pumping system

The water pumping system based on biomass gasifier is composed of dual fuel for diesel engine associeted with a centrifugal pump and a biomass gasfier[8]. The gasification process consists of transforming solid/liquid fuel into gaseous fuel (pro-

ducer gas) which is a mixture of calorific with hydrogen , nitrogen , methane and carbon monoxide and it can be utilized in dual fuel diesel engines by substituting 65-70 % of diesel.

### 1.4.2 Biogas water pumping system

Biogas can be used as a fuel to power the internal combusting engines for water pumping systems[8]. Moreover, the farmers have the possibilty to install a bigas generation unit to produce biogas.

The matenaince and operating of this water pumping systems configuration are higher. In addition, the presence of energy losses during the transmission of power engine/pump.

## 1.5 Hybrid renewable energy water pumping system

The combinaison of more forms of energy sources to feed the water pumping system can be used[15][16]. It makes the operating of the system more flexible and reliable compared to water pumping system based on one form of renewable energy sources due to the intermittence of this source.

## 1.6 Photovoltaic water pumpig system

The pumping water based on solar photovoltaic consists of using the electricity produced by the PV panels to feed the pump. The PV water pumping system is mainly constituted of the following components :

- Photovoltaic array
- DC-DC converter
- Inverter

- Motor
- Pump

Based on the system components, PV water pumping system can be classified into the following categories :

- On the basis of energy storage
  - → Battery-coupled
  - → Direct driven
- On the basis of type of motor
  - → DC motor
  - →AC motor
- Basis of categories of pumps
  - → Basis of types of pumps
    - ▶ Surface mounted pump set
    - ▶ Deep well pump set.
  - → Basis of applications of pumps
    - ▶ Dynamic pumps
    - ▶ Positive displacement pumps
- Basis of tracking of power source
  - → Fixed PV panels
  - → Tracking PV panels

### 1.6.1 On the basis of energy storage

The produced electricity from the PV array can be used to drive the pump or stored in storage batteries.

#### 1.6.1.1 Battery-coupled

During daylight hours, the electrical current produced by the solar panel charges the batteries. The stored energy is then used to pump water[17]. The advantages of using the batteries consist of prolonging the water pumping duration and ensuring to operate the water pumping system at all time. Moreover, the energy provides from the batteries can be used for others applications. However, the use of the storage batteries is not recommended because they increase the cost of the PV system, the maintenance is required and can reduce the efficiency of the water system. In addition, the voltage supplied by the batteries can be lower than that produced by the PV panels during the maximum sunlight conditions. Fig 1.1 illustrates the block diagram of block diagram of PVWPS with battery storage.

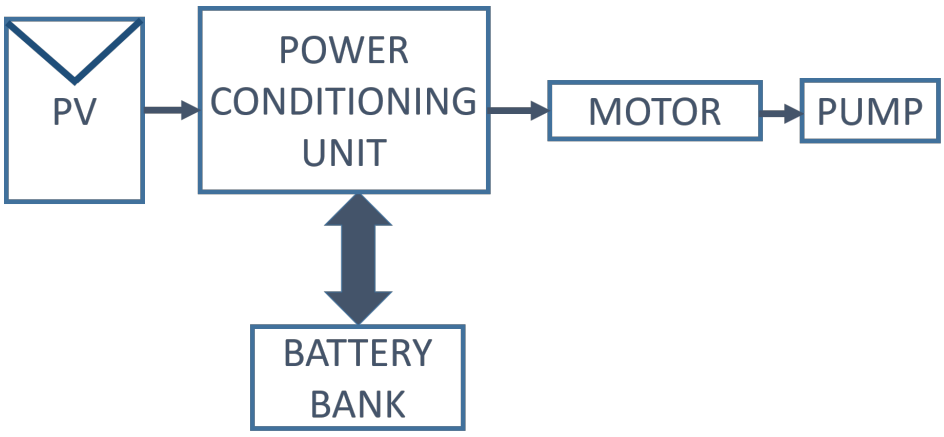


FIGURE 1.1 – Block diagram of PVWPS with battery storage

#### 1.6.1.2 Direct driven

In this PV water pumping system, the electricity produced by the PV panels feeds directly the pump[18]. The system operates only when the solar energy is available, this is due to absence of backup power. The direct driven PV water pumping system is battery free, which is simpler, less expensive and requires less maintenance compared to the previous system with storage batteries. However, the pump doesn't

operate during the night. Moreover, during late afternoon, early morning and cloudy days, the efficiency of the pump is reduced which leads to a little amount of pumped water. The volume of pumped water depends on the angle and intensity of the irradiance which is constantly changing. Extra volume of water pumped can be stored in water storage tank which is more economical than battery storage backup. Fig 1.2 illustates the block diagram of a direct coupled PVWPS.

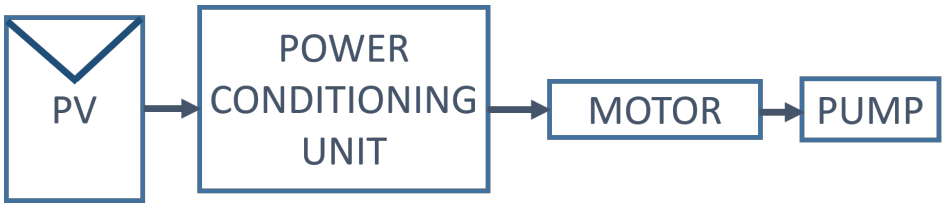


FIGURE 1.2 – Block diagram of a direct coupled PVWPS

### 1.6.2 On the basis of type of motor

The PV array produces a direct current (DC) which can be converted into alternating current (AC) thanks to an inverter[19][20].

#### 1.6.2.1 DC Motors

Different types of DC motors have been used for pumping water. These engines are attractive as they can directly connect to the PV array and generally utilized for low power solar water pumping system (above 7KW)[8][21]. The conventional DC motors use carbon brushes in order to transfer electrical power from PV panels to motor shaft. However, these brushes must be changed frequently because they wear out. Therefore, the maintenance and operation cost of the motor increase, especially for submersible DC water pumps where the pump must be removed frequently from the deep well for maintaining and replacing the brushes.

To overcome these drawbacks, a brushless DC (BLDC) motors are introduced

which are consist of a self-synchronous machine with an electronic commutator[22]. PV power is transferred to motor shaft based on the magnetic induction principle. Authors used permanent magnet synchronous (PMSM) brushless DC motor with a centrifugal pump. It was reported that the proposed configuration is a better alternative than a DC motor for low power direct coupled PV water pumping due to high efficiency, the absence of brushes, low maintenance requirements and high reliability. Other authors proposed a switched reluctance motor (SRM) which is supplied by a DC voltage through a switching circuit. The efficiency of the SRM is found to be a better than that of DC motor and it is cheaper than DC motor. Fig 1.3 illustates the block diagram of PV DC water pumping system.

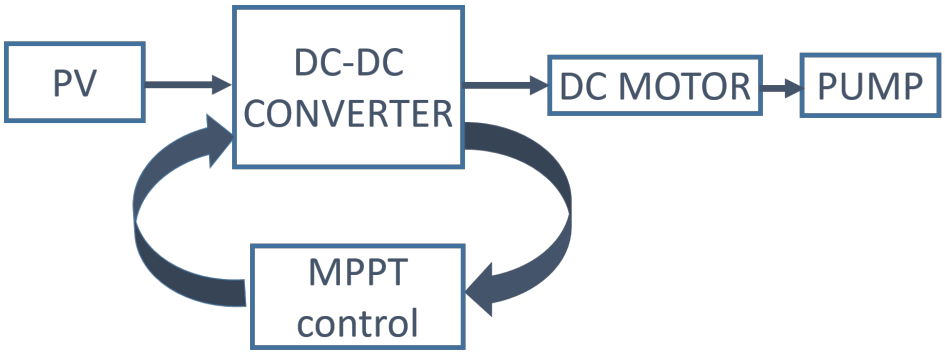


FIGURE 1.3 – Block diagram of PV DC water pumping system

#### 1.6.2.2 AC Motors

AC motors can be used to drive the pump. In this case, an inverter must be introduced to convert DC to AC electrical power since the PV array produces DC electricity[23]. This type of engines can run even on grid power in case of non-availability of PV power (no light or less light), moreover the maintenance cost is reduced. However, the overall efficiency of PV water pumping system is reduced due to the losses of the inverter.Fig 1.4 illustates the block diagram of PV AC water pumping system.

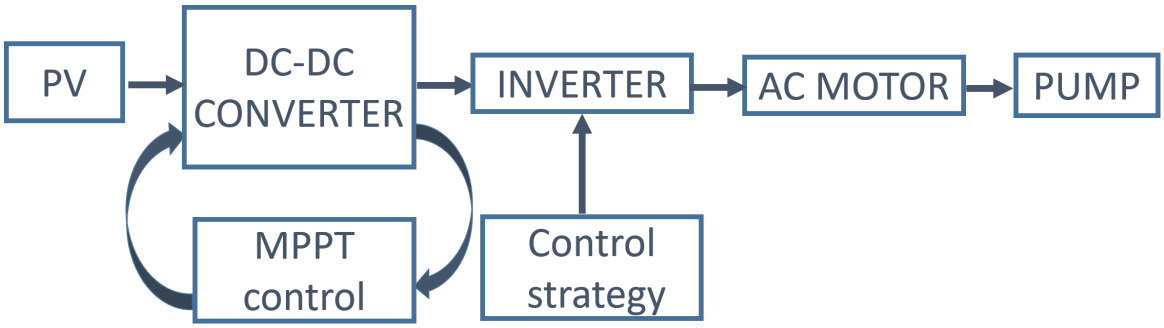


FIGURE 1.4 – Block diagram of PV AC water pumping system

Solar inverter has special characteristics adapted for use with PV panels, including anti-islanding protection and maximum power point tracking. Solar inverters can be classified into four major categories [24][25][26][27] :

- Solar pump inverters.
- Stand-alone inverters or off-grid inverter.
- Grid-tie inverters.
- Intelligent hybrid inverters.

Solar pump inverters generate AC electricity from DC electricity produced by solar arrays without using the batteries.

Stand-alone inverters use DC energy provided from batteries which are fed by photovoltaic panels. This type of inverter can include integral battery chargers to recharge the battery from an AC source.

Grid-Tie inverters are connected to the grid in order to send back energy from the surplus of solar photovoltaic generation and any unused energy to the grid. Moreover they generate a pure sine wave that is appropriate with the AC waveform generated by the grid.

Intelligent hybrid inverters manage the components associated directly to the unit such as battery storage, photovoltaic array and utility grid and they are able to discharge and charge solar batteries bank.

### 1.6.3 Basis of categories of pumps

Different types of pumps can be used in PV water pumping system, each one has its pros and cons. In this section, the solar pumps are classified according to their types and applications[8][28].

#### 1.6.3.1 Basis of types of pumps

- **Submersible pump**

  The pumps are either submersible, surface or floating. The submersible pump is designed to draw water from deep wells and it must be completely submerged in liquid for operating. The advantages of the submersible pump are simple to install, more protected from the environment, less likely to be damaged from running dry and utilize the groundwater as a natural priming fluid. However, its maintenance is difficult.

- **Surface pump**

  The surface pump is designed to draw water from shallow wells, rivers, springs, ponds or tanks. This type of pump cannot be submerged in water and its suction is limited when used in deep wells. Different manufactures specified that the typical suction abilities for this category is between 10 and 20 ft. Contrarily to submersible pump, the surface pumps are less protected because they are exposed to the extreme climate (freezing and harsh weather). Moreover, the cavitation is a frequent problem with these pumps and the loss of priming water can lead to burning the motor. The dynamics of pulling water up from a well causes a higher rate of mechanical problems and failure. The major drawbacks of these pumps are the high cost of the installation and the power losses in the shaft bearing which reduce the efficiency.

- **Floating pump**

  The floating water pump is designed to draw water from reservoirs with ad-

justing height ability. These pumps are ideal for irrigation pumping from open wells and canals. Moreover, the floating unit sets are easily portable and the chance of the irrigation pump running dry is negligible.

#### 1.6.3.2 Basis of applications of pumps

The pump can be splitted into two categories : dynamic pumps and positive displacement ones.

- **Dynamic pumps**

  Dynamic pumps can be utilized where a change in flow is not a problem and high volumes are required. Centrifugal pump is dynamic pump and it's commonly used because it generates more head than other dynamic pumps at a variable speed, simple, low cost, necessitates less torque to start and it's characterized by its low maintenance. Compared to positive displacement pumps, the efficiency of dynamic pumps is lower. This configuration can be functioned for short time with the discharge valve closed.

- **Positive displacement pumps (volumetric pumps)**

  Positive displacement pumps or volumetric pumps are not well adapted to be associated directly to PV array. Hence, maximum power point tracking system and a power conditioning unit must be introduced. These pumps have different speed–torque characteristics and are used when relatively small but precise volumes are required. In volumetric pumps, the water output is almost independent of head and directly proportional to the speed of pump and the operating with the discharge valve closed will damage the pump. Piston pump and Screw pump are volumetric pumps.

### 1.6.4 Basis of tracking of power source

The PV water pumping system can be operated with or without a tracking system[29][30].

#### 1.6.4.1 Fixed PV panels

In this configuration, the PV panels are arranged on metallic structures inclined at a fixed tilt angle. The latitude angle of the pumping site is generally equal to the value of tilt angle. The PV system without a tracking system is caracterized by a low cost and low performance compared to the PV system based on tracking system.

#### 1.6.4.2 Tracking PV panels

Other PV systems are equipped with sun trackers in order to maximize the PV power by keeping the PV panel always perpendicular to the light rays during the day. The solar tackers can have one direction : a horizontal single- axis tracker to track the sun toward south and north or vertical single- axis tracker to track the sun toward east and west. The solar trackers can have also two directions (both vertical and horizontal axis) to increase the power gain. The tracking system improves the efficiency of the PV water pumping system, while the cost of the installation and maintenance are considerably higher. Solar tracking should not be confused with Maximum Power Point Tracking (MPPT) which is a control algorithm to extract the maximum PV power rather than a physical device. MPPT algorithms will be discussed in the next section.

## 1.7 Literature review of control strategies applied to PVWPS system

Several solar water pumping technologies have been developed by researchers to efficiently operate PVWPS. The majority of the PV water pumping system in the beginning days operated using DC motors because it can be directly associated with PV array as it produces direct current.

In [19] the authors proposed fuzzy logic controller to control the level of the tanks and the speed of the DC motors based on the irradiation levels in PV. A technique which allows to identify the reference speed for the control of the DC motors is presented. The suggested system optimizes the energy obtained from the PV panels, minimizes the cost of the PV water pumping system and it controls the tanks in real time to provide water.

In [31], PV water pumping system using shunt DC motor is presented. A single step-up converter associated to DC motor, is controlled by an unique duty ratio which allows to achieve optimum operation under various irradiation levels. The proposed control improves the efficiency of the PV water system and eliminates the requirement for permanent adjustments of the duty ratio.

In [32] the authors introduce a buck-boost converter in order to keep a constant voltage at the terminals of the DC motor for each solar radiation levels. A sinusoidal pulse width modulation technique is introduced to control DC-DC converter. A mathematical analysis of the proposed PV water pumping system is carried out. DC motors give an important starting torque but they need regular maintenance. For this reason, brushless DC motors are utilized.

In [33] the authors proposed a solar water pumping system based on BLDC motor. A zeta converter is controlled through the incremental conductance technique with the aim of achieving soft starting of the BLDC motor used to drive a pump. The selection of the fundamental switching frequency of the inverter is effectuated by using an electronic commutation. A proposed technique for low valued DC link capacitor is presented. The PV system is modeled and tested using Matlab /Simulink under different operating conditions.

In[34], an entire design of the solar powered water pumping system for an agricultural land is presented. Cuk converter is controlled by perturb and observe (P&O) technique and it adjusts the dc link voltage to feed three phase inverter connected to BLDC motor. Numerical simulation using Matlab/Simulink and practical im-

plementation using Arduino UNO have been carried out to validate the proposed control.

Ghasem Shokri et al.[35] developed a control strategy for directly coupled solar photovoltaic water pumping system. The suggested system consists of BLDC motor controlled by direct torque control strategy. Buck-Boost converter is utilized to ensure optimal operation of BLDC motor. Bacterial Foraging Optimization (BFO) algorithm is used to tune PI controllers to reduce the complexity of classical control techniques. A comparative study between the proposed algorithm, PWM current control and conventional hysteresis is effectuated to evaluate the performance of the PV water pumping system under different conditions. The simulations results show the robustness of BFO algorithm.

Rajan Kumar et al.[36] proposed a single solar PV water pumping system. The purpose consists of eliminating the DC-DC conversion stage in order to reduce the size, cost, complexity and increase the efficiency. The proposed control strategy of BLDC motor is simple and allows the PV array to work at its peak power without using any additional control associated for the soft start of moto-pump and its speed control. Simulation and experimental results validated the suitability of proposed system.

R. Akkaya et al .[37] proposed genetic assisted, multi-layer perceptron neural network method to control DC–DC boost converter. A proportional integral (PI) speed control loop of BLDC motor is introduced. A real time implementation of the overall system using DSP unit is effectuated. The suggested method is compared with other systems. The proposed technique allows the functioning of the PV system for longer periods of time through the day.

In [38] the authors have presented standalone photovoltaic water pumping system driven by a brushless DC (BLDC) motor. Perturb and observe and fuzzy logic control algorithms are used to get the maximum power and compared to evaluate the performance of the PV system. BLDC motor has high efficiency and reliability

but the rotor position of this engine is identified by using hall sensors which make the system complex and increase the cost.

Terki et al. [39] introduced the fuzzy logic (FL) control to improve the performance of the PV. FL speed controller is used to overcome the drawbacks provided by the conventional PI controller such as larger overshoot, oscillation and lower response. The characteristics of the PV system using (PI) and a fuzzy logic (FL) speed controllers are studied. The dynamic behaviors of PV water pumping system based on FL controller ensure better performance.

Ahmed M. Kassem developed a technique based on artificial neural network (ANN) to operate the BLDC motor at the high available efficiency [40]. The proposed method allows to ensure the optimum chopping ratio of buck–boost converter and design a state feedback static controller for PV water pumping system at any irradiation. A comparative study between the proposed controller and PID controller has effectuated. From the obtained results, the proposed control strategy provides good performance.

In [41], authors proposed a sizing of a standalone photovoltaic water pumping system using permanent magnet DC motor. The proposed method is based on multi-objective optimization algorithm to enhance the size of the photovoltaic water pumping system according to technical and economic objectives. The performance of the system is evaluated based on the meteorological data of the target for one year. The proposed system is able to attain balance between cost , reliability, and excess water of the PV water pumping system.

S. Sashidhar et al.[42] developed single-stage sensorless control of Permanent magnet brushless dc motor based photovoltaic water PV water pumping system. The aim is to improve the control of the motor with hall-effect based position sensor. Therefore, a position sensorless control scheme is introduced. The experimental results show the improvement of reliability of the overall PV system.

In [43] , an optimization based on genetic algorithms (GA) was effectuated for

two MPPT algorithms which are perturb and observe and fuzzy technique. On the other hand, the permanent magnet DC (PMDC) motor is used to drive the pump. GA is usually utilized to optimize other algorithms based on principles of biological evolution. The use of this kind of motor for water pumping is still not popular as it suffers from non-availability of rare earth magnet and cost constraints.

In PV pumping applications, an induction motor shows good performance compared to other commercial motors because of its greater robustness, lower cost, availability in local markets, higher efficiency and lower maintenance cost. Saber KRIM et al.[44] proposed a method to improve the control of the PV water pumping system. To fix the switching frequency and improve the DTC performances. Space Vector Modulation (SVM) is introduced. On the other hand, P&O is used to control the DC-DC converter. Hardware co-simulation based on FPGA is carried out to evaluate the efficiency of the proposed induction motor control. comparative studies between the proposed method, the conventional DTC and different MPPT algorithms are effectuated. It can be noticed that compared to dSpace, FPGA reduces the execution time. Therefore, the commutation losses of the inverter are minimized.

An approach based on Open-End Winding IM for PV fed water-pump drive system is proposed by Sachin Jain et al.[45]. The dual inverter is utilized to obtain low value DC bus voltage. The proposed technique incorporates the two control strategies which are V/f control and Maximum Power Point Tracking for the efficient utilization of the PV water pumping system. The proposed control scheme reduces the number of sensors, which leads to reduce the cost of the PV system.

In [46] authors proposed a control strategies for single stage PV water pumping system which consists of using a dual Maximum Power Point Tracking technique to achieve the maximum power from two PV generators. The three-phase Open-End Winding Induction Motor (OEWIM) is controlled by V/f control and used to drive the centrifugal pump. The results of the analysis indicated that the torque ripples

are reduced and the performance of PV system is improved. Moreover, the proposed technique can be used for multiple PV panels.

A designed induction motor for PV water pumping system is developed by Khusro Khan et al.[47] . The stator and rotor slots are modified. The proposed method eliminates the use of mechanical sensor ,which reduces the complexity and the cost . The induction motor is controlled by field-oriented control based on artificial neural network current control strategy. A robust speed adaptive technique is proposed. A prototype is developed in laboratory to evaluate the proposed control of PV water system. The proposed method illustrates better performance in terms of cost, saving energy, starting current and torque.

João Victor Mapurunga Caracas et al.[48] suggested a new converter to drive an induction motor used for photovoltaic water pumping system. The proposed system consists of a Full-Bridge Three-phase Voltage Source Inverter and Resonant Two Inductor Boost Converter. This latter is improved by using a non-isolated recovery snubber along with a hysteresis controller. In addition, a constant duty cycle control is introduced to enhance the efficiency. Experimental results show the robustness of the proposed PV water system

Rashmi Rai et al.[49] developed an efficient speed sensorless control for PV water pumping system. The sliding mode based DC link voltage regulator is used for regulating the speed and the motor power for PV water pumping system. The integral sliding mode observer based speed estimation of induction motor and sliding mode current control for decoupling of current are introduced to avoid the disadvantages of motor parameters variation. The proposed sliding mode based control is compared with the proportional integral (PI) controller based speed sensorless control for motor parameter variation. Based on the simulation and experimental results, the control of the PV water pumping system is optimal using the proposed technique.

In [50],an incremental conductance (INC) based MPPT control technique is utilized to obtain the peak power from the PV array and scalar control for induction

motor drive operation, the authors used the INC method based on fixed step size. The scalar control strategy is characterized by its simple structure, easy design and low cost.

On the other hand, variable step size incremental conductance and Field oriented control strategies are proposed in [51]. The aim is to achieve a better control of PV water pumping system without battery storage. The proposed technique is applied in two cities in Morocco which are fez and Marrakech using real climatic conditions. The simulation results illustrate that the proposed technique offers better performance in Marrakech .

J. Linares-Flores et al.[52] developed a control of solar powered induction motor drive for water pumping system. Field-Oriented Control is used. A maximum power point tracking algorithm based on the exact Static Error Dynamics Passive Output Feedback controller technique and an Algebraic Estimator is proposed. This technique determines the impedance between the boost converter and the inverter. The suggested control strategies allow starting softly by an angular speed drive, using the PV array. Field-Oriented Control technique is implemented using dSPACE system, while the MPPT algorithm is implemented in the DSP board.

In [53] the authors suggested direct torque control based fuzzy logic controller for induction motor driven double stage PV water pumping system. It consists of replacing the hysteresis controllers by fuzzy logic controller to improve the performance of the conventional direct torque control. The performance of the proposed system is evaluated for three different months of the year and compared with the conventional method. The simulation results demonstrate superiority of the proposed PV water pumping system in terms of pumped water, torque and flux ripples and tracking of flux reference.

Abla Khiareddine et al.[54] proposed double stage PV water pumping system with battery storage. The authors proposed an optimal power management approach of the PV water pumping system and designed three new supervisory controllers

which are a fuzzy controller, algorithm controller and neuro fuzzy controller. The vectorial control is utilized for the induction motor. A combination of vectorial control and neuro fuzzy controller worth to be implemented in agricultural applications.

## 1.8 Performance of PVWPS

The use of solar photovoltaic in the water pumping process is the better option because there is a natural relationship between requirement of water and the availability of solar power. However, the initial cost of the PV system is higher and the performance of the PVWPS is affected by weather conditions and the efficiency of the PV technology conversion.

## 1.9 MPPT algorithms

The electrical power produced by the PV panels depends on the sunshine, temperature and the overall aging of the system[55]. For these reasons, the PV array can provide only a maximum power for a particular voltage and current. This operating at maximum power depends on the load at its terminals. To extract the maximum power available at the terminals of the PV array and transfer it to the load, an adaptation stage must be integrated between them (PV array and the load)[56]. The latter must be able to operate the PV array at its maximum power. To achieve this objective, the used adaptation stage is composed of a DC-DC converter controlled by the duty cycle which is adapted using MPPT algorithms.

Various MPPT techniques have been reported in literature, each method has its own specification, limitation and application. The MPPT algorithms can be classified into three major groups[57] :

1. Conventional methods including Constant voltage controller (CVC) method, Perturb & Observe (P&O) method, Incremental Conductance (IC) method ;

these kinds of algorithms use PV current, PV voltage, irradiance and temperature for maximum power extraction and they are characterized by its simple implementation.

2. artificial intelligence-based methods including Fuzzy logic controller technique, Artificial neural network control strategy and Adaptive Neuro-fuzzy Inference method. These algorithms have fast response, good MPP tracking accuracy and offer better performance than the conventional methods but they are complex to implement.
3. Hybrid methods including Modified Perturb and Observe method (Modified P&O), PI modified Fuzzy logic controller (PI-FLC) method and Neural-Fuzzy logic (N-FL) method, these algorithms combine the conventional and artificial intelligence-based methods to achieve greater efficiency and tracking accuracy.

The two most MPPT algorithms are perturb and observe ( P&O) and incremental conductance (INC). Good performance is obtained using conventional MPPT methods based on fixed step, but they are slow and present oscillations around the PPM and the results are not satisfactory during sudden change of climatic conditions. A fast follow-up can be realized by increasing step, but the oscillations appear in steady state[58]. Many contributions have been introduced using a variable step, where the algorithm automatically changes the step size. Therefore, variable step size incremental conductance algorithm and variable step size perturb and observe technique have been chosen for the purpose of comparison.

### 1.9.1 Variable step size perturb and observe

The P&O algorithm is used by the majority of authors because it's easy and simple to implement ant low-cost[59]. Based on the measuring of PV voltage and current, the PV power is calculated. It is compared to the previous power in order to deduce the value of the duty cycle $\alpha$ Fig 1.5. In fact, the Perturb and Observe algorithm is functioned as follows :

- if $\frac{dP_{pv}}{dV_{pv}} > 0$ : the working point is on the left of the MPP ;
- if $\frac{dP_{pv}}{dV_{pv}} < 0$ : the working point is on the right of the MPP ;
- if $\frac{dP_{pv}}{dV_{pv}} \approx 0$ : the working point is at the MPP ;

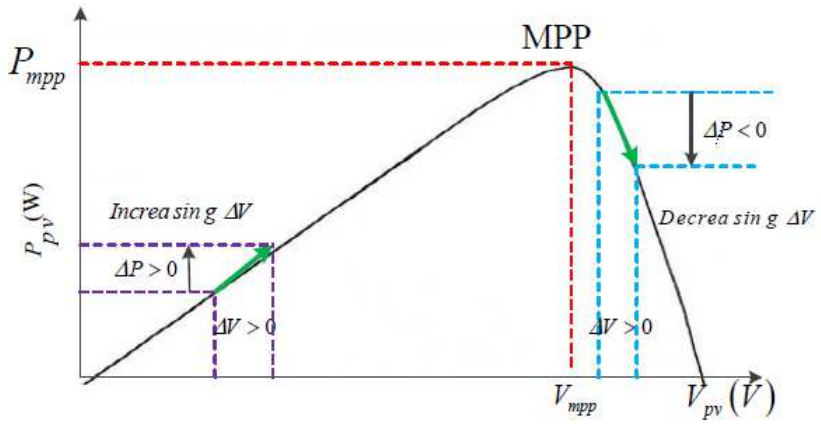


FIGURE 1.5 – Methodology to locate the Maximum Power Point using the Power versus Voltage curve

The conventional P&O MPPT is based on fixed step, smaller step causes slower response and larger step results in higher oscillations. To overcome this drawback, a variable step size is used which consists in choosing automatically the step.

The step size is determined by equation (1.1).Fig 1.6 shows the flowchart of VSS P&O algorithm.

$$Offset = Offset_0 \times \frac{\Delta_P}{\Delta_V} \tag{1.1}$$

### 1.9.2 Variable step size incremental conductance

Incremental conductance algorithm has been proposed which is based on the derivative of the $P_pv$ with respect to $V_pv$ to avoid the disadvantages of the P&O algorithm. The principal advantage of the incremental conductance (INC) algorithm

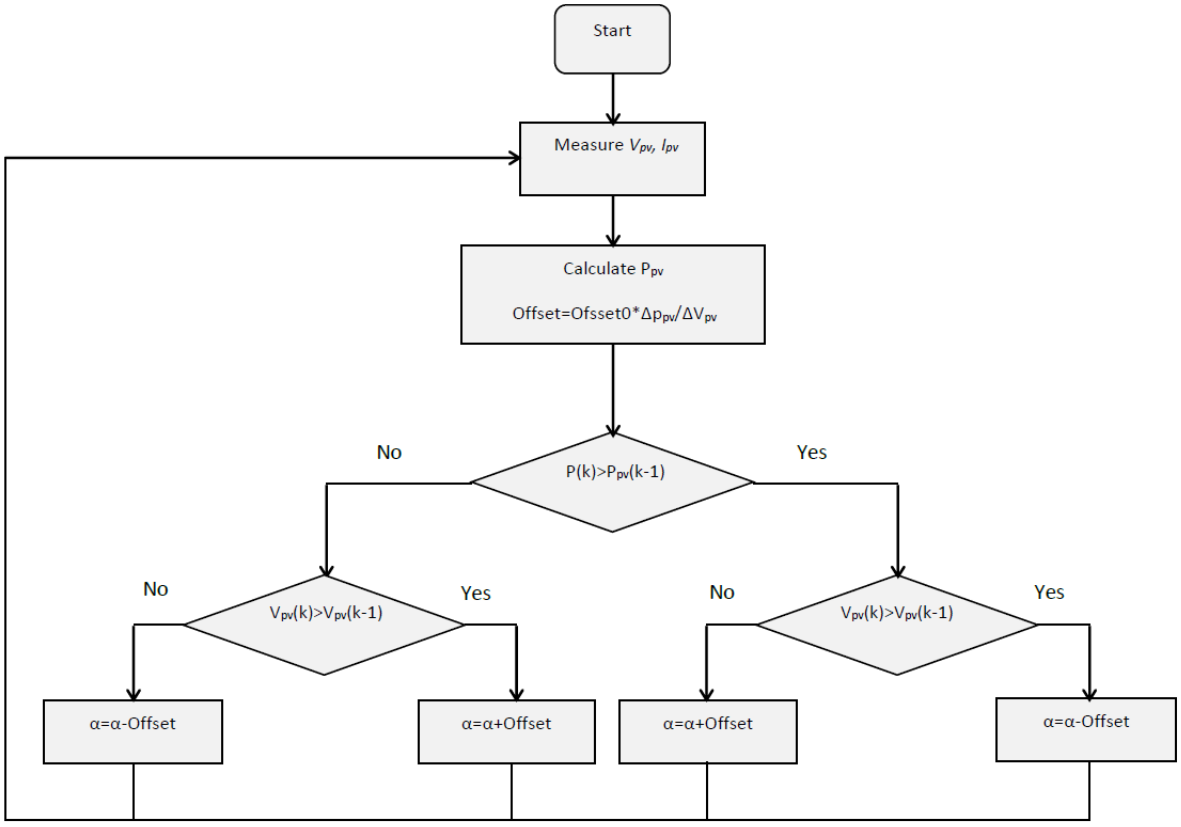


FIGURE 1.6 – Variable step size P&O

is that it provides a good performance under rapidly changing atmospheric conditions. This technique uses the slope of the $P_pv$ characteristics in order to track MPP. Therefore, incremental conductance algorithm is operating as follows :

- $\frac{V_{pv}}{I_{pv}} = -\frac{\Delta V_{pv}}{\Delta I_{pv}}$ : at MPP ;
- $\frac{V_{pv}}{I_{pv}} < -\frac{\Delta V_{pv}}{\Delta I_{pv}}$ : left to MPP ;
- $\frac{V_{pv}}{I_{pv}} > -\frac{\Delta V_{pv}}{\Delta I_{pv}}$ : right to MPP ;

The drawback of the incremental conductance method is the use of a fixed tracking step size. For this, the variable step size incremental conductance is used in this chapter. Fig 1.7 shows the flowchart of VSS INC algorithm.

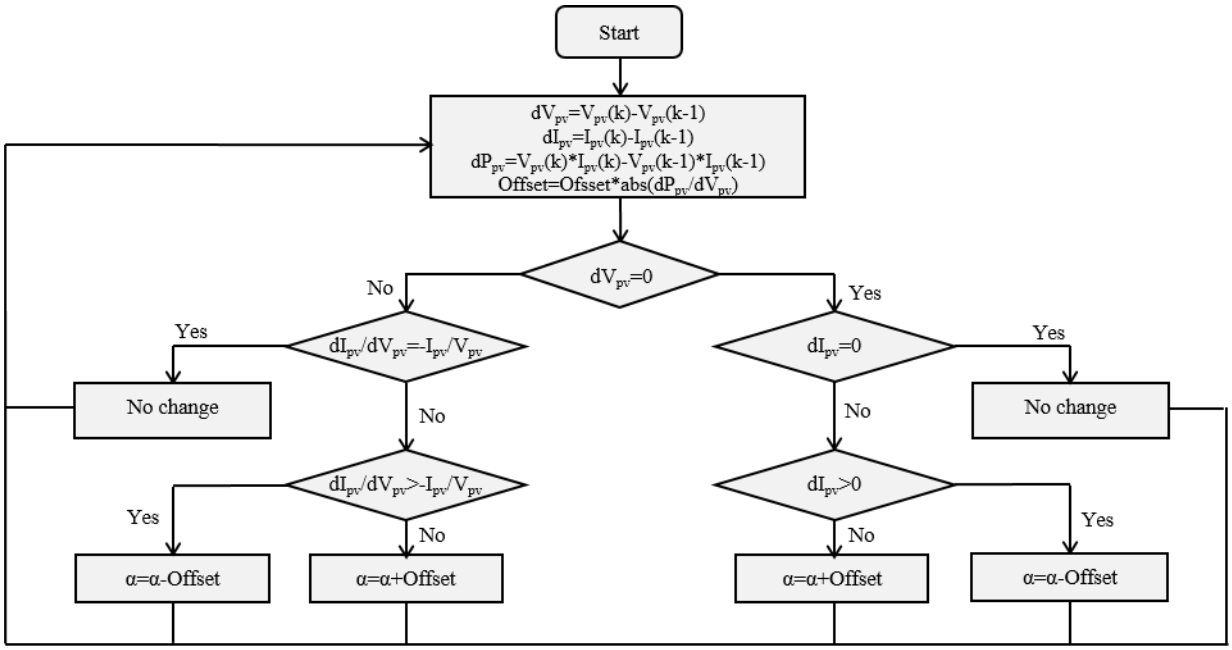


FIGURE 1.7 – Variable step size incremental conductance

# Conclusion

This chapter presents a state of the art about different configurations of the water pumping system based on renewable energy sources such as solar photovoltaic, solar thermal, wind, biomass and hybrid forms of energy. Depending on the components in the system, PV water pumping system has been classied by mentioning the relative advantages and disadvantages of each conguration. Then, the most used MPPT algorithms which are perturb and observe (P&O) and incremental conductance(INC) based on variable step size are presented.

# Chapter 2

## Modeling of the PV water pumping system

## 2.1 Introduction

To evaluate and control the system elements, an essential step consists in modeling the PV system components. Therefore, we present the used model of the photovoltaic panels, the DC-DC converter, the inverter, the induction motor and the pump.

## 2.2 PV array

The researchers proposed different models for PV panels [60][61], In particular the model with a single diode and the model with two diodes, and consequently the choice of an adequate model is a little difficult. Two diode model is very precise and gives satisfactory results when the irradiation is low[62], but it's complex considering the number of parameters intervening in this model[63][64]. The four parameters model (4-p), in which the effect of the shunt resistance is negligible[65] is used to simulate photovoltaic panels and improved the performance of pumping system installations[63]. The five parameters model (5-p) introduces a parallel resistance in the equivalent circuit of the photovoltaic cell[66], the leakage current of the P-N junction is described by this resistance[67]. This model is the most used because it presents a compromise between precision and simplicity[63]. Comparative studies

have been made between the 4-p and 5-p models, the results have shown that the 4-p model is less accurate than the 5-p model[66]. So we can be satisfied with this model to do our research.

### 2.2.1 Modeling of PV cell

The equivalent model of PV cell, studied in this work, is presented in Fig 2.1. It contains a current source, shunt and series resistors, and a diode[68][69][70].

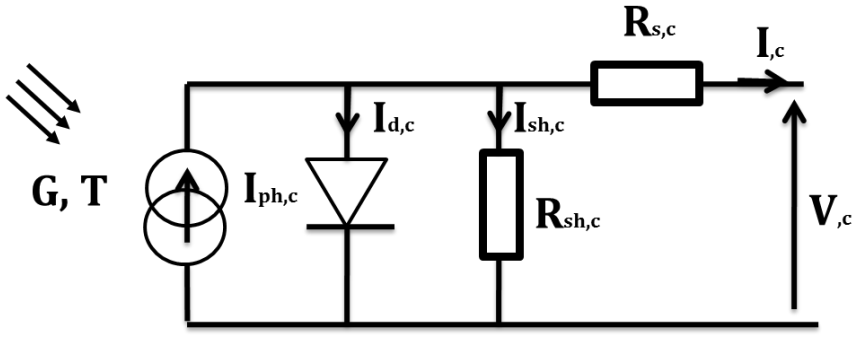


FIGURE 2.1 – Equivalent model of a PV cell

The mathematical model for the current-voltage characteristic of a PV cell is expressed by [71] :

$$I_{,c} = I_{ph,c} - I_{o,c}(\exp \frac{q(V_{,c} + R_{s,c}I_{,c}}{aKT} - 1) - \frac{(V_{,c} + I_{,c}Rs, c)}{Rsh, c} \tag{2.1}$$

Where $I_{ph,c}$ is the photocurrent of a cell,$I_{0,c}$ is the reverse saturation current of the diode, q, a, T, and K are the electron charge, the ideality factor of the diode, the junction temperature, the Boltzmann's constant respectively. $V_{,c}$ is the output voltage of PV cell, $I_c$ is the output current of PV cell, $R_{s,c}$and $R_{sh,c}$ are the series and shunt resistors of the cell.

### 2.2.2 Model of the PV panel

The PV panel used in this study consists of Ns cells coupled in series in order to increase the voltage, and therefore the functioning of our photovoltaic panel can be modeled by the following approximate analytical expression[72]

$$I = I_{ph} - I_o e^{\frac{q(V+R_s I)}{aKTN_s}-1} - \frac{(V+IR_s)}{R_{sh}} \tag{2.2}$$

$$I_{ph} = (I_{sc} + K_i(T - 298.15)\frac{G}{1000}) \tag{2.3}$$

$$I_o = \frac{I_{sc} + K_i(T - 298.15)}{e^{(\frac{q(V_{oc}+K_v(T-298.15)}{akTN_s})} - 1} \tag{2.4}$$

Where $I_{ph}$ is the photocurrent $I_0$ is the reverse saturation current of the diode, $N_s$ is the number of cells coupled in series, I is the current generated by the panel, G is the solar irradiation in $W/m^2$, $R_{sh}$ and $R_s$ are the shunt and series resistors of the panel. The cells are connected in series, so :

$I_{ph}$= $I_{ph,c}$

$I_0$= $I_{0,c}$

$V = V_{,c} \times N_s$

$R_s = R_{s,c} \times N_s$

$R_{sh} = R_{sh,c} \times N_s$

### 2.2.3 MATLAB/Simulink Based Modelling of Photovoltaic Panel

#### 2.2.3.1 Extract the lacked parameters of a PV panel

Some electrical parameters such as (ideality factor a diode saturation current, the series resistance $R_s$, the light-generated current $I_{ph}$, and shunt resistance $R_{sh}$ are not given by the manufacturer. Therefore, to adjust the PV panel, these missing parameters must be determined. Hence, many researchers have worked on the

identification of these parameters [60][73]. Mathworks provides a tool that allows determining these parameters based on the parameters mentioned in manufacturer specifications. The tool displays and adjusts the missing parameters.

| Photovoltaic Panel CSUN235-60P | |
|---|---|
| Maximum Power, $P_m$ | 235 W |
| Open Circuit Voltage, $V_{oc}$ | 36.8 V |
| Short Circuit Current, $I_{sc}$ | 8.59 A |
| Maximum Power Voltage $P_m, V_m$ | 29.5 V |
| Maximum Power Current $P_m, I_m$ | 7.97 A |
| Standard Test Condition | 1000 $W/m^2$ , 25$^{\circ}C$, AM 1.5 |
| Number of cell | 60 |
| Temperature coefficient of open-circuit voltage $V_{oc}, K_v$ | -0.37% / $^{\circ}C$ |
| Temperature coefficient of short-circuit current $I_{sc}, K_i$ | 0.07% / $^{\circ}C$ |

TABLE 2.1 – Electrical characteristics of the csun235-60p photovoltaic module

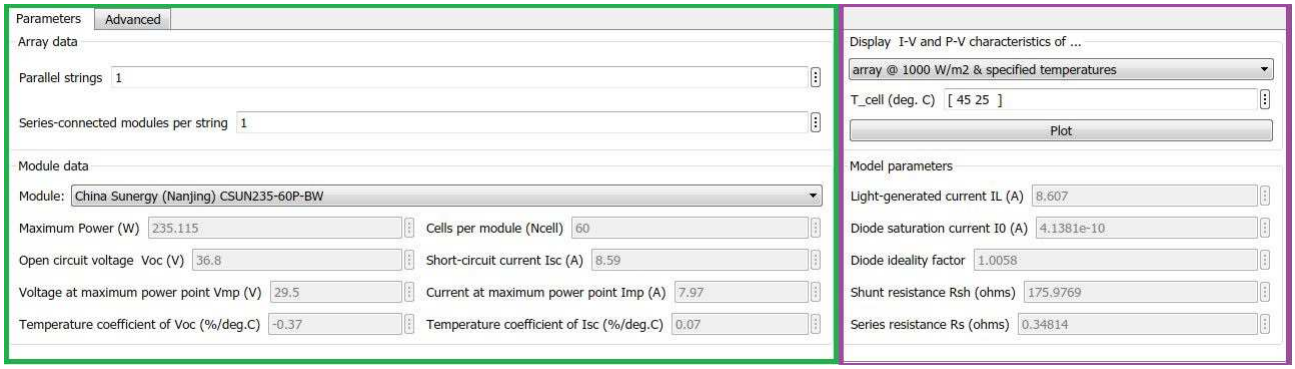


FIGURE 2.2 – Mathworks PV tool

#### 2.2.3.2 Simulink model of PV panel

Based on the equations (2.2), (2.3) and (2.4), below is the model developed by Matlab/Simulink tool. Fig 2.4 shows the I-V and P-V curves obtained by the PV panel Simulink model under STC. From the equations (2.2),(2.4),it can be seen that the physical behavior of the PV panel depends on solar irradiation, the shunt and series resistances and temperature. Hence, in this section, the influence of these parameters on the output of the PV panel is studied.

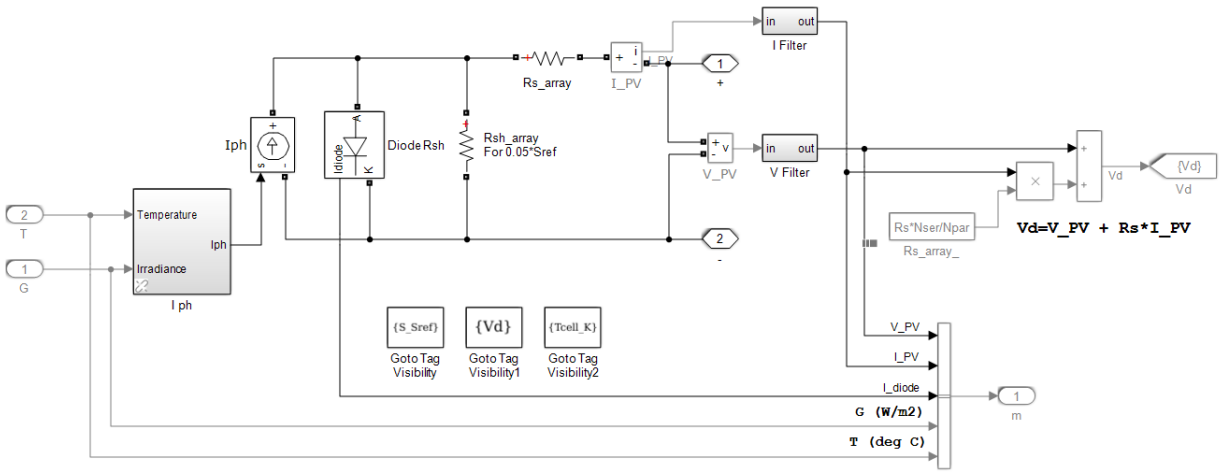


FIGURE 2.3 – Simulink model of PV panel

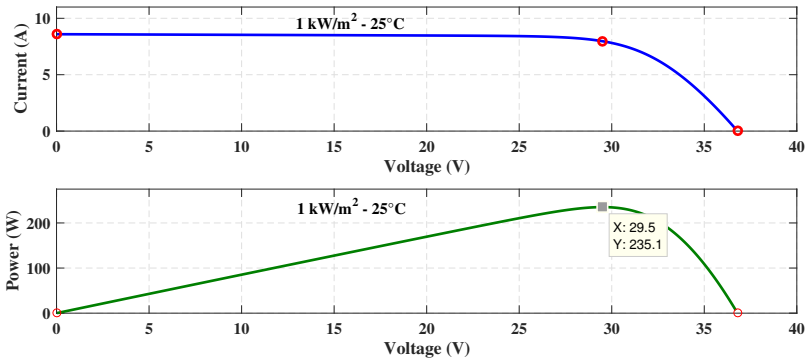


FIGURE 2.4 – I-V and P-V curves of CSUN235-60P PV panel

- **Effect of solar radiation variation**

  Fig 2.5(a) clearly shows that the current produced by the PV depends strongly on the solar irradiation. Fig 2.5(b) presents P-V curve, the voltage increases by 1.5V when solar irradiation has increased from 400 $W/m^2$ to 1000 $W/m^2$.

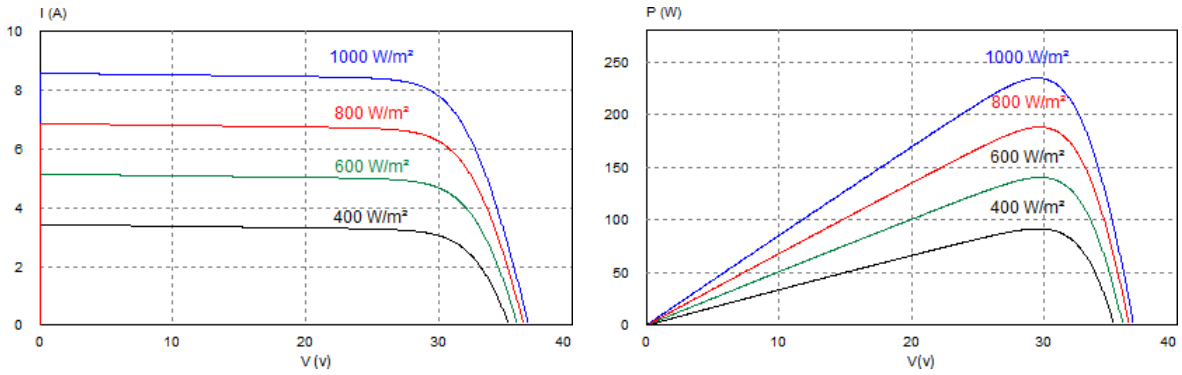


(a) (b)

FIGURE 2.5 – (a)I-V curves for different solar radiation and (b) P-V curves for different solar radiation

- **Effect of temperature variation**

  In general, for a given solar radiation, when the temperature raises, the open-circuit voltage $V_{oc}$ decreases slightly, while the short-circuit current increases. This behavior is validated and presented in Fig 2.6 .

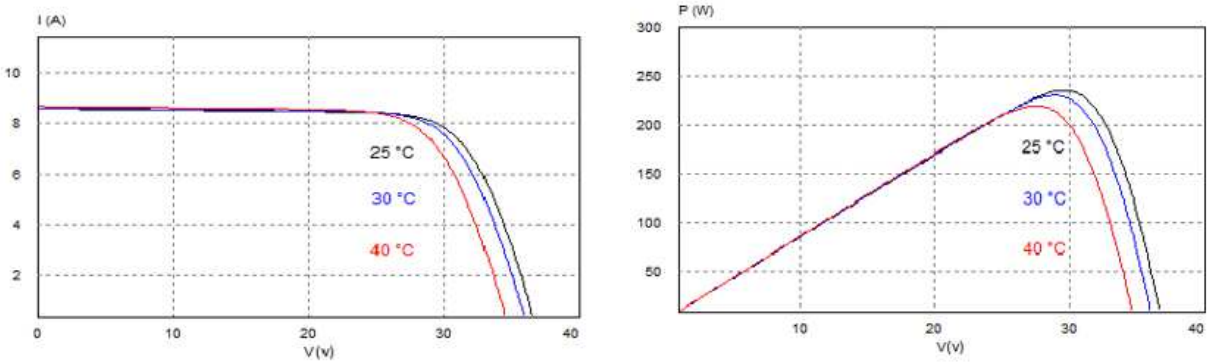


(a) (b)

FIGURE 2.6 – (a)I-V curve for different temperature values and (b) P-V curves for different temperature values

- **Effect of series resistance variation**

  The value of the series resistance is very low, and in some cases it can be neglected. Nevertheless, to make the model suitable for any given photovoltaic panel. We can vary this resistor in order to predict the influence of its variation on the outputs of the PV panel.

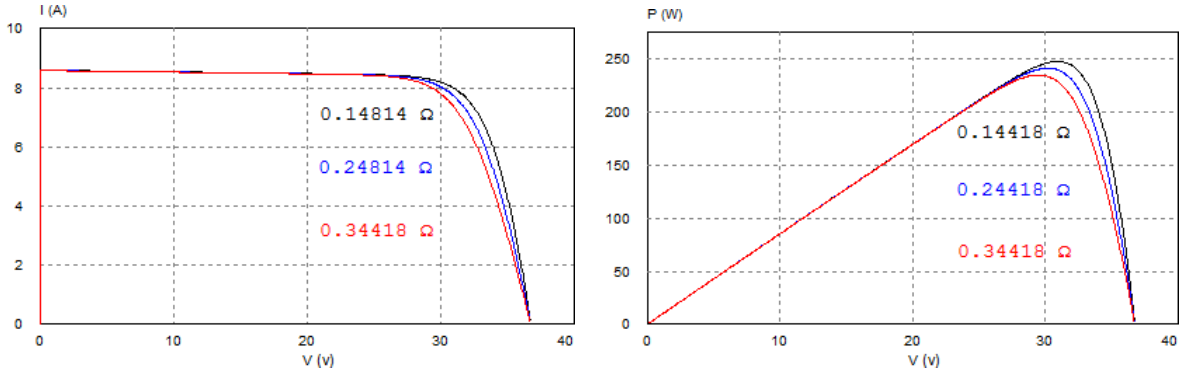


(a) (b)

FIGURE 2.7 – (a)I-V curves for different values of $R_s$ and (b) P-V curves for different values of $R_s$

According to Fig 2.7, the variation of $R_s$ affects the angle of curve I-V by causing a deviation of the slope of the maximum power point. The simulation was done for three different $R_s$ values, 0.14418 Ω, 0.24418 Ω and 0.34418 Ω. We have shown that the higher $R_s$ values reduce the output power. The fill factor, given by equation (2.5) decreases as $R_s$ increases.

$$FF = \frac{P_{max}}{V_{oc} \times I_{sc}} \tag{2.5}$$

- **Effect of shunt resistance variation**

  The shunt resistance must be large enough to have better output power and a good fill factor. For a low shunt resistance, the current collapses more strongly so that there will be a high-power loss and a low fill factor as shown in Fig 2.8.

- **Effect of diode saturation current variation**

  The curves of Fig 2.9 show the behavior of the PV panel for different saturation current values.

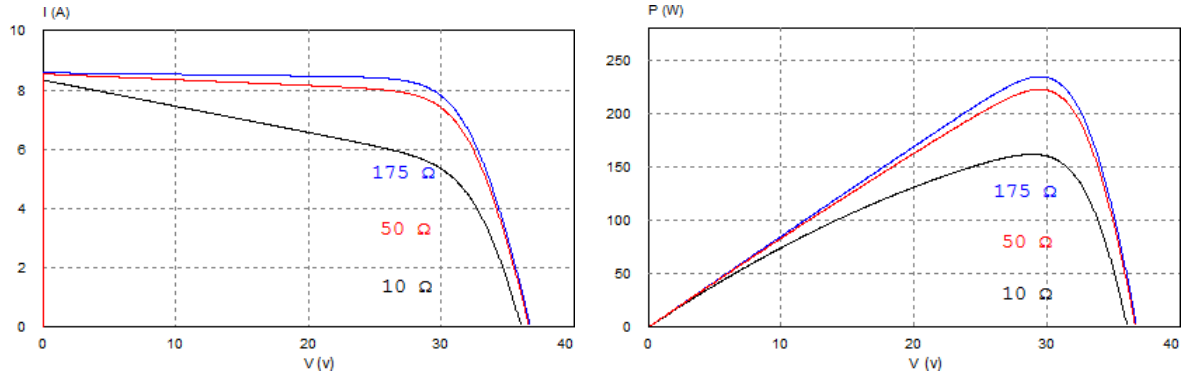


(a) (b)

FIGURE 2.8 – (a)I-V curves for different values of $R_{sh}$ and (b) P-V curves for different values of $R_{sh}$

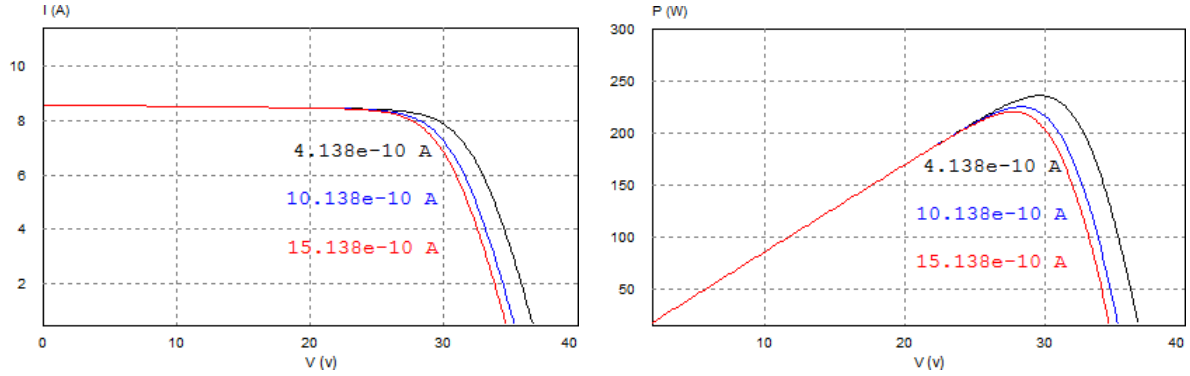


(a) (b)

FIGURE 2.9 – (a)I-V curves for different saturation current values and (b) P-V curves for different saturation current values

## 2.3 Boost converter

The DC /DC converter is placed between the PV panel and the inverter in order to increase the voltage and maximizing the power from the panel Fig 2.10[74][75].

### 2.3.1 Operation

The operation of the boost converter can be divided into two distinct states depending on the state of the switch S.

*S=1* : the switch is closed (Fig 2.11) which produces an augmentation in the

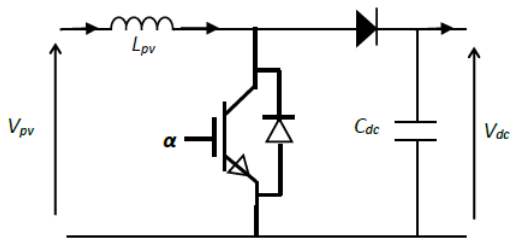


FIGURE 2.10 – Boost converter topology

inductor current. Therefore, a quantity of energy is stored in form of magnetic energy. The diode is blocked and the load is disconnected from the power supply. The equations that represent this state are :

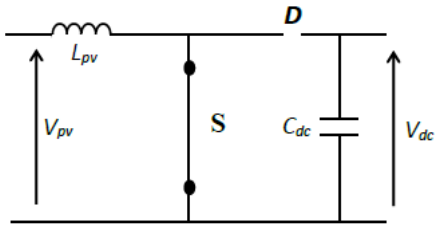


FIGURE 2.11 – Boost converter configuration switch turned ON

$$V_{pv} = L\frac{dI_{L_{pv}}}{dt} \tag{2.6}$$

$$0 = C\frac{dV_{dc}}{dt} + Idc \tag{2.7}$$

*S=0* : the switch is opened Fig 2.12, the inductor current crosses the diode, the capacitor and the load connected to the boost. This leads in transferring the energy accumulated in the inductance during the On-state into the capacitor. The equations that represent this state are :

$$V_{pv} = L\frac{dI_{L_{pv}}}{dt} + V_{dc} \tag{2.8}$$

$$I_{L_{pv}} = C\frac{dV_{dc}}{dt} + Idc \tag{2.9}$$

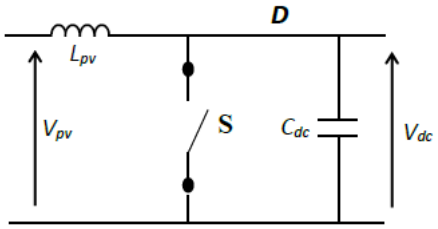


FIGURE 2.12 – Boost converter configuration switch turned OFF

## 2.4 Voltage source inverter

Fig 2.13 illustrates the model of two level voltage source inverter (VSI) which is composed of six IGBT transistors with anti-parallel diodes[76]. The inverter is controlled by the logic values $S_i$, where :

$S_i$= 0, $T_i$ is switched off and $\bar{T}_l$ is switched on.

$S_i$= 1, $T_i$ is switched on and $\bar{T}_l$ is switched off. with : i= a, b, c.

The voltage vector expression of two-level VSI can be given as follows :

$$V = \sqrt{\frac{2}{3}} V_{dc}[S_a + S_b e^{j\frac{2\pi}{3}} + S_c e^{j\frac{4\pi}{3}}] \tag{2.10}$$

Where : $V_{dc}$ is the DC link voltage

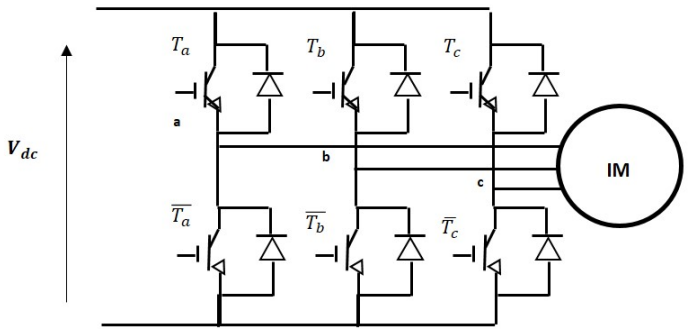


FIGURE 2.13 – Schema of the three-phase inverter

The VSI is composed of six active switching states (V1, V2, V3, V3, V4, V5, V6) and two zero switching states ($V_0$,$V_7$). The switching states are indicated as space

vectors in Fig 2.14.

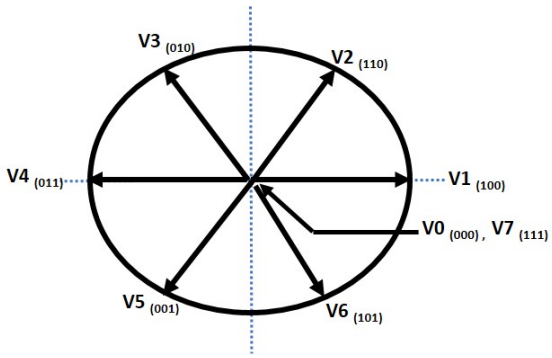


FIGURE 2.14 – Space vector diagram of two-level inverter

## 2.5 Machine model

### 2.5.1 Model of Induction Motor in a (d, q) frame

The dynamic equation's model of the IM which is dedicated for indirect field oriented control can be written in reference frame $d$-$q$ as follows[77][78] : The stator voltage components in $d$-$q$ coordinate system :

$$V_{ds} = R_s i_{ds} + \frac{d}{dt}\phi_{ds} - w_s \phi_{qs} \tag{2.11}$$

$$V_{qs} = R_s i_{qs} + \frac{d}{dt}\phi_{qs} + w_s \phi_{ds} \tag{2.12}$$

The rotor voltage components in $d$-$q$ coordinate system :

$$0 = R_r i_{dr} + \frac{d}{dt}\phi_{dr} - w_{sr} \phi_{qr} \tag{2.13}$$

$$0 = R_r i_{qr} + \frac{d}{dt}\phi_{qr} + w_{sr} \phi_{dr} \tag{2.14}$$

The stator flux components in $d$-$q$ coordinate system :

$$\phi_{ds} = l_s i_{ds} + M i_{dr} \tag{2.15}$$

$$\phi_{qs} = l_s i_{qs} + M i_{qr} \tag{2.16}$$

The rotor flux components in $d$-$q$coordinate system :

$$\phi_{dr} = l_r i_{dr} + M i_{ds} \tag{2.17}$$

$$\phi_{qr} = l_r i_{qr} + M i_{qs} \tag{2.18}$$

The developed electromagnetic torque :

$$T_{em} = \frac{PM}{l_r}(\phi_{dr} i_{qs} - \phi_{qr} i_{ds}) \tag{2.19}$$

### 2.5.2 Model of Induction Motor in $(\alpha,\beta)$ frame

The dynamic equation's model of the IM which is dedicated for direct torque control can be written in reference frame $(\alpha,\beta)$ as follows[7] :

$$\frac{d}{dt}\begin{bmatrix} i_{s\alpha} \\ i_{s\beta} \\ \phi_{s\alpha} \\ \phi_{s\beta} \end{bmatrix} = \begin{bmatrix} -\frac{1}{\sigma}(\frac{1}{\tau_s}+\frac{1}{\tau_r}) & -w_r & \frac{1}{\sigma L_s \tau_r} & \frac{w_r}{\sigma L_s} \\ w_r & -\frac{1}{\sigma}(\frac{1}{\tau_s}+\frac{1}{\tau_r}) & -\frac{w_r}{\sigma L_s} & \frac{1}{\sigma L_s \tau_r} \\ -R_s & 0 & 0 & 0 \\ 0 & -R_s & 0 & 0 \end{bmatrix} . \begin{bmatrix} i_{s\alpha} \\ i_{s\beta} \\ \phi_{s\alpha} \\ \phi_{s\beta} \end{bmatrix} + \begin{bmatrix} \frac{1}{\sigma L_s} & 0 \\ 0 & \frac{1}{\sigma L_s} \\ 1 & 0 \\ 0 & 1 \end{bmatrix} \begin{bmatrix} V_{s\alpha} \\ V_{s\beta} \end{bmatrix} \tag{2.20}$$

The developed electromagnetic torque :

$$T_{em} = \frac{3}{2} P(\phi_{\alpha s} i_{\beta s} - \phi_{\beta s} i_{\alpha s}) \tag{2.21}$$

With : $\sigma = 1 - \frac{M^2}{L_s L_r}$ $\tau_s = \frac{R_s}{L_s}$ $\tau_r = \frac{R_r}{L_r}$ Where : $i_s$, $i_r$ : the stator and rotor currents $\phi_s$, $\phi_r$ : components of the stator and rotor flux $R_s$,$R_r$ : Stator and rotor resistances $L_s$,$L_r$ : Stator and rotor inductances M : Mutual inductance The dynamic model of the induction motor is demonstrated and detailed in Appendix (A.1)

## 2.6 Centrifugal pump

Centrifugal pump is dynamic pump and it's commonly used because it generates more head than other dynamic pumps at a variable speed, simple, low cost, necessitates less torque to start and it's characterized by its low maintenance. The flow head characteristic of a centrifugal pump can be estimated using the model of "Pleider-Peterman" and expressed as follows :

$$H = a_0 w^2 + a_1 w Q + a_2 Q^2 \tag{2.22}$$

Where : Q : Flow rate ($m^3/h$) H : total height (m) $a_0$,$a_1$, $a_2$ : geometric parameters characterizing the pump.

The Q-H characteristic of the pipe network is given by :

$$H = H_g + \psi Q^2 \tag{2.23}$$

Where : $H_g$ : geodetic head $\psi$ : constant which depends on conduit diameter and all frictional losses of pipe network. As shown in eq (2.25), the centrifugal pump load torque $T_p$ is given as :

$$T_p = K_p \Omega^2 \tag{2.24}$$

The centrifugal pumps verify the similarity laws (2-26), from a characteristic curve (P, H, Q) established for a rotation speed N of the impeller pump, the characteristic ($P^{'}$, $H^{'}$, $Q^{'}$) can be obtained for any rotation speed $N^{'}$[72][79].

$$Q^{'} = Q \times (\frac{N^{'}}{N}); \;\; H^{'} = H \times (\frac{N^{'}}{N})^2; \;\; P^{'} = P \times (\frac{N^{'}}{N})^3 \tag{2.25}$$

# Conclusion

This chapter presents the modeling of the PV water pumping system components which are the PV panel, the boost converter, the voltage source inverter (VSI), the induction motor and the centrifugal pump. Moreover, the missing parameters of the PV panel are determined using the tool provided by Mathworks. Hence by using these parameters, a PV panel modeled on Matlab/Simulink. Moreover, the impact of the shunt and series resistances, diode saturation current, solar irradiation and temperature on the output of the PV panel is investigated.

# Chapter 3

# Optimization and control of water pumping PV systems using fuzzy logic controller

## 3.1 Introduction

The induction motor is the principal element of the pumping systems[5]. DC motors were used for speed controls because of their simple design in controlling flux and torque[80]. However, DC motors need regular maintenance[7]. To surmount this weakness, Brushless permanent-magnet motors have been proposed[8]. But, these engines are limited for low-power PV systems[21]. Then, PV pumping systems based on AC motors have been used because they are more efficient, maintenance-free and low cost[9][81]. However, the flux, torque and speed controls of these induction motors are complex due to its nonlinear model[7]. Field oriented control (FOC) is the most used technique to drive the IM [82], it consists of two control techniques : indirect FOC (IFOC)[83][84] and direct FOC (DFOC)[7][85]. The reason behind using this type of control is to obtain torque and flux decoupling even with their complex mathematical equations for IM. These methods have been used by numerous researchers in several studies because of the high performance of controller in IM drives[84][86]. However, the FOC technique is complex and the system performances are influenced by external load disturbances, uncertainties and parameter variations[87][88][89][90].To surmount these drawbacks, a new control method which

is Direct Torque Control (DTC) was proposed[7]. Several studies showed that DTC presents some advantages compared to FOC[85]. However, DTC has major drawbacks which are high ripples of the flux and electromagnetic torque and variable switching frequency due to the use of hysteresis controllers[91]. These disadvantages produce undesirable acoustic noise and mechanical vibrations which lead to a deterioration of the machine performances and generate high current distortion which degrades the quality of the output power. Researchers proposed several solutions to improve DTC. D. Mohan et al and D.isalm et al used multilevel inverters, this method reduces the ripples, but the switching losses and the cost are increased due to the high number of power devices[92][93]. In Refs [94][95], the authors propose space vector modulation (SMW), however, this technique needs accurate design of torque and flux controllers. DTC is also improved by sliding mode control as given in [96], but the chattering phenomenon appeared which presents the main problem of this method. In the recent years, the use of artificial intelligent techniques like neural network-based DTC have been used by many researchers to improve the controller performances. This technique provides high performance, but it requires the training process which retards the performance of the controller [97]. Fuzzy logic controller is an intelligent control strategy which is characterized by its logical resemblance to a human operator[98]. The structure of FLC is adjusted based on the components of its internal configuration like Fuzzy rules, fuzzification and defuzzification blocks. The main advantages of Fuzzy logic controller are adapted to the nonlinear control command and not based on the model of the induction machine[99]. It has very effective techniques for complicated and imprecise processes where there does not exist any mathematical model. These features make the FLC not only easy to use, but also easy to design[100]. Many authors introduced FLC for doubly fed induction machine (DFIM), doubly fed induction generator (GFIM) and permanent magnet synchronous motor (PMSM)[101][102]. In fact, the use of FLC results in reducing torque and flux ripples. However, to the author's best knowledge, the previous stu-

dies about photovoltaic water pumping systems do not use fuzzy logic controllers to control the induction motor (IM). For this, an improved DTC of IM based water pumping system using FLC is proposed. The proposed method consists of substituting the hysteresis controllers and the look-up table by fuzzy logic switching vector selection scheme. To show the performance of the proposed method, a comparative study between the proposed method and the conventional DTC is presented under different operating conditions. Simulation results demonstrate the superiority of the proposed method in terms of daily cumulative water, power and the overall efficiency. Moreover, the quality of current signals is improved with a THD around 3.06 %. To ensure the maximum power point whatever the climatically conditions, variable step size P&O are used to track maximum power of photovoltaic pumping system.

## 3.2 Direct torque control of induction motor

The direct Torque Control (DTC) strategy was introduced by Takahashi in 1984 and proposed by Depenbrock in 1985 for the control applications of induction motors. This type of control is characterized by its fast dynamic response, simple implementation and robustness to the rotor parameter variation without the need for a complex field orientation block and inner current regulation loop. The basic principle in DTC for induction motors is to directly select stator voltage vectors, which makes the flux rotate and produce the desired torque.

### 3.2.1 Control of stator flux and electromagnetic torque

#### 3.2.1.1 Control of stator flux

The stator flux is determined in the reference frame $(\alpha, \beta)$ as follows :

$$\bar{V_s} = R_s \bar{i_s} + \frac{d\bar{\phi_s}}{dx} \tag{3.1}$$

And

$$\bar{\phi_s} = \bar{\phi_{s0}} + \int_0^t (\bar{V_s} - R_s\bar{i_s})dt \tag{3.2}$$

For high speeds, the voltage drop due to the stator resistance can be neglected. Therefore, the eq (3.2) can be expressed as follows :

$$\bar{\phi_s} \approx \bar{\phi_{s0}} + \int_0^t \bar{V_s}dt \tag{3.3}$$

During the sampling time period $T_Z$ , the voltage vector applied to IM remains constant.

$$\bar{\phi_s}(K+1) \approx \bar{\phi_s}(K) + \bar{V_s}(K)T_z \tag{3.4}$$

From eq (3.4), it is clear that the variation of stator voltage vector is proportional to the stator flux vector. The voltage vector imposes the direction of the stator flux vector's extremity and making a circular trajectory Fig 3.1. The flux regulation can

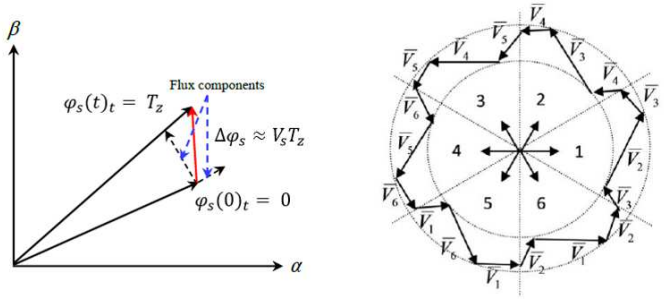


FIGURE 3.1 – Evolution of stator flux vector in the complex plan

be realized using two-level hysteresis comparator which allows to maintain the stator flux vector extremity in a circular trajectory as shown in Fig 3.2[103].
The logical outputs of the flux controller are expressed as :

$$\begin{aligned} S_{\phi_s} &= 1 \;\; if \;\; \Delta\phi_s > h_{\phi_s} \\ S_{\phi_s} &= 0 \;\; if \;\; \Delta\phi_s \leq -h_{\phi_s} \end{aligned} \tag{3.5}$$

$h_{\phi_s}$ is hysteresis band of stator flux.

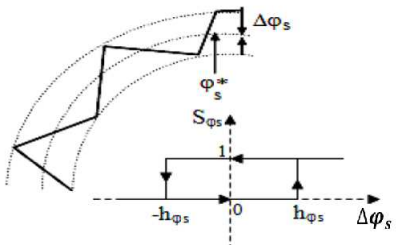


FIGURE 3.2 – Two-level hysteresis comparator for stator flux control

The stator flux error is calculated by subtracting the reference value of flux from its actual estimated value :

$$\Delta\phi_s = |\phi_s^*| - |\phi_s| \tag{3.6}$$

#### 3.2.1.2 Control of electromagnetic torque

The electromagnetic torque is determined from the stator and rotor flux as follows :

$$T_{em} = p\frac{M}{\sigma L_s L_r}\phi_s\phi_r \tag{3.7}$$

$$|T_{em}| = p\frac{M}{\sigma L_s L_r}|\phi_s||\phi_r|sin(\varepsilon) \tag{3.8}$$

Equation (3.8) means that the electromagnetic torque is controlled by the stator and rotor flux amplitudes. If those parameters remain unchanged, the torque can be controlled by means of the angle $\varepsilon$.

A three-level hysteresis comparator is used for torque regulation to control the motor in both rotation senses (Fig 3.3). The two-level comparator can be also used but it allows to operate in one rotation sense[103].

The logical outputs of the torque controller are expressed as :

$$\begin{aligned} S_{T_{em}} &= 1 \qquad\quad \Delta T_{em} > h_{T_{em}} \\ S_{T_{em}} &= 0 \quad if \quad -h_{T_{em}} \leq \Delta T_{em} \leq h_{T_{em}} \\ S_{T_{em}} &= 1 \qquad\quad \Delta T_{em} < -h_{T_{em}} \end{aligned} \tag{3.9}$$

$h_{Tem}$ is hysteresis band of torque.

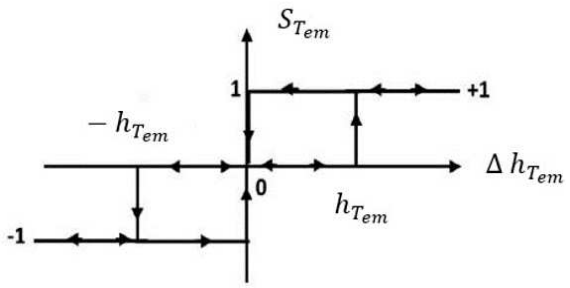


FIGURE 3.3 – Three level hysteresis comparator for electromagnetic torque control

The torque error is calculated by subtracting the reference value of torque from its actual estimated value :

$$\Delta T_{em} = |T^*_{em}| - |Tem| \tag{3.10}$$

### 3.2.2 Estimation of stator flux and electromagnetic torque

This technique needs to determine several parameters in order to estimate the electromagnetic torque and the stator flux[104]. The components of the stator voltage $(V_{s\alpha}, V_{s\beta})$ are calculated using Concordia transformation on the output voltage of the three-phase voltage source inverter :

$$\begin{bmatrix} V_{s\alpha} \\ V_{s\beta} \end{bmatrix} = \begin{bmatrix} 1 & -\frac{1}{2} & -\frac{1}{2} \\ 0 & \frac{\sqrt{3}}{2} & -\frac{\sqrt{3}}{2} \end{bmatrix} \begin{bmatrix} V_{sa} \\ V_{sb} \\ V_{sc} \end{bmatrix} \tag{3.11}$$

The input stator voltages of the induction motor which are the output voltages of voltage source inverter are expressed by :

$$\begin{aligned} V_{sa} &= \tfrac{V_{dc}}{3}(2S_a - S_b - S_c) \\ V_{sb} &= \tfrac{V_{dc}}{3}(2S_b - S_c - S_a) \\ V_{sc} &= \tfrac{V_{dc}}{3}(2S_c - S_a - S_b) \end{aligned} \tag{3.12}$$

The components of the stator current $(i_{s\alpha}, i_{s\beta})$ can be calculated by applying Concordia transformation on the measured current :

$$i_{s\alpha} = \sqrt{\frac{2}{3}} i_{sa} \tag{3.13}$$

$$i_{s\beta} = \frac{1}{\sqrt{2}}(i_{sb} + 2i_{sc}) \tag{3.14}$$

#### 3.2.2.1 Estimation of stator flux

From the stator voltages and currents of the induction motor, the stator flux components can be determined as follows[105] :

$$\begin{aligned} \hat{\phi_{s\alpha}} &= \int_0^t (v_{s\alpha} - R_s.i_{s\alpha})dt \\ \hat{\phi_{s\beta}} &= \int_0^t (v_{s\beta} - R_s.i_{s\beta})dt \end{aligned} \tag{3.15}$$

The stator flux magnitude and flux angle are donated as :

$$\hat{\phi_s} = \sqrt{\hat{\phi_{s\alpha}^2} + \hat{\phi_{s\beta}^2}} \tag{3.16}$$

$$\theta_s = \arctan \frac{\hat{\phi_{s\beta}}}{\hat{\phi_{s\alpha}}} \tag{3.17}$$

#### 3.2.2.2 Estimation of electromagnetic torque

The electromagnetic torque can be determined using current components, pair-pole number and flux components of the induction machine :

$$T_{em} = p.(\hat{\phi_{s\alpha}}.i_{s\beta} - \hat{\phi_{s\beta}}.i_{s\alpha}) \tag{3.18}$$

### 3.2.3 Switching table construction

#### 3.2.3.1 Six sector switching table

The stator flux ($\phi_s^*$) and torque references ($T_{em}^*$) are compared with the corresponding estimated values. The torque error is the input of a three-level hysteresis comparator (Fig 3.3), where the error stator flux magnitude is the input of a two-level hysteresis comparator (Fig 3.2). The stator flux space is composed of six sectors of 60° each (Fig 3.4). The outputs of the flux hysteresis, torque hysteresis and flux sector are used to select the switching vector of voltage source inverter (VSI)[106].

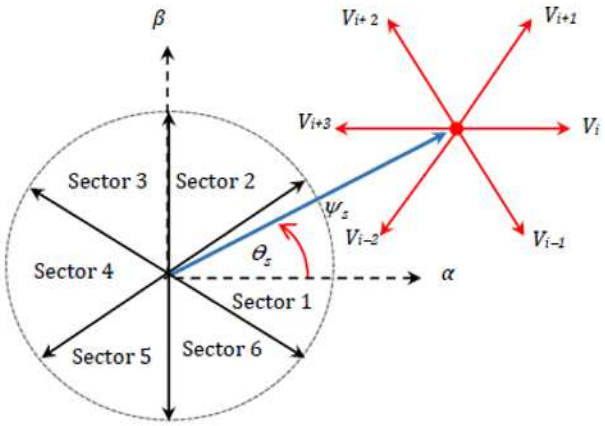


FIGURE 3.4 – Partition of the complex plan in six angular sectors

When the stator flux vector is situated in the sector i , we obtain :

- If $V_{i+1}$is selected, the flux increases and the torque increases ;
- If $V_{i-1}$is selected, the flux increases and the torque decreases ;
- If $V_{i+2}$is selected, the flux decreases and the torque increases ;
- If $V_{i-2}$is selected, the flux decreases and the torque decreases ;

Whereas, the vector $V_0$ or $V_7$ decrease the torque, keep the amplitude of flux unvaried and stop the rotation of flux. Switching table allows to determine the VSI switching vector as illustrated in table 3.1. The VSI is composed of six active switching states and two zero switching states.

| $E_\phi$ | $E_{T_{em}}$ | S1 | S2 | S3 | S4 | S5 | S6 |
|---|---|---|---|---|---|---|---|
| | 1 | V2 | V3 | V4 | V5 | V6 | V1 |
| 1 | 0 | V7 | V0 | V7 | V0 | V7 | V0 |
| | -1 | V6 | V1 | V2 | V3 | V4 | V5 |
| | 1 | V3 | V4 | V5 | V6 | V1 | V2 |
| 0 | 0 | V0 | V7 | V0 | V7 | V0 | V7 |
| | -1 | V5 | V6 | V1 | V2 | V3 | V4 |

TABLE 3.1 – Switching Table

| $E_\phi$ | $E_{T_{em}}$ | S1 | S2 | S3 | S4 | S5 | S6 | S7 | S8 | S9 | S10 | S11 | S12 |
|---|---|---|---|---|---|---|---|---|---|---|---|---|---|
| | 2 | V2 | V3 | V3 | V4 | V4 | V5 | V5 | V6 | V6 | V1 | V1 | V2 |
| | 1 | V2 | V2 | V3 | V3 | V4 | V4 | V5 | V5 | V6 | V6 | V1 | V1 |
| 1 | -1 | V1 | V1 | V2 | V2 | V3 | V3 | V4 | V4 | V5 | V5 | V6 | V6 |
| | -2 | V6 | V1 | V1 | V2 | V2 | V3 | V3 | V4 | V4 | V5 | V5 | V6 |
| | 2 | V3 | V4 | V4 | V5 | V5 | V6 | V6 | V1 | V1 | V2 | V2 | V3 |
| 0 | 1 | V4 | V4 | V5 | V5 | V6 | V6 | V1 | V1 | V2 | V2 | V3 | V3 |
| | -1 | V5 | V5 | V6 | V6 | V1 | V1 | V1 | V2 | V2 | V3 | V4 | V4 |
| | -2 | V5 | V6 | V6 | V1 | V1 | V2 | V2 | V3 | V3 | V4 | V4 | V5 |

TABLE 3.2 – Look up switching table with twelve sectors

V1, V2, V3, V4, V5, V6 represent the six active vectors produced by a voltage source inverter (VSI). V0 and V7 are the two zero voltage.

#### 3.2.3.2 Twelve sectors switching table

In the conventional DTC, the stator flux space is composed of six sectors. For each sector, we find two switching states are not considered. This causes an ambiguity in torque command. Hence, the decomposition of the sector will be changed which gives a new switching table. It consists of taking the first sector from (0 to $\frac{\pi}{3}$) instead of ($\frac{11\pi}{6}$ *to* $\frac{\pi}{6}$). In the same way, each sector contains two unused vectors which causes an ambiguity in flux[107]. To solve this problem, the stator flux space will be divided into twelve sectors instead of six sectors. Therefore, six switching states per sector will be utilized. Then, a twelve-sectors look-up table is presented in 3.2. Based on studies in literature, the augmentation of the number of sectors provides a slight

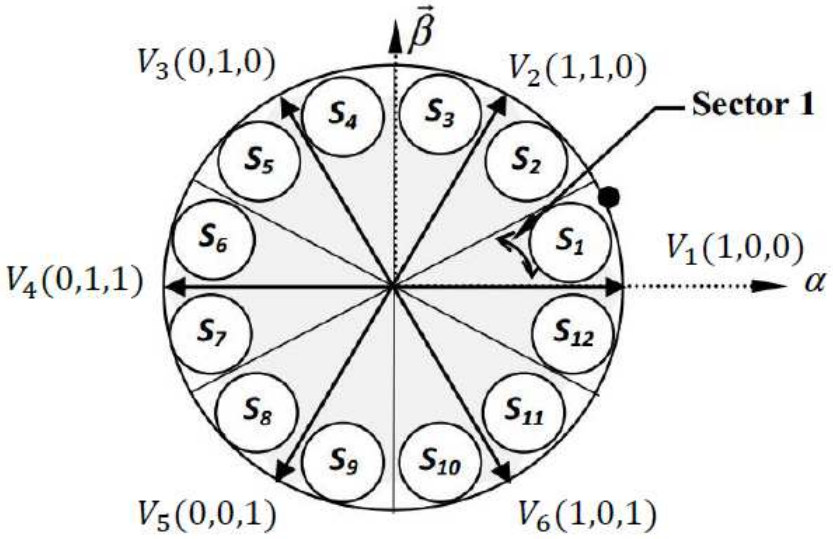


FIGURE 3.5 – Voltage space vector in 12 sectors cases

effect on minimizing the current harmonics and high ripples. Moreover, DTC based on twelve sectors gives good dynamic in low and high speed.

### 3.2.4 Global scheme of conventional direct torque control

The global control scheme of conventional direct torque control technique is presented in Fig 3.6 and composed of :

- Decoupled flux and torque hysteresis controllers
- An association of VSI-Induction motor
- Speed regulation loop using PI controller
- Look-up switching table
- Flux/torque estimators with position/sector determination
- Voltage and current calculation blocks with $\frac{3}{2}$ (Concordia) transformation

## 3.3 Fuzzy logic control

Fuzzy logic is an approach of artificial intelligence which aims the reasoning algorithms utilized in applications where process data cannot be represented in binary

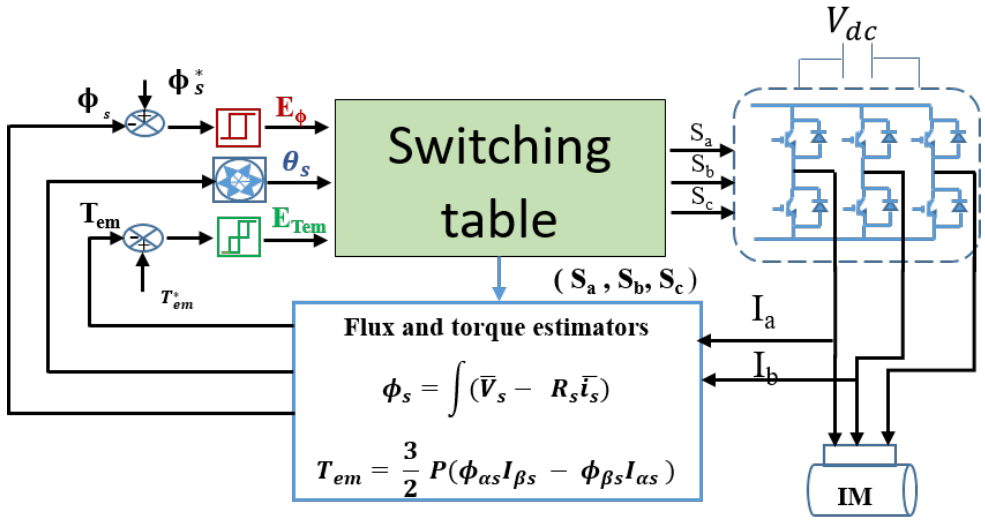


FIGURE 3.6 – Global control scheme of basic direct torque control

form in order to emulate the decision making in machines and human thinking. Fuzzy logic examines vague declarations as these so that they make logical impression.Fuzzy logic control deals with the relative importance of precision. Among of the reasons for using fuzzy logic controller is its logical similarity to a human operator which consists of functioning based on foundations of a knowledge base which in turn rely upon the various if then rules, resembling a human operator. Fuzzy logic controller is characterized by its simplicity because it requires no complex mathematical knowledge. Moreover, it' s easy to design because it requires just a qualitative knowledge of the system The use of fuzzy logic is beneficial for :

- Complex system which its modeling is impossible or difficult
- System commanded by human expert
- System composed of continuous and complex outputs and inputs
- System based on human observation as the basis for rules or inputs.

### 3.3.1 Components of FLC

The inputs of the fuzzy logic controller are defined using the linguistic variables which in turn are determined based on the membership functions. The membership functions defined while respecting that they cover the whole of the universe of discourse. The adjacent fuzzy sets overlap each other in order to avoid any discontinuity with respect to minor variations in the inputs. The three essential parts in Fuzzy Logic Controller are[100][108] :

- Fuzzifier or Fuzzification
- Inference System.
- Defuzzufier or Defuzzification

#### 3.3.1.1 Fuzzification

In this step, the appropriate inputs of the fuzzy logic controller must be chosen. These input variables represent the dynamical system completely. The linguistic variables are used instead of numerical variables for processing information. However, the inputs of the fuzzy logic controller are represented in the form of numerical variables (or other words). Hence, they must be converted into linguistic variables. The operation of converting the crisp sets into fuzzy sets is effectuated by the fuzzifier. The fuzzification process consists of determining the membership functions for the inputs which should cover the whole universe of discourse and each one illustrates a linguistic variable or a fuzzy set. The crisp inputs are converted into fuzzy sets. The membership functions can be Triangular, Trapezoidal Bell, Generalized Bell or Sigmoidal. Moreover, a hybrid of the above Membership Functions can be also used.

#### 3.3.1.2 Inference System

- **Rule Base :**

  It composed of a number of If-Them rules in which the "IF" is named the

antecedent while the "THEN" is named the consequence. The developed rules are identical to the human thought process. Moreover, the computer utilizes the linguistic variables obtained after fuzzification to execute the rules. The programming of the FLC becomes simple because the rules are simple to understand and write.

- **Database :**

  It composed of the all determined membership functions that are to be utilized by the rules .

- **Reasoning Mechanism :**

  It effectuates the inference process on the data and the rules provided to ensure a reasonable output. The all knowledge and the rules are processed by the code of the software based on a particular situation. it employs a human brain type of attribute to methodically perform the inference process for treating the information.

#### 3.3.1.3 Defuzzification

This operation is the opposite function of fuzzifier step which consists of converts the fuzzy variables to crisp sets. This step is important because in the real world, the crisp values can only be considered as inputs to the other systems. The fuzzy sets are similar to the human thought process, their functionality is restricted only to the above processes. Generally, a defuzzufier is needed just when the Mamdani fuzzy model is employed for designing a controller. Mandani model follows the Compositional Rule of Inference which makes it preferable. Contrary to Mamdani model, the outputs are determined using a specific function for the other two models (first order polynomial in the input variables) and therefore, the output is crisp. The fuzzy model must be able to the fuzziness from inputs to outputs in a suitable manner. Hence, the designing of the Fuzzy Logic Controller (based on Mamdani Fuzzy Model) necessitates :

- The selection of suitable inputs and their fuzzification.
- The description of the output membership functions and input
- The determination of the Fuzzy Rule Base.
- The defuzzification of the output achieved after the processing of the linguistic variables using a proper defuzzification technique.

### 3.3.2 Advantages of Fuzzy Logic for System Control

→ Fewer values, rules, and decisions are required [109].

→ More observed variables can be evaluated.

→ Linguistic, not numerical, variables are used, making it similar to the way human think.

→ It relates output to input, without having to understand all the variables, permitting the design of a system that may be more accurate and stable than one with a conventional control system.

→ Simplicity allows the solution of previously unsolved problems.

→ Rapid prototyping is possible because a system designer doesn't have to know everything about the system before starting work.

→ They're cheaper to make than conventional systems because they're easier to design.

→ They have increased robustness.

→ They simplify knowledge acquisition and representation.

→ A few rules encompass great complexity.

## 3.4 DTC base on Fuzzy logic controller

In this section, a fuzzy approach is proposed to improve the DTC (Fig 3.13), the fuzzy logic controller is used to determine the desired inverter vector state. Fig 3.11

shows the proposed diagram of the fuzzy logic DTC of induction motor. The FLC is composed of tree inputs which are torque error, the stator error, the stator flux angle and one output. An FLC generally consists of four principal steps :

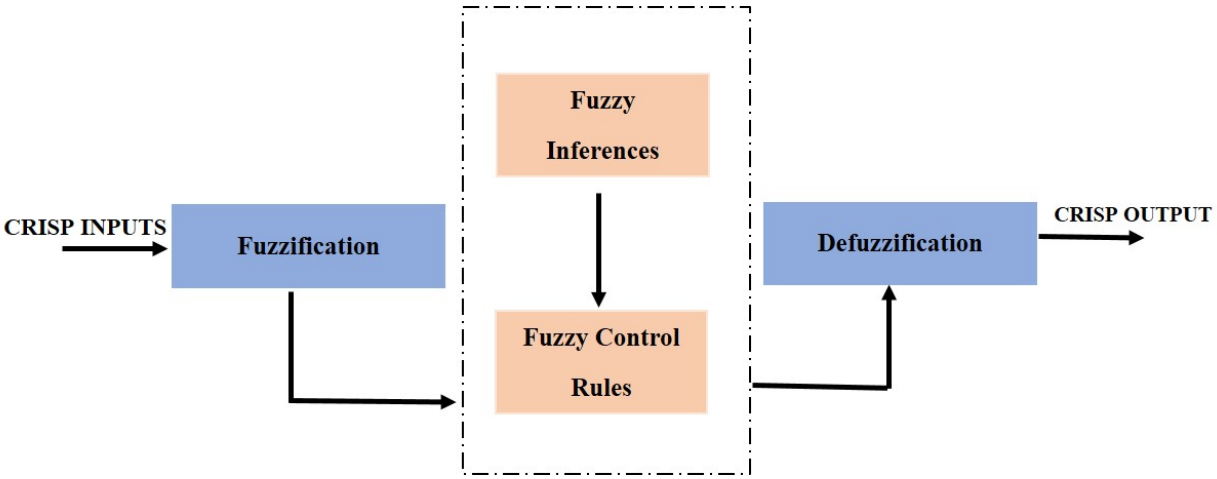


FIGURE 3.7 – Block diagram of Fuzzy controller

- A fuzzifier :

  The analog inputs are converted into fuzzy variables which are produced by using membership functions (MF), the fuzzy system performance is described using a fuzzy rule base that stores fuzzy rules. An approximative reasoning will be done by associating input variable with fuzzy rules using a fuzzy inference engine. During the defuzzification step, the FLC output is converted to a crisp value for the actual system input. The shape of the membership function, the fuzzy reasoning rules and the defuzzification method influence the response of the FLC. In order to make the stator flux variations medium, the stator flux error is composed of three linguistic variables : negative (N), zero (Z) and positive (P). The (N) and (P) variables are represented by two symmetric trapezoidal membership functions and Z by an equidistant isosceles triangular (Fig 3.8). To make the torque error variations smaller, the torque error is divided into five linguistic variables : negative large (NL) negative small (NS) zero (Z) positive small (PS) and positive large (PL). The torque error mem-

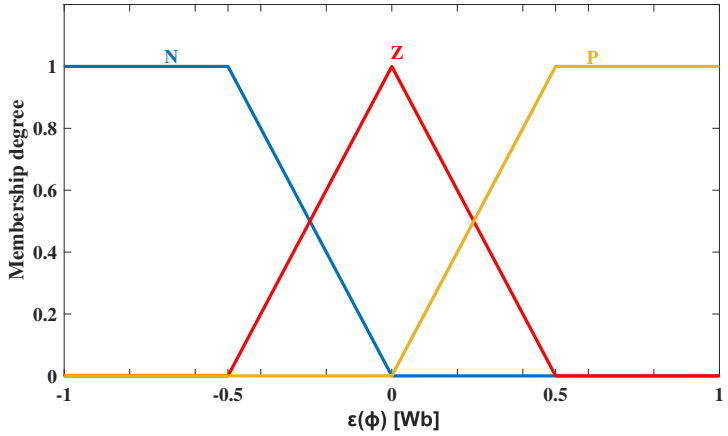


FIGURE 3.8 – The fuzzy membership functions of $\varepsilon_\phi$

bership function is represented by three equidistant isosceles triangular and two symmetric trapezoidal (Fig 3.9). The stator flux angle is divided into six

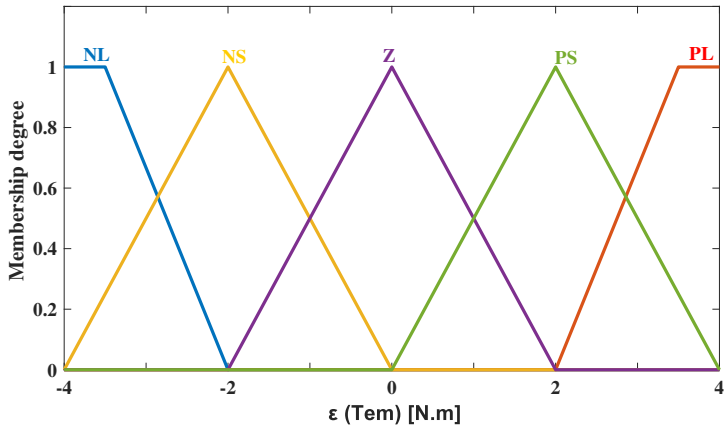


FIGURE 3.9 – The fuzzy membership functions of $\varepsilon$ $T_{em}$

sectors, for more precision, the universe of discourse is divided into 12 fuzzy sets. The stator flux angle membership function is represented by twelve equidistant isosceles triangular of 60° wide and an overlap of 30°with neighborhood fuzzy sets which each fuzzy set works for an angle of 30°(Fig 3.10(a)).

The Fig 3.10(b) shows the output variable of the fuzzy controller which is composed of seven switching states (one zero switching state and six active switching states).

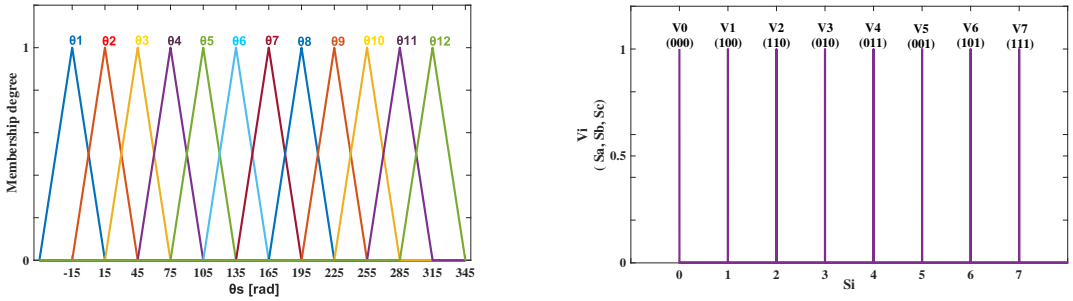


(a) (b)

FIGURE 3.10 – (a)The fuzzy membership functions of $\theta_s$ (b) The fuzzy membership functions of the output

- Fuzzy control rules :

  The optimal switching state is given by fuzzy rules. The fuzzy rules are established using expert knowledge and intuition in order to govern the behavior of the fuzzy controller. Stator flux angle, torque error and flux error : these elements are based on the choice of the sector of stator flux. In order to obtain the desired references values of the flux and the motor torque, the right switching state has to be chosen. Table 3.3 shows the fuzzy rule base with 180 rules which can be obtained from membership functions for three inputs (3×5×12).

- Fuzzy inferences :

  In this work, the inference method is developed using Mamdani's procedure based on min-max decision[110]. μAi(e$\phi$), μBi(eT)and μCi($\theta$) represent the membership values of torque error, flux error and stator flux angle. $\alpha_i$ is the weighting factor for ith rule and it's can be written as Eq (3.19) :

$$\alpha_i = min(\mu A_i(e\phi), \mu B_i(eT), \mu C_i(theta)) \tag{3.19}$$

$$\mu' V_i(V) = max(\alpha_i, \mu V_i(V)) \tag{3.20}$$

- Deffuzifier :

| $\theta_s$ | | Θ1 | Θ2 | Θ3 | Θ4 | Θ5 | Θ6 | Θ7 | Θ8 | Θ9 | Θ10 | Θ11 | Θ12 |
|---|---|---|---|---|---|---|---|---|---|---|---|---|---|
| $\varepsilon_\phi$ | $\varepsilon_{T_{em}}$ | | | | | | | | | | | | |
| | PL | V2 | V3 | V3 | V4 | V4 | V5 | V5 | V6 | V6 | V1 | V1 | V2 |
| | PS | V2 | V2 | V3 | V3 | V4 | V4 | V5 | V5 | V6 | V6 | V1 | V1 |
| P | Z | V0 | V7 | V7 | V0 | V0 | V7 | V7 | V0 | V0 | V7 | V7 | V0 |
| | NS | V1 | V1 | V2 | V2 | V3 | V3 | V4 | V4 | V5 | V5 | V6 | V6 |
| | NL | V6 | V1 | V1 | V2 | V2 | V3 | V3 | V4 | V4 | V5 | V5 | V6 |
| | PL | V2 | V3 | V3 | V4 | V4 | V5 | V5 | V6 | V6 | V1 | V1 | V2 |
| | PS | V2 | V3 | V3 | V4 | V4 | V5 | V5 | V6 | V6 | V1 | V1 | V2 |
| Z | Z | V7 | V0 | V0 | V7 | V7 | V0 | V0 | V7 | V7 | V0 | V0 | V7 |
| | NS | V7 | V0 | V0 | V7 | V7 | V0 | V0 | V7 | V7 | V0 | V0 | V7 |
| | NL | V6 | V1 | V1 | V2 | V2 | V3 | V3 | V4 | V4 | V5 | V5 | V6 |
| | PL | V3 | V4 | V4 | V5 | V5 | V6 | V6 | V1 | V1 | V2 | V2 | V3 |
| | PS | V4 | V4 | V5 | V5 | V6 | V6 | V1 | V1 | V2 | V2 | V3 | V3 |
| N | Z | V7 | V7 | V0 | V0 | V7 | V7 | V0 | V0 | V7 | V7 | V0 | V0 |
| | NS | V5 | V5 | V6 | V6 | V1 | V1 | V2 | V2 | V3 | V3 | V4 | V4 |
| | NL | V5 | V6 | V6 | V1 | V1 | V2 | V2 | V2 | V3 | V4 | V4 | V5 |

TABLE 3.3 – Voltage vector fuzzy control table

This operation converts the fuzzy values back into a numerical value at the output, which are one zero voltage (V0 or V7) and six non-zero voltage vectors (Fig 3.10(b)). For this step, the max method is used and expressed by the Eq (3.21). By this method, the value of fuzzy output which has the maximum possibility distribution is used as control output.

$$\mu' V_{out}(V) = max_{i=1}^{180} max(\mu' V_i(V)) \tag{3.21}$$

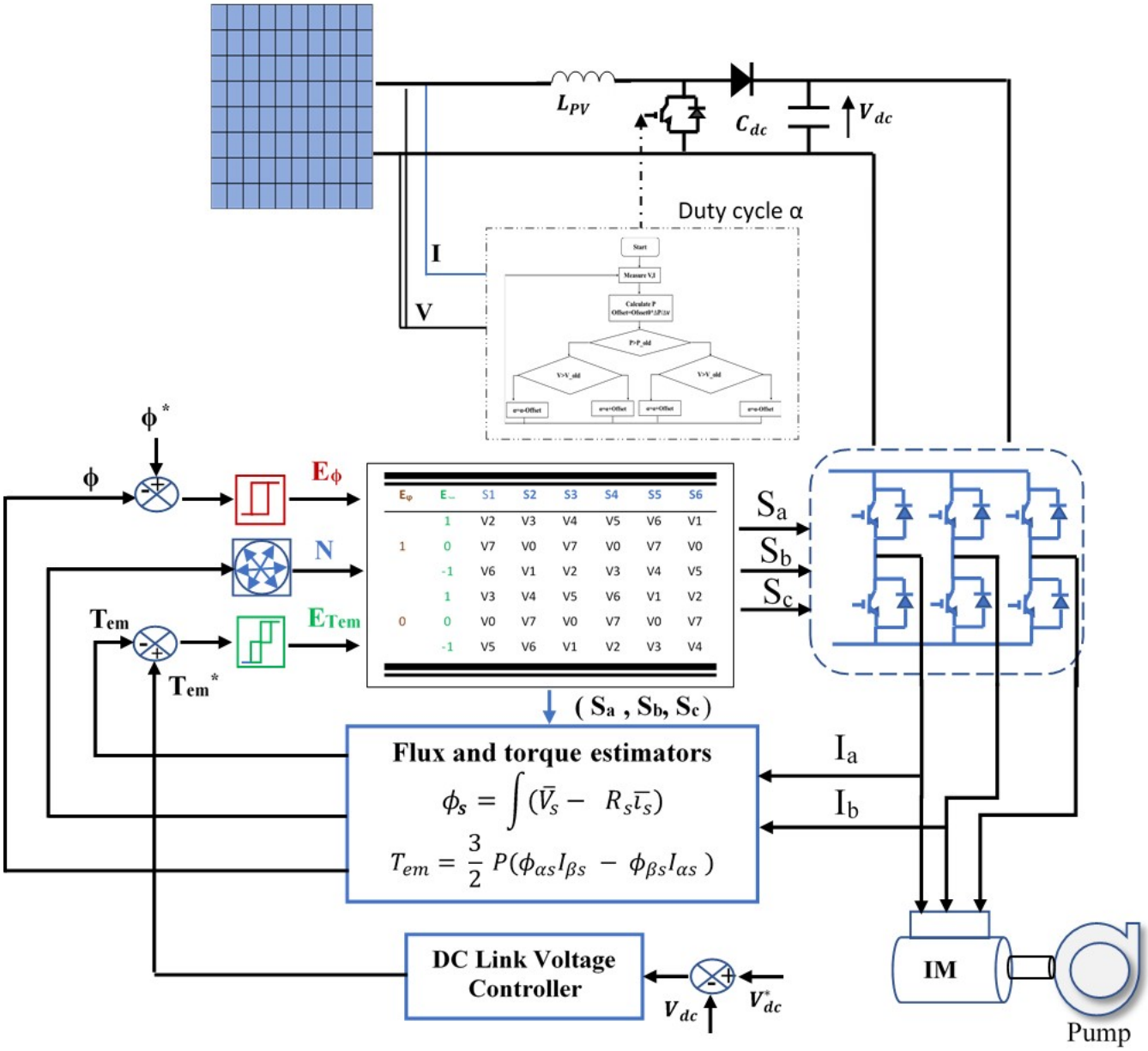


FIGURE 3.11 – Photovoltaic water pumping system based on Conventional DTC

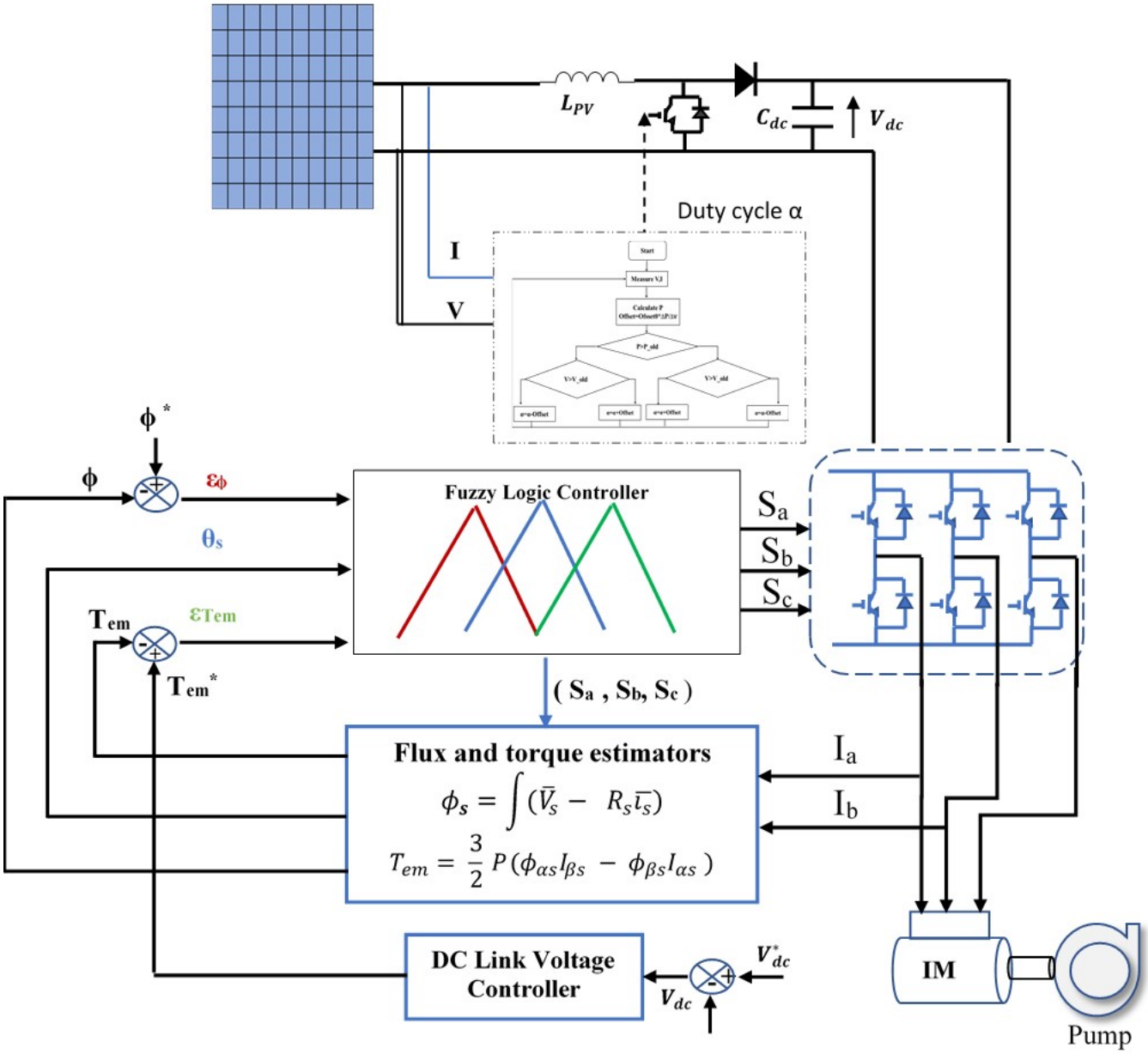


FIGURE 3.12 – Photovoltaic water pumping system based on FLC - DTC

## 3.5 Simulation Results

In this proposed system, a 1880 W is extracted from CSUN 235-60P modules (table 2.2) in order to feed the centrifugal pump. The extracted power is higher than the motor rating because some losses are existing into the PV system. For this, our pumping system is composed of 8 modules which must be connected in series. The sizing of the photovoltaic system components is summarized in table 3.4. The parameters of the IM are shown in appendices (A.2).

| Component | Expression | Used value |
|---|---|---|
| $V_{dc}^{*}$ | $V_{dc} = \frac{2\sqrt{2}}{\sqrt{3}} V_{LL}$ | 400V |
| $C_{dc}$ | $C_{dc} = \frac{6aV_{LL}I_t}{{V_{dc}^{*}}^2 - {V_{dc1}}^2}$ | $2000\mu F$ |
| $\alpha$ | $\alpha = \frac{V_{dc} - V_{mp}}{V_{dc}}$ | 0.26 |
| $L_{pv}$ | $L_{pv} = \frac{\alpha V_{mp}}{\Delta I f_s}$ | 3 mH |

TABLE 3.4 – Design of parameters of the system

With the aim of testing and evaluating the effectiveness of the proposed control strategy, a simulation test is carried out in *MATLAB/SIMULINK* environment. Using the real data of solar radiation from (Fes, Maroc) for three different months where the climatics conditions are differents : Warm month (Summer), Mild month (Spring), Cold month (Winter).

Figs 3.13 (a),(b), 3.14(a) ,(b) and 3.15(a),(b) show the evolution of the solar radiance and the PV power corresponding to Warm month (June 2016), mild month (Mars 2016), Cold month (December 2016). Figs 3.13(c) 3.14 (c) and 3.15(c) show the characteristics of electric speed using the conventional and the suggested method. The simulation results show that in rapid changing in atmospheric conditions, the proposed method shows better response as compared to the conventional one in terms of tracking speed.

Figs 3.13(d),3.14(d) and 3.15(d) illustrate the pumped water volume obtained

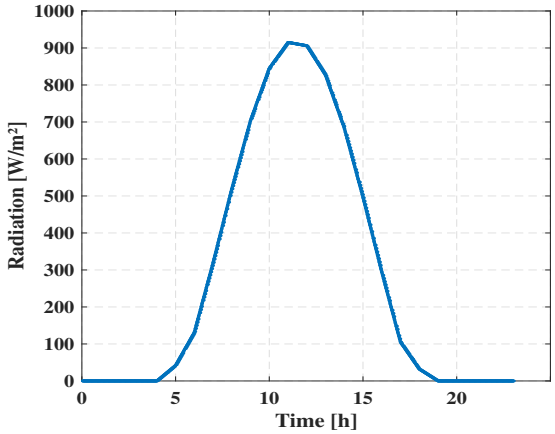


(a) Irradiation profile in June at Fez,Morroco

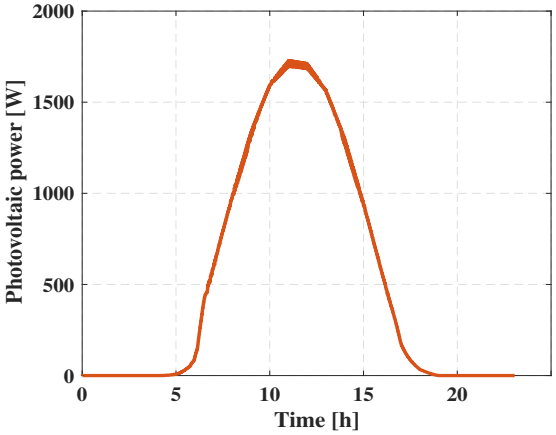


(b) Photovoltaic power

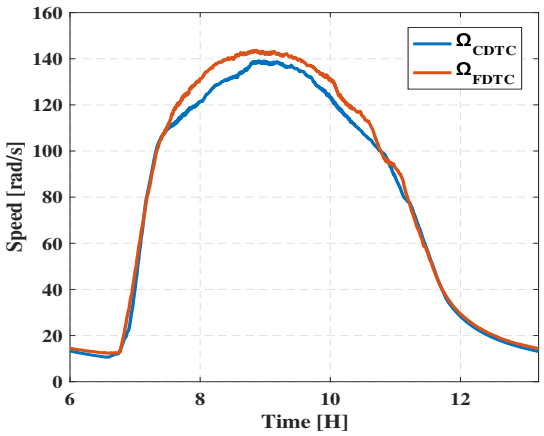


(c) Electric speed

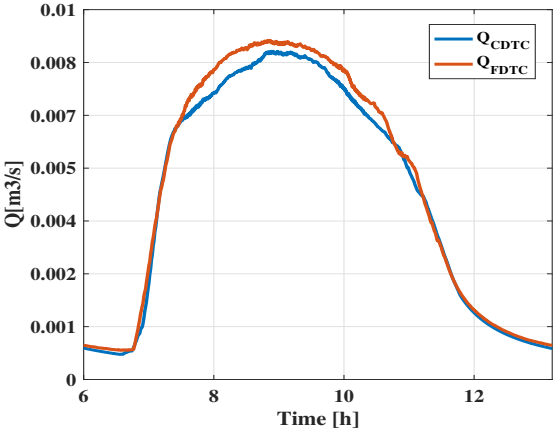


(d) Water Flow

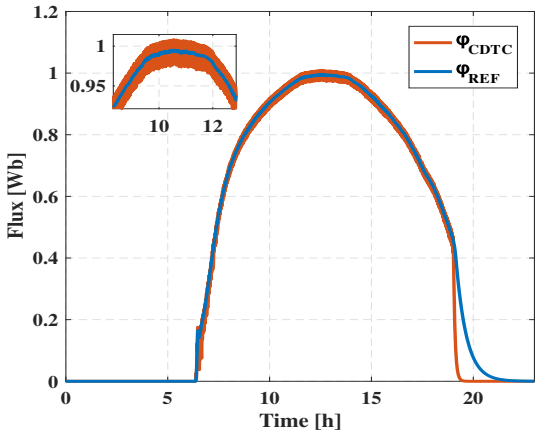


(e) Stator flux responses using CDTC

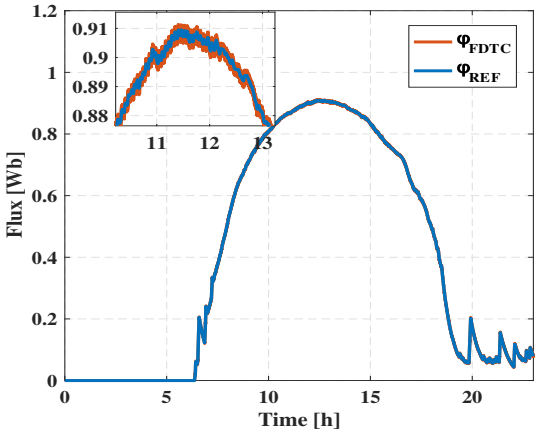


(f) Stator flux responses using FDTC

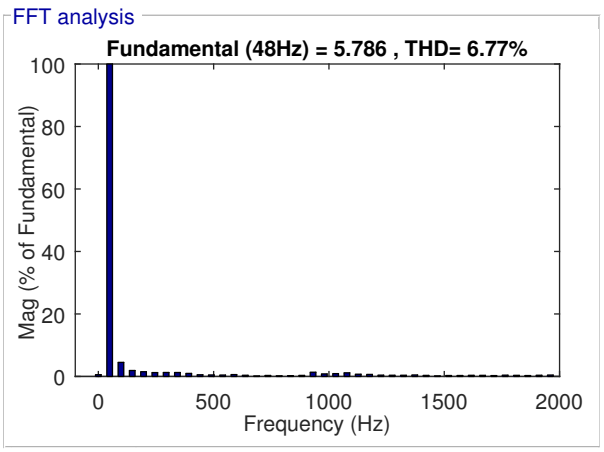


(g) FFT analysis of stator current using CDTC

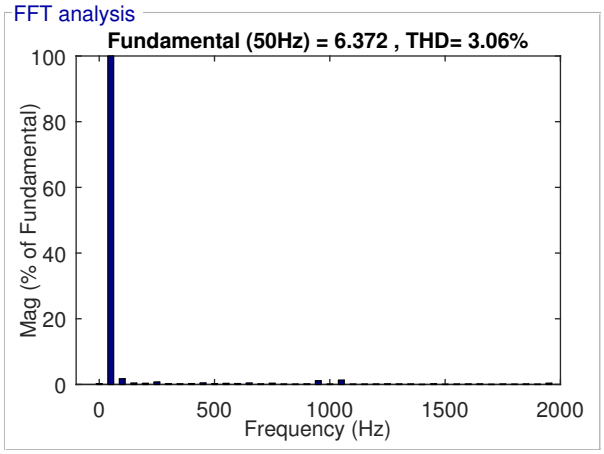


(h) FFT analysis of stator current using FDTC

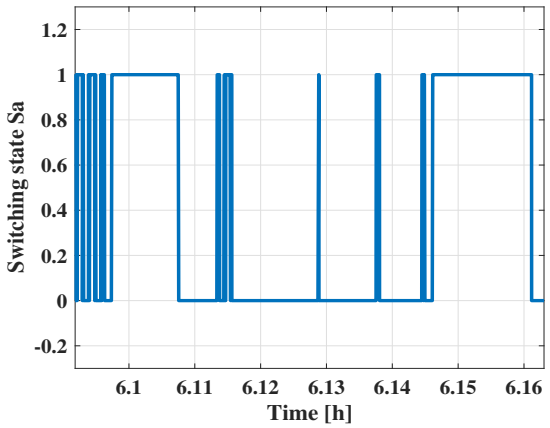


(i) Inverter switching state for CDTC

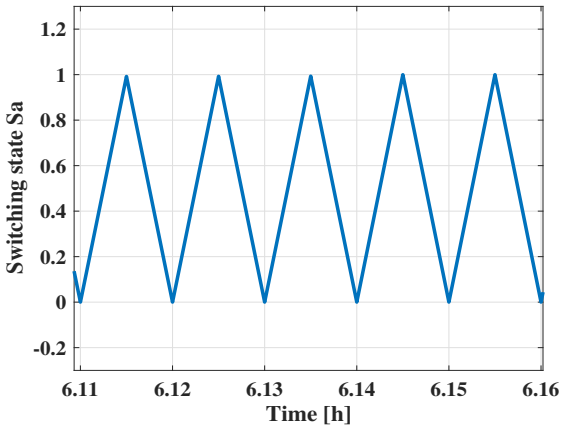


(j) Inverter switching state for FDTC

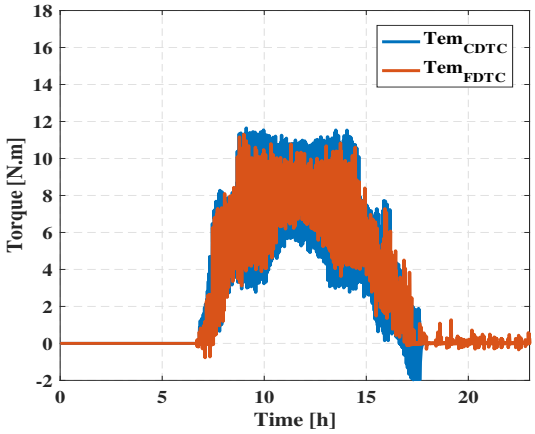


(k) Electromagnetic torque

FIGURE 3.13 – Characteristics of PV water pumping system in June

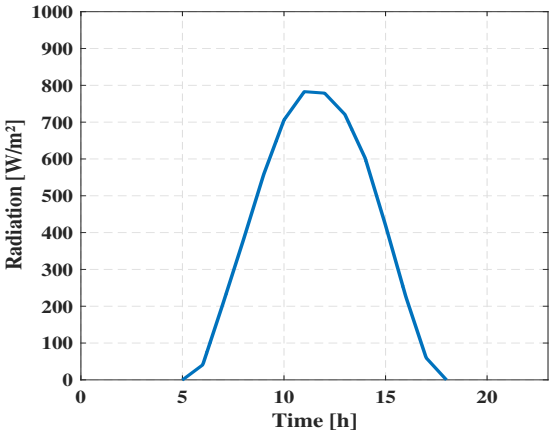


(a) Irradiation profile in March at Fes

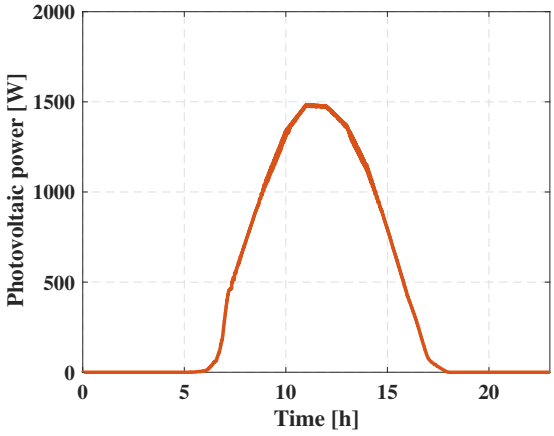


(b) Photovoltaic power

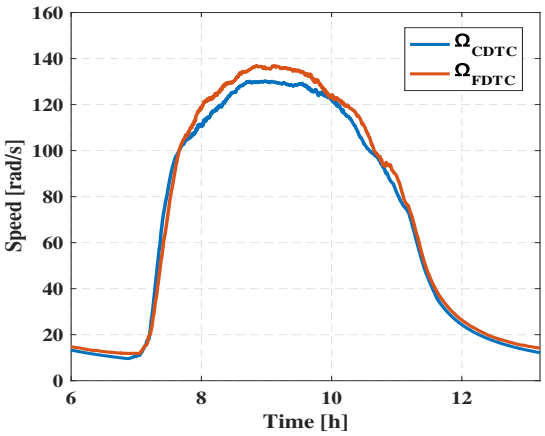


(c) Electric speed

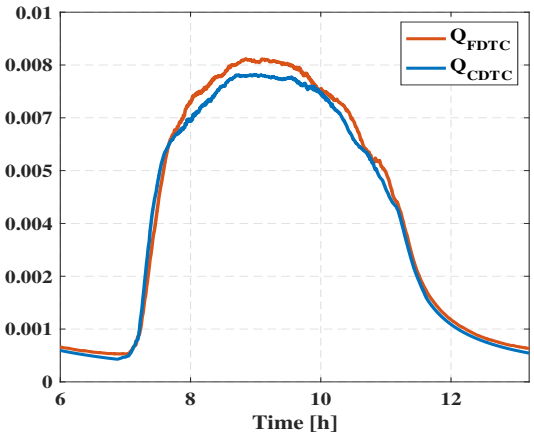


(d) Water Flow

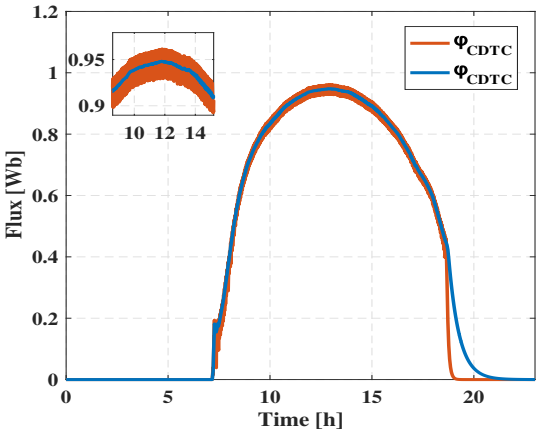


(e) Stator flux responses using CDTC

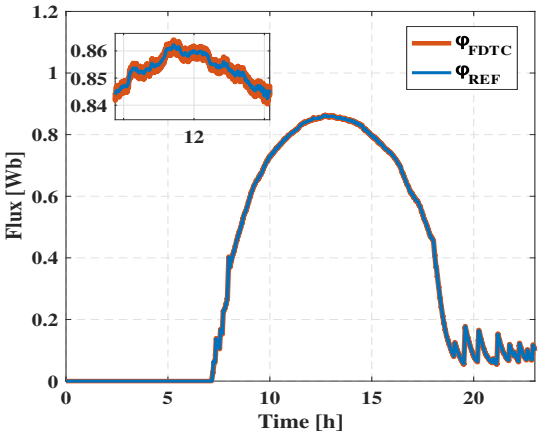


(f) Stator flux responses using FDTC

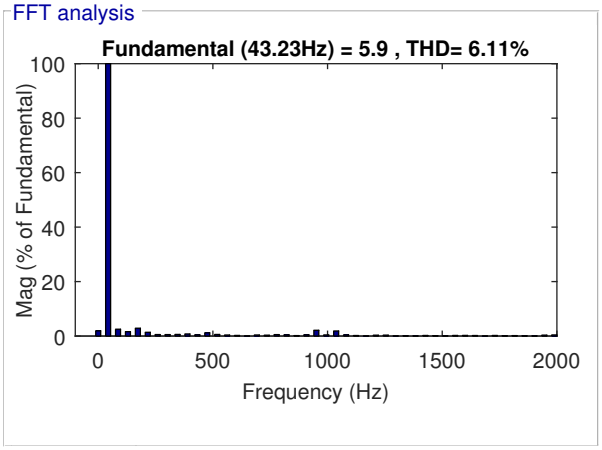


(g) FFT analysis of stator current using CDTC

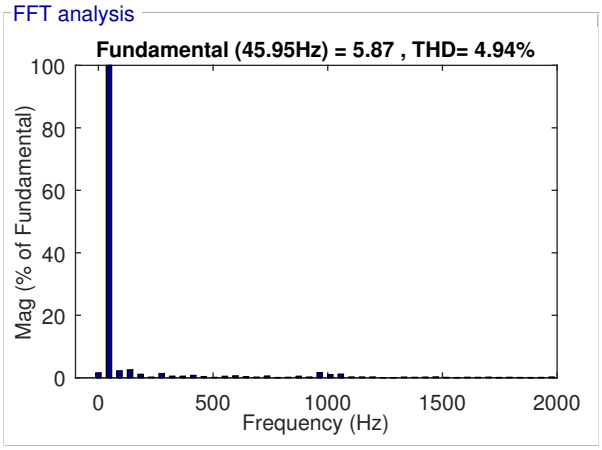


(h) FFT analysis of stator current using FDTC

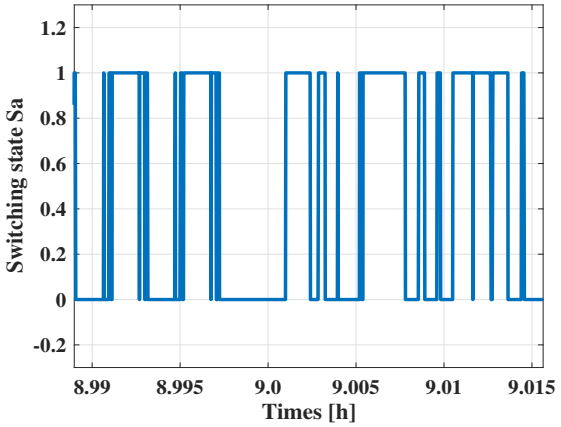


(i) Inverter switching state for CDTC

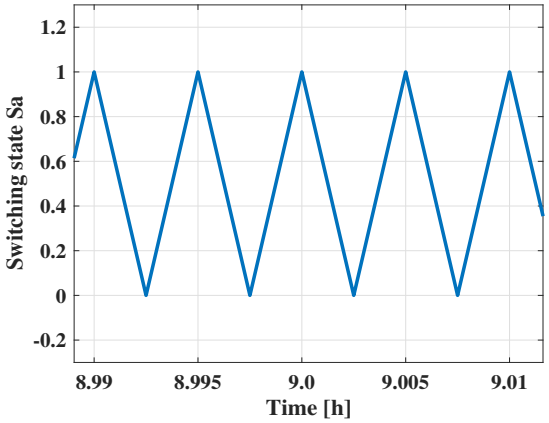


(j) Inverter switching state for FDTC

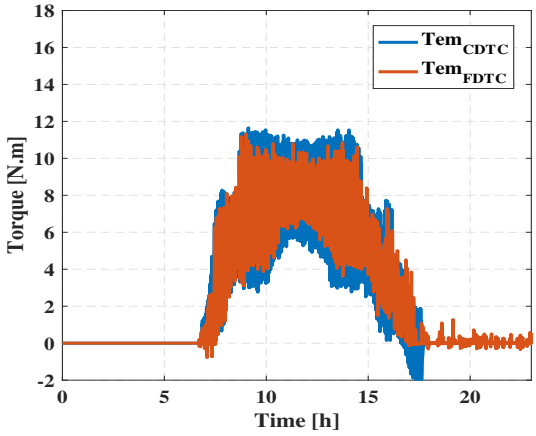


(k) Electromagnetic torque

FIGURE 3.14 – Characteristics of PV water pumping system in March

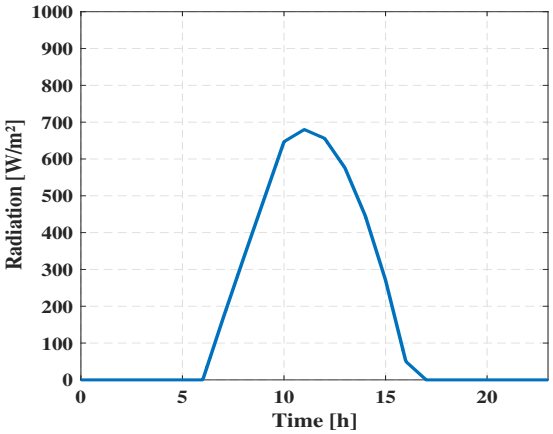


(a) Irradiation profile in December at Fes

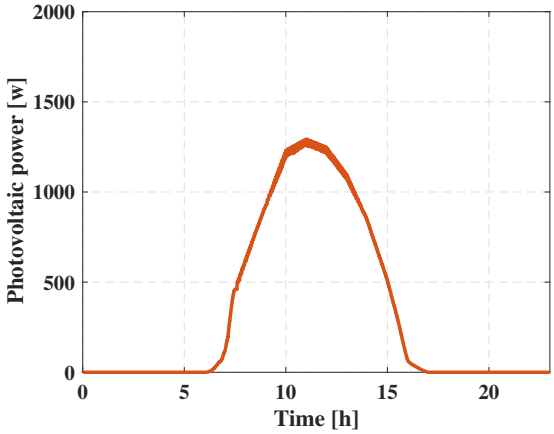


(b) Photovoltaic power

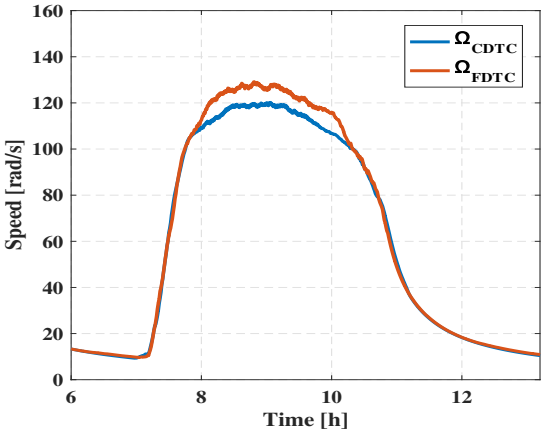


(c) Electric speed

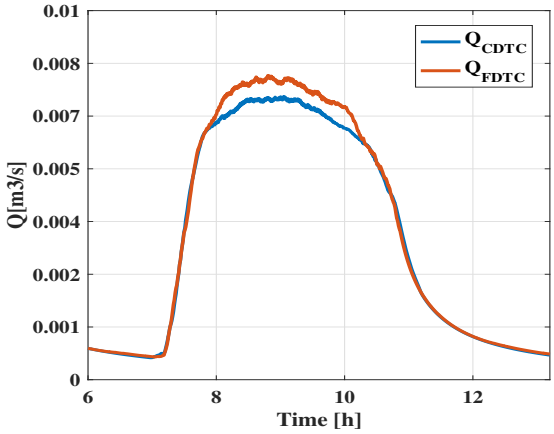


(d) Water Flow

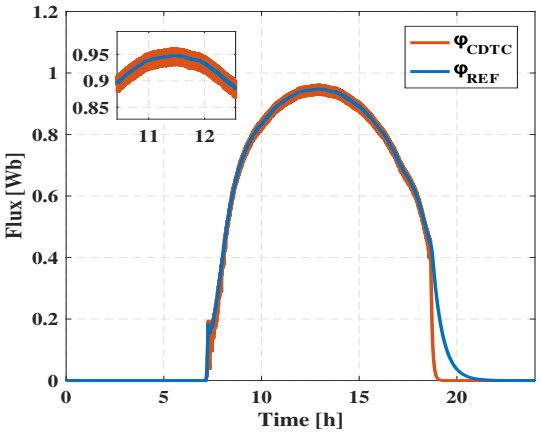


(e) Stator flux responses using CDTC

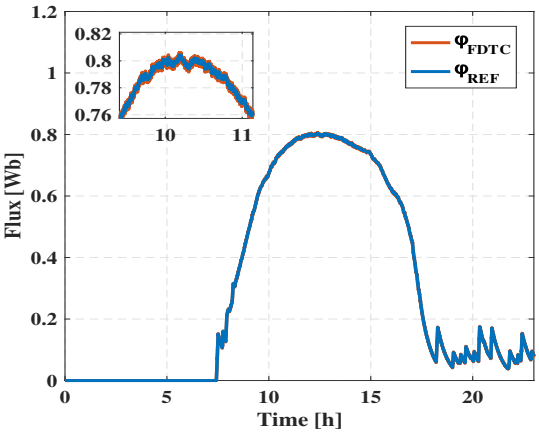


(f) Stator flux responses using FDTC

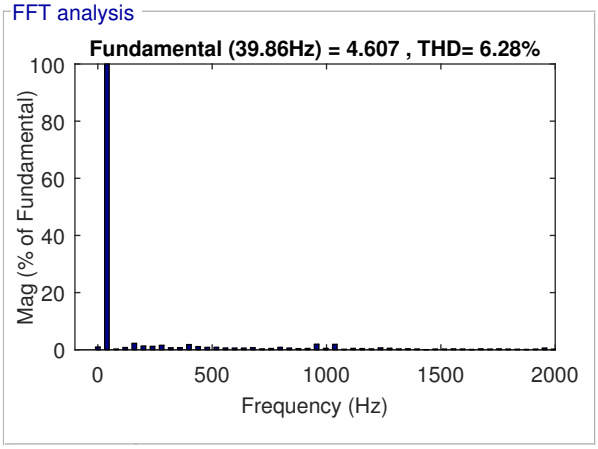


(g) FFT analysis of stator current using CDTC

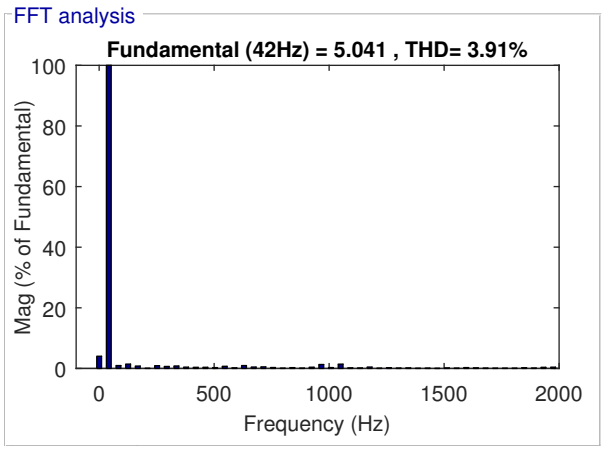


(h) FFT analysis of stator current using FDTC

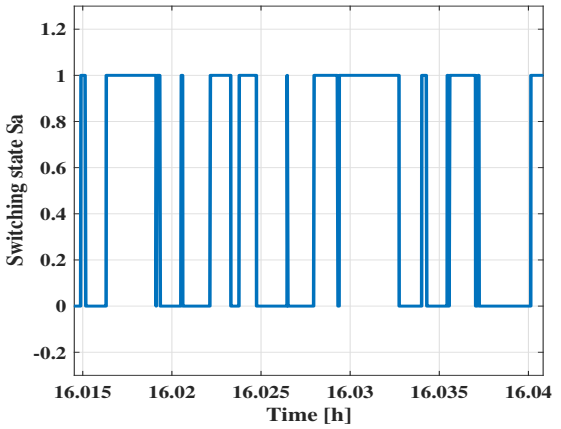


(i) Inverter switching state for CDTC

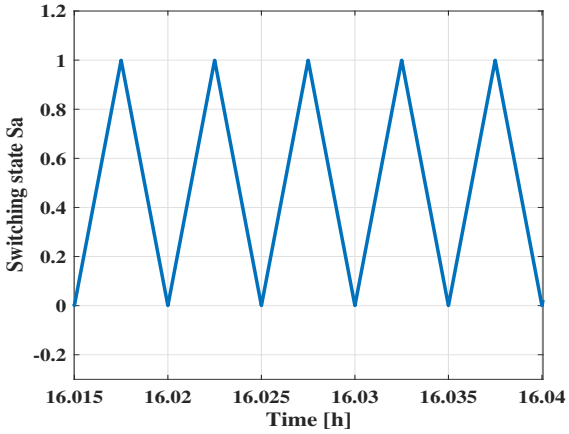


(j) Inverter switching state for FDTC

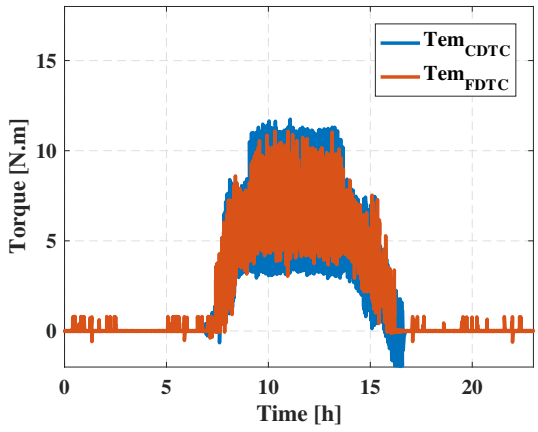


(k) Electromagnetic torque

FIGURE 3.15 – Characteristics of PV water pumping system in December

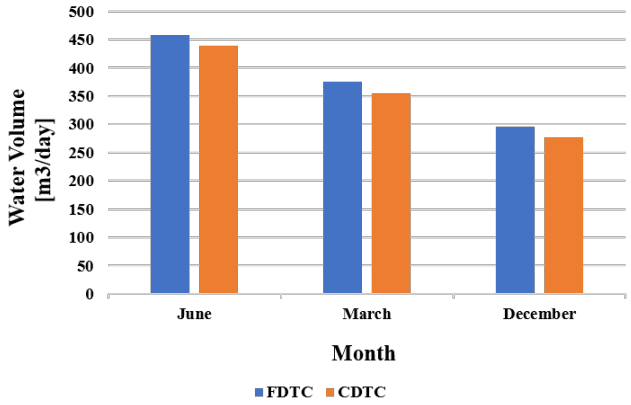


FIGURE 3.16 – Water volume comparison

| Season | Volume Obtained with FDTC ( $m^3/day$) | Volume Obtained with CDTC ( $m^3/day$) |
|---|---|---|
| Hot season | 458.64 | 438.48 |
| Moderate season | 375.84 | 354.96 |
| Cold season | 297.3 | 277.26 |

TABLE 3.5 – Pump flow using the Conventional and FLC-DTC Methods

using the conventional DTC and FLC-DTC in the three seasons : cold, medium, and hot seasons.

Fig 3.16 and table 3.5 show that, using the FLC-DTC, the pumped volume is clearly higher than using the conventional method.

Figs 3.13 (e),(f), 3.14 (e),(f) and 3.15 (e),(f) show the developed flux responses of IM drive with zoom-in view using the conventional and the proposed method. The hysteresis band of flux is limited to $\pm$ 1. The simulation results illustrate that the response of stator flux magnitude of fuzzy DTC represents low oscillations compared with conventional DTC and better tracking reference. To illustrate the impact of the CDTC and the proposed method on the quality of the signal, a FFT (Fast Fourier Transform) analysis of the stator current waveforms is done. Figs 3.13(g),(h),3.14(g),(h) and 3.15(g),(h) show the frequency spectrum. It can be seen that, the FDTC provides a lower total harmonic distortion (THD) in comparison with the CDTC.

| Performance \ Season | | | June | March | December |
|---|---|---|---|---|---|
| T*(N.m)* | $\Delta T$ | DTC- Conventionnel | ±3.85 | ± 2.89 | ±4.135 |
| | | DTC-FLC | ±2.29 | ±2 | ±3.3365 |
| | Improvement(%) | | 40.5 | 30.7 | 18.6 |
| $\phi(Wb)$ | $\Delta\phi$ | DTC- Conventionnel | 0.037 | 0.028 | 0.03 |
| | | DTC-FLC | 0.003 | 0.003 | 0.004 |
| | Improvement(%) | | 91.8 | 89.2 | 86.8 |
| THD*(%)* | $\Delta\phi$ | DTC- Conventionnel | 6.77 | 6.11 | 6.28 |
| | | DTC-FLC | 3.06 | 4.94 | 3.91 |

TABLE 3.6 – Torque, flux ripples and THD of the CDTC and FDTC

Figs 3.13(i),(j),3.14(i),(j) and 3.15(i),(j) show the inverter switching state of the first voltage phase ($S_a$) for both techniques, we can see that the switching frequency is variable, which is a major disadvantage in the conventional DTC. Contrariwise, the switching frequency is constant using FLC-DTC, therefore, the commutation losses are reduced. Figs 3.13(i),3.14(i) and 3.15(i) show the corresponding torque responses for the conventional DTC and the proposed DTC using fuzzy logic controller. The hysteresis band of torque is limited to ± 4. The torque response clearly shows that the torque's ripples with the proposed method are reduced significantly compared with conventional DTC.

The torque and flux ripples of the proposed method compared to conventional DTC are calculated and shown in table 3.6. From the presented data, our method has good performances than the Conventional DTC with maintaining a good torque response and respect to reducing the torque and flux ripple.

The improvement is calculated using Eq (3.22) and presented in table 3.6.

$$Improvement(\%) = \frac{V_{CDTC} - V_{FDTC}}{V_{CDTC}} \tag{3.22}$$

## 3.6 Conclusion

An optimal process of a photovoltaic water pumping system (PVWPS) based on an induction machine and driving a centrifugal pump is investigated. The PV system was studied using conventional DTC which contains a hysteresis controller in order to improve the efficiency of PV systems, Fuzzy Logic Control has been proposed. The performances of FLC applied to induction motor has been tested and compared with the conventional DTC. The simulation results show the increase of both the daily pumped quantity and reduction in the torque, stator current and flux ripples due to the use of a comparator with hysteresis reached by FLC.

# Chapter 4

## Improvement control of photovoltaic based water pumping system without energy storage

## 4.1 Introduction

Two types of stand-alone PV systems are used : the first one uses battery storage which stores the surplus power from PV, therefore, the cost of PV system increases by 10% - 50%[79][111]. The second one does not use the battery storage, the water pumped is stored in a tank for any use[28]. Different types of motors are used with PV based water pumping system in order to drive the pump, the choice depends on the efficiency, the availability, the price and the reliability. DC motors are used into pumping because they are easy to operate[112]. However, this kind of motors need regular maintenance due to brushes and commutator [113]. To surmount this weakness, Brushless DC motors have been proposed, these motors are characterized by a simple control, high reliability and ruggedness[8][9]. PV pumping systems based on AC motors, particularly induction motors (IM) are also used, these engines are rugged, they have high efficiency, maintenance free and low cost[50]. Two typical configurations of a PV water pumping systems based on IM are used. The first one is the dual stages water pumping system which is composed of a PV panel, a DC-DC converter for boosting the PV voltage array and maximizing the power, a DC-AC inverter for the conversion from DC voltage to variable voltage / variable frequency

power source and a pump driven by IM [22]. The second one is the single stage water pumping system which does not contain the DC-DC converter, because the DC-AC inverter with a tracking algorithm allows to perform the same task, and generate a variable voltage / variable frequency power supply to feed the IM. In addition, the PV panels must be connected in a series arrangement[114]. Researchers proposed several control strategies for IM[115][116][117][118][119]. Indirect Field Oriented control is the most used method to drive the IM[5][82], this control strategy ensures good and faster response [10][51]. The aim is to control the IM in a similar way to a DC motors by ensuring a decoupling between the flux and the torque. However, IFOC has its main difficulties namely :

i) Transformation synchronization, current regulators and PWM complicate this control strategy ;

ii) IFOC is influenced by parameter variations ;

iii) Delay to the torque response due to the use of PI controllers [77].

Different research studies have been proposed using intelligent approaches in order to improve the efficiency of the indirect field-oriented control.

Asma Chihi et al have proposed a method which is designed by IFOC based on Sliding Mode technique[5], this control strategy is robust and fast but it presents undesirable chattering[120]. Z.Kamaran et al have proposed a smart control system based on an Adaptive Fuzzy Logic Controller[121]. Fuzzy controller needs several rules based on the extensive experiments which makes it difficult to implement[7][53]. Artificial neural network is also used with conventional IFOC schemes[122]. Other researchers are combined different modern techniques : Saleh Masumpoor et al have proposed a technique consists of using sliding-mode and type-2 neuro fuzzy systems in order to improve the control of system [123]. Bouhoune et al have used Hybrid control of the three-phase induction machine using artificial neural networks and fuzzy logic[124]. All these intelligent control techniques are used to enhance the performance of the IFOC, but they need a high-speed processor for implementation[125].

The control using a constant value of the reference flux can be non-optimal for some operations, particularly, regarding the power losses and the absorbed currents, therefore, the efficiency of the IM can be reduced. The operating with variable flux reference can be able to optimize certain quantities without significant degrading in the dynamic performances. This chapter aims to present a new approach to the indirect field-oriented control strategy with loss minimization of induction machine (IM) drive which is proposed for the PV water pumping systems. This strategy consists to choose the optimal rotor flux by minimizing the copper losses, consequently maximizing the efficiency of PV pumping systems and energy saving. The proposed method is compared to conventional indirect field-oriented control and implemented using a dSpace system with DS1005 controller board under various operating conditions.

## 4.2 Indirect field oriented control

When the indirect Field Oriented Control is used, the flux is not regulated. This is given by the setpoint value and oriented from the angle $\theta_s$ which is obtained from the stator pulsation $w_s$. Hence, this method eliminates the use of the sensor or observer. In synchronous reference frame, the equations of the stator and rotor voltages of the induction machine can be expressed by[126] :

$$\begin{aligned} V_{ds} &= R_s i_{ds} + \tfrac{d}{dt}\phi_{ds} - w_s \phi_{qs} \\ V_{qs} &= R_s i_{qs} + \tfrac{d}{dt}\phi_{qs} + w_s \phi_{ds} \end{aligned} \tag{4.1}$$

$$\begin{aligned} 0 &= R_r i_{dr} + \tfrac{d}{dt}\phi_{dr} - w_{sr} \phi_{qr} \\ 0 &= R_r i_{qr} + \tfrac{d}{dt}\phi_{qr} + w_{sr} \phi_{dr} \end{aligned} \tag{4.2}$$

The implementation of rotor flux-oriented vector control is based on the orientation of the rotating coordinate system of axes $d$-$q$, such that the axis d is coincident with the direction of $\phi_r$.

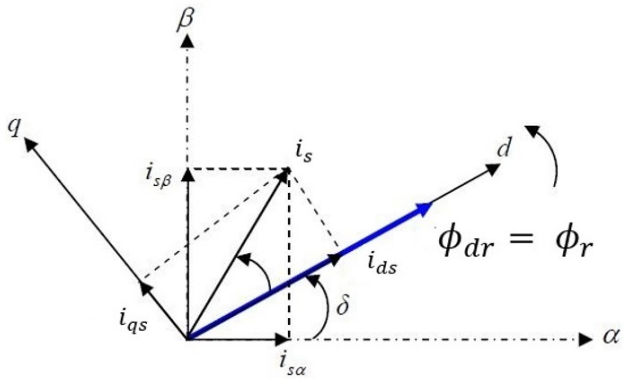


FIGURE 4.1 – Vector diagram in stationary and rotating reference frame

This means that the flux component is oriented on the d-axis, that implies[78] :

$$\begin{aligned} \phi_{dr} &= \phi_r \\ \phi_{qr} &= 0 \end{aligned} \tag{4.3}$$

Therefore, the rotor voltages are expressed by :

$$\begin{aligned} 0 &= R_r i_{dr} + \tfrac{d}{dt}\phi_{dr} \\ 0 &= R_r i_{qr} + w_{sr}\phi_{dr} \end{aligned} \tag{4.4}$$

And the components of flux are given by :

$$\begin{aligned} \phi_{ds} &= l_s \sigma i_{ds} + \tfrac{M}{l_r}\phi_{dr} \\ \phi_{qs} &= l_s \sigma i_{qs} \end{aligned} \tag{4.5}$$

Hence, the stator voltages are expressed by :

$$\begin{aligned} V_{ds} &= R_s i_{ds} + \sigma l_s \tfrac{d}{dt} i_{ds} + \tfrac{M}{l_r}\tfrac{d}{dt}\phi dr - w_s \sigma l_s i_{qs} \\ V_{qs} &= R_s i_{qs} + \sigma l_s \tfrac{d}{dt} i_{qs} + w_s \tfrac{M}{l_r}\phi qr + w_s \sigma l_s i_{ds} \end{aligned} \tag{4.6}$$

### 4.2.1 Estimation of $w_s$ and $\theta_s$

In this control strategy, the stator pulsation is determined indirectly from the measurement of the mechanical speed as follows :

$$w_{sr} = \frac{M}{T_r}\frac{i_{qs}}{\phi_{dr}} \tag{4.7}$$

Therefore, we obtain :

$$w_s = p\Omega + \frac{M}{T_r}\frac{i_{qs}}{\phi_{dr}} \tag{4.8}$$

We can note that the appearance of the rotor time constant ($T_r$) influences on the performance of this control strategy. The position of stator flux is given by :

$$\theta_s = \int w_s dt \tag{4.9}$$

### 4.2.2 Electromagnetic torque

The expression of the electromagnetic torque becomes[127] :

$$T_{em} = p\frac{M}{L_r}\phi_r i_{qs} \tag{4.10}$$

Eq (4.10) shows that by applying the indirect field oriented control, the electromagnetic torque can be controlled with q-axis stator current. The equations of the induction motor can be expressed as :

$$\begin{gathered}
V_{ds} = (R_s + R_r\frac{M^2}{l_r^2})i_{ds} + \sigma l_s\frac{d}{dt}i_{ds} - \frac{M}{l_r^2}R_r\phi_{dr} - w_s\sigma l_s i_{qs} \\
V_{qs} = (R_s + R_r\frac{M^2}{l_r^2})i_{qs} + \sigma l_s\frac{d}{dt}i_{qs} + \frac{M}{l_r}w\phi_{dr} + w_s\sigma l_s i_{ds} \\
w_s = p\Omega + \frac{M}{T_r}\frac{i_{qs}}{\phi_{dr}} \\
T_r\frac{d}{dt}\phi_{dr} + \phi_{dr} = Mi_{ds} \\
T_{em} = p\frac{L_m}{L_r}\phi_r i_{qs} \\
J\frac{d\Omega}{dt} = T_e - T_l - f_v\Omega
\end{gathered} \tag{4.11}$$

The equations of the induction motor can be also written by considering $\phi_{qr} = 0$ as follows :

$$\begin{aligned} \frac{d}{dt}i_{ds} &= -\frac{1}{\sigma l_s}(R_s + R_r\frac{M^2}{l_r^2})i_{ds} + w_s i_{qs} + \frac{1}{\sigma l_s}(\frac{M}{l_r^2}R_r)\phi_{dr} + \frac{1}{\sigma l_s}V_{ds} \\ \frac{d}{dt}i_{qs} &= -w_s i_{ds} - \frac{1}{\sigma l_s}(R_s + R_r\frac{M^2}{l_r^2})i_{qs} - \frac{1}{\sigma l_s}(\frac{M}{l_r})w_s\phi_{dr} + \frac{1}{\sigma l_s}V_{ds} \\ \frac{d}{dt}\phi_{dr} &= \frac{M}{l_r}R_r i_{ds} - \frac{R_r}{l_r}\phi_{dr} \\ J\frac{d}{dt}\Omega &= T_e - T_l - f_v\Omega \end{aligned} \tag{4.12}$$

From Eq (4.12), It can be seen that the stator voltages $V_{ds}$ and $V_{qs}$ depend on both current components $i_{ds}$ and $i_{qs}$ which leads to influence on the flux and the torque. Therefore, a decoupling process must be introduced.

### 4.2.3 Decoupling controller

Different decoupling techniques are proposed in literature. In this paper, the decoupling compensator technique is used. Therefore, Eq (4.6) can be written as follows[128] :

$$\begin{aligned} V_{ds} &= (R_s + s\sigma l_s)i_{ds} - w_s\sigma l_s i_{qs} \\ V_{qs} &= (R_s + s\sigma l_s)i_{qs} + w_s\frac{M}{l_r}\phi_r + w_s\sigma_s i_{ds} \end{aligned} \tag{4.13}$$

Where s is the derivative operator. The decoupling is achieved by choosing voltage commands such that :

$$\begin{aligned} V_{ds}^* &= (R_s + s\sigma l_s)i_{ds} = V_{ds} + w_s\sigma l_s i_{qs} = V_{ds} + e_{ds} \\ V_{qs}^* &= (R_s + s\sigma l_s)i_{qs} = V_{qs} - (w_s\frac{M}{l_r}\phi_r + w_s\sigma l_s i_{qs}) = V_{qs} - eqs \end{aligned} \tag{4.14}$$

Hence, the actions on the *(d,q)* axis are decoupled and illustrated in the figure. The voltages $V_{ds}$ and $V_{qs}$ are obtained from the voltages $V_{ds}^*$ and $V_{qs}^*$

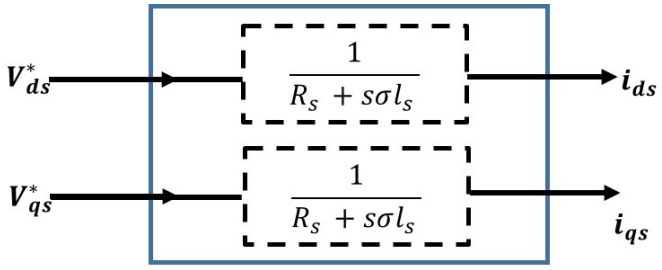


FIGURE 4.2 – The obtained controls

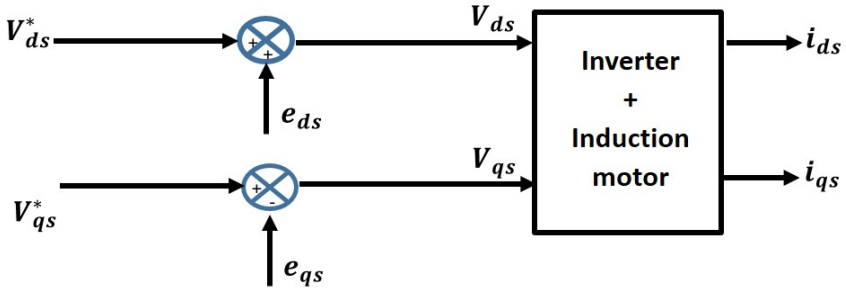


FIGURE 4.3 – Reconstruction of $V_{sd}$ and $V_{sq}$

## 4.3 Global scheme of indirect field-oriented control

The global control scheme of indirect field oriented control is shown in Fig 4.4 it's composed of :

- Coordinate transformations
- PWM algorithm
- Current controllers
- Speed regulation loop using PI controller
- An association of VSI-Induction motor.

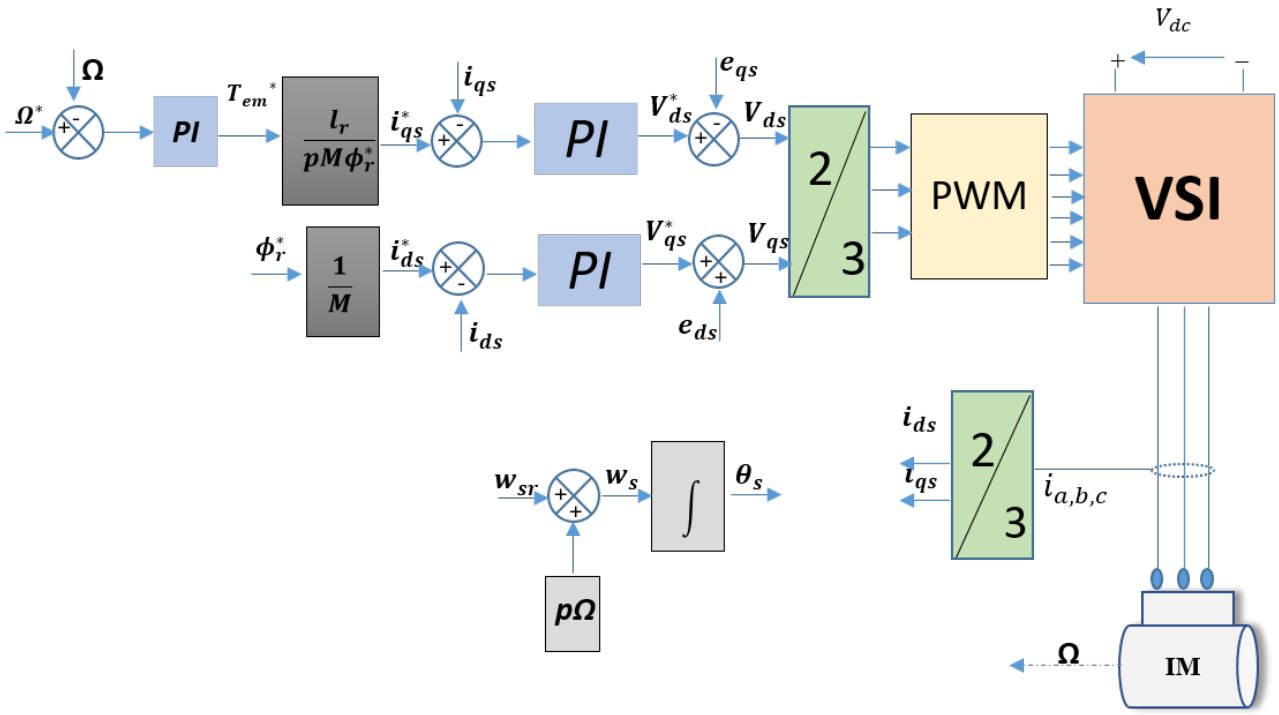


FIGURE 4.4 – The global control scheme of indirect field oriented

## 4.4 Pulse Width Modulation *(PWM)*

### 4.4.1 The 3-phase Inverter

As mentioned above, the scheme of a two-level voltage source inverter is shown in Figure 4.5, where $V_a$, $V_b$, $V_c$ are the voltages applied to the star-connected motor windings, and $V_{dc}$ presents the continuous inverter input voltage. The two level VSI is composed of six switches that can be BJT, GTO, IGBT... depending of the used system and the operating of these devices must respect the following conditions :

- Three switches must all time be ON and three all time OFF
- In order to avoid the vertical conduction and to ensure that there is no overlap in the power switch transitions, the upper and the lower switches located in the same leg are controlled by two complementary pulsed signals.

Different PWM techniques have been developed to control the VSI. The choice of the technique depends on several parameters such as : the type of machine that will

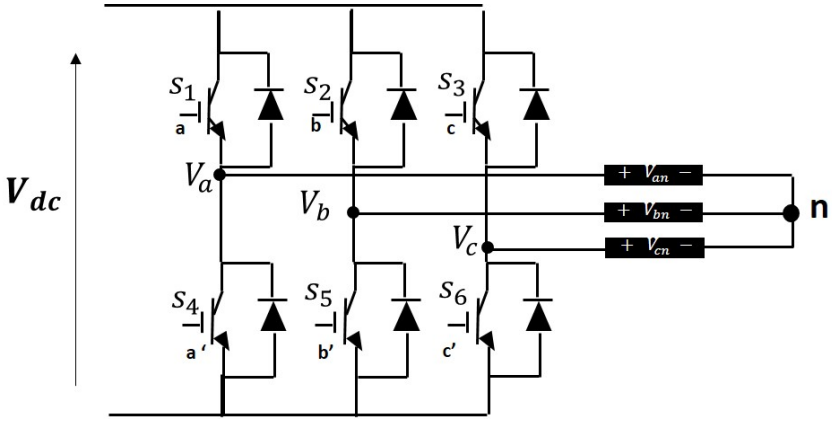


FIGURE 4.5 – Two level VSI

be controlled, the semiconductors used in the inverter, the value of the power...

Table 4.1 shows the eight switching vectors, output line to neutral voltage (phase voltage), and output line-to-line voltages which must be multiplied by DC-link Vdc. Fig. 4.6 illustrates the eight inverter voltage vectors (V0 to V7). In this section,

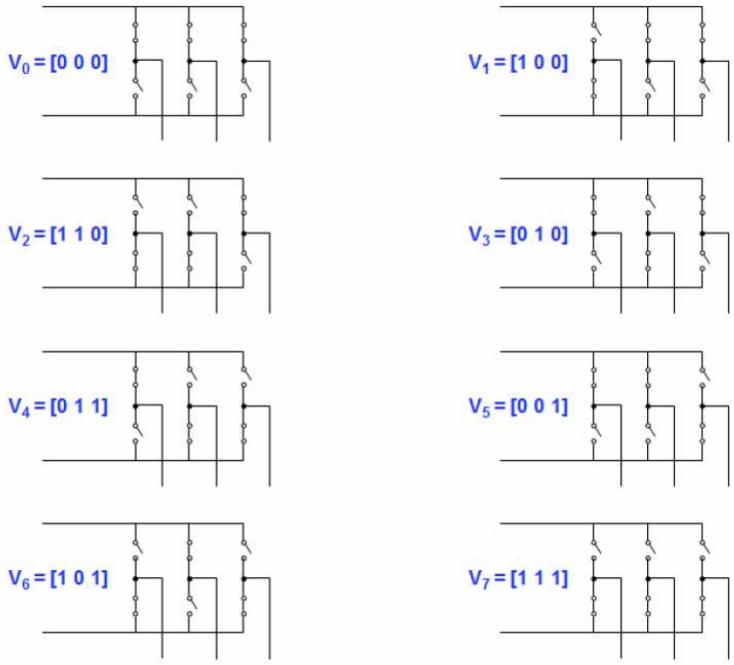


FIGURE 4.6 – The eight inverter voltage vectors (V0 to V7)

two PWM technique which are Sinusoidal PWM (SPWM) and Space Vector Pulse Width Modulation (SVPWM) will be presented[129].

| *Voltage vectors* | *Switching vectors* | | | *Line to neutral voltage* | | | *Line to line voltage* | | |
|---|---|---|---|---|---|---|---|---|---|
| | $a$ | $b$ | $c$ | $V_{an}$ | $V_{bn}$ | $V_{cn}$ | $V_{ab}$ | $V_{bc}$ | $V_{ca}$ |
| $V_0$ | 0 | 0 | 0 | 0 | 0 | 0 | 0 | 0 | 0 |
| $V_1$ | 1 | 0 | 0 | $\frac{2}{3}$ | -$\frac{1}{3}$ | -$\frac{1}{3}$ | -1 | 0 | -1 |
| $V_2$ | 1 | 1 | 0 | $\frac{1}{3}$ | $\frac{1}{3}$ | -$\frac{2}{3}$ | 0 | 1 | -1 |
| $V_3$ | 0 | 1 | 0 | -$\frac{1}{3}$ | $\frac{2}{3}$ | -$\frac{1}{3}$ | -1 | 1 | 0 |
| $V_4$ | 0 | 1 | 1 | -$\frac{2}{3}$ | $\frac{1}{3}$ | $\frac{1}{3}$ | -1 | 0 | 1 |
| $V_5$ | 0 | 0 | 1 | -$\frac{1}{3}$ | -$\frac{1}{3}$ | $\frac{2}{3}$ | 0 | -1 | 1 |
| $V_6$ | 1 | 0 | 1 | $\frac{1}{3}$ | -$\frac{2}{3}$ | $\frac{1}{3}$ | 1 | -1 | 0 |
| $V_7$ | 1 | 1 | 1 | 0 | 0 | 0 | 0 | 0 | 0 |

TABLE 4.1 – Switching vectors, phase voltages and output line to line voltages

### 4.4.2 Sinusoidal PWM (SPWM)

This technique consists in comparing three sine waves phase shifted by 120° based on the frequency of the desired output voltage with a very high frequency carrier triangle. The two signals are introduced in a comparator (Fig 4.8). The output depends on the state of the signals(Fig 4.7) :

- The comparator output is high when the sine wave (the modulation signal) is greater than the triangle
- The comparator output is low when the sine wave is smaller than the triangle.

This sinusoidal PWM Process is shown in Figure 4.7. The use of the SPWM technique is characterized by its simplicity and allows to eliminate specific harmonics.

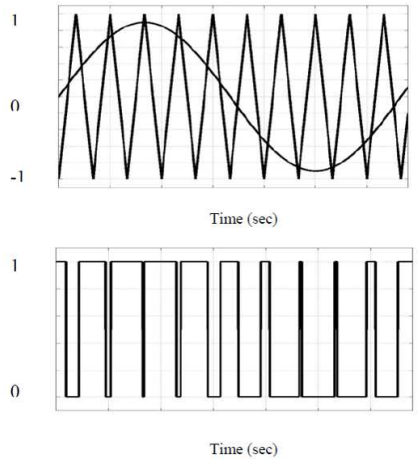


FIGURE 4.7 – PWM illustration by the sine-triangle comparison method (a) sine-triangle comparison (b) switching pulses

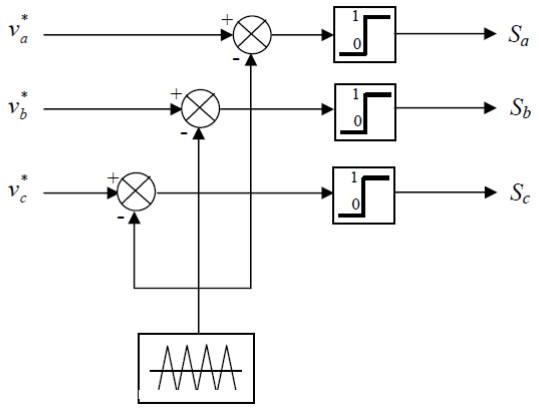


FIGURE 4.8 – SPWM technique

### 4.4.3 Space Vector Pulse Width Modulation (SVPWM)

Space Vector PWM (SVPWM) refers to a special technique of determining the switching sequence of the six power semiconductor switches of a two-level voltage source inverter (VSI). The use of this technique allows to produce less harmonic distortion in the output voltages or current in the windings of the motor load. In this method, the reference voltage vector $V_{ref}$ is approximated by the eight switching patterns. One simple technique of approximation is to produce the average output of the two-level voltage source inverter in a small period, T to be the same as that

of $V_{ref}$ in the same period. The space vector diagram of two level inverter is divided into 6 sector of 60° each whose the non-zero vectors form the axes of a hexagon Fig 4.9.

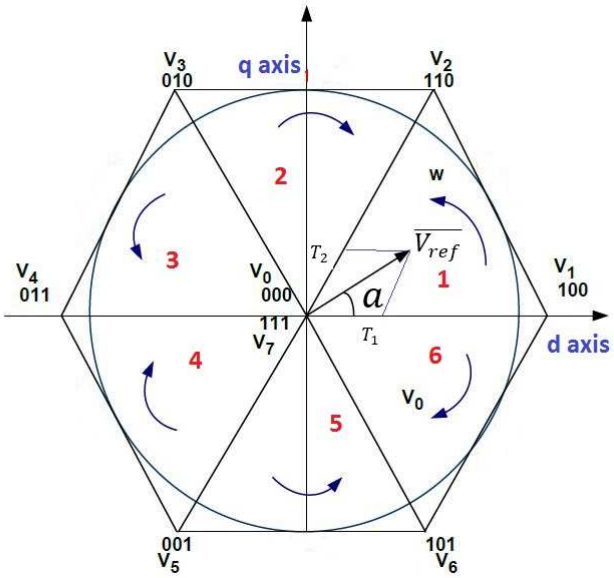


FIGURE 4.9 – Basic switching vectors and sectors

The implementation of SVPWM for two-level inverter can be effectuated by considering the following steps :

- Determination of : $V_d$, $V_q$, $V_{ref}$, and angle ($\alpha$)
- Determination of time duration $T_0$, $T_1$ and $T_2$
- Determination of the switching time of each transistor (S1 to S6)

#### 4.4.3.1 Determination of : $V_d$, $V_q$, $V_{ref}$ and angle ($\alpha$)

From Fig 4.10, the $V_d$, $V_q$, $V_{ref}$ and angle ($\alpha$) can be expressed by :

$$V_d = V_{an} - V_{bn} \times \cos 60 - V_{cn} \times \cos 60 \tag{4.15}$$

$$V_d = V_{an} - \frac{1}{2}V_{bn} - \frac{1}{2}V_{cn} \tag{4.16}$$

$$V_q = 0 + V_{bn} \times \cos 30 - V_{cn} \times \cos 30 \tag{4.17}$$

$$V_q = V_{an} - \frac{\sqrt{3}}{2}V_{bn} - \frac{\sqrt{3}}{2}V_{cn} \tag{4.18}$$

$$\begin{bmatrix} V_d \\ V_q \end{bmatrix} = \frac{1}{2}\begin{bmatrix} 1 & -\frac{1}{2} & -\frac{1}{2} \\ 0 & \frac{\sqrt{3}}{2} & -\frac{\sqrt{3}}{2} \end{bmatrix}\begin{bmatrix} V_{an} \\ V_{bn} \\ V_{cn} \end{bmatrix} \tag{4.19}$$

$$|\overline{V_{ref}}| = \sqrt{V_d^2 + V_q^2} \tag{4.20}$$

$$\alpha = \arctan(\frac{Vq}{Vd}) = wt = 2\pi ft \tag{4.21}$$

Where f is the fundamental frequency

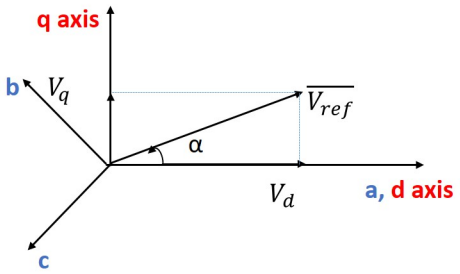


FIGURE 4.10 – The relationship of abc reference frame and stationary dq reference frame

#### 4.4.3.2 Determination of time duration $T_0$, $T_1$, $T_2$

From Fig 4.11, the switching time duration can be expressed as follows :

- Switching time duration at sector 1 :

$$\int_0^{T_Z} \overline{V_{ref}} = \int_0^{T_1} \overline{V_1}dt + \int_{T_1}^{T_1+T_2} \overline{V_2}dt + \int_{T_1+T_2}^{T_z} \overline{V_0}dt \tag{4.22}$$

$$T_z\overline{V_{ref}} = (T_1\overline{V_1} + T_2\overline{V_2}) \tag{4.23}$$

$$T_z|\overline{V_{ref}}|\begin{bmatrix} \cos\alpha \\ \sin\alpha \end{bmatrix} = T_1\frac{2}{3}V_{dc}\begin{bmatrix} 1 \\ 0 \end{bmatrix} + T_2\frac{2}{3}V_{dc}\begin{bmatrix} \cos\frac{\pi}{3} \\ \sin\frac{\pi}{3} \end{bmatrix} \tag{4.24}$$

Where $0 \leq \alpha \leq 60^{\circ}$

$$T_1 = T_Z \; a \; \frac{\sin(\frac{\pi}{3} - \alpha)}{\sin(\frac{\pi}{3})} \tag{4.25}$$

$$T_2 = T_Z \; a \; \frac{\sin(\alpha)}{\sin(\frac{\pi}{3})} \tag{4.26}$$

$$T_0 = T_Z - (T_1 + T_2) \tag{4.27}$$

Where $T_z = \frac{1}{f_z}$ and $a = \frac{|\overline{V_{ref}}|}{\frac{2}{3}V_{dc}}$

- Switching time duration at any sector

$$\begin{aligned} T_1 &= \tfrac{\sqrt{3}T_z|\overline{V_{ref}}|}{V_{dc}}(\sin(\tfrac{\pi}{3} - \alpha + \tfrac{n-1}{3}\pi)) \\ T_1 &= \tfrac{\sqrt{3}T_z|\overline{V_{ref}}|}{V_{dc}}(\sin(\tfrac{n}{3}\pi - \alpha)) \\ T_1 &= \tfrac{\sqrt{3}T_z|\overline{V_{ref}}|}{V_{dc}}(\sin\tfrac{n}{3}\pi\cos\alpha - \cos\tfrac{n}{3}\pi\sin\alpha) \end{aligned} \tag{4.28}$$

$$\begin{aligned} T_2 &= \tfrac{\sqrt{3}T_z|\overline{V_{ref}}|}{V_{dc}}(\sin(\alpha - \tfrac{n-1}{3}\pi)) \\ T_1 &= \tfrac{\sqrt{3}T_z|\overline{V_{ref}}|}{V_{dc}}(-\cos\alpha\sin\tfrac{n-1}{3}\pi - \sin\alpha\cos\tfrac{n-1}{3}\pi) \end{aligned} \tag{4.29}$$

$$T_0 = T_z - T_1 - T_2 \tag{4.30}$$

Where : n=1 through 6 ( Sector 1 to 6 ) and $0 \leq \alpha \leq 60^{\circ}$

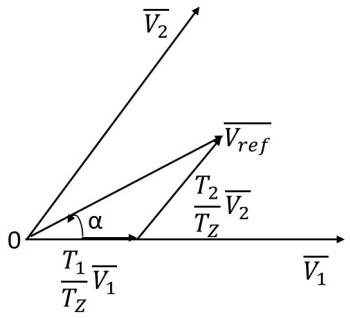


FIGURE 4.11 – Reference vector as a combination of adjacent vectors at sector 1

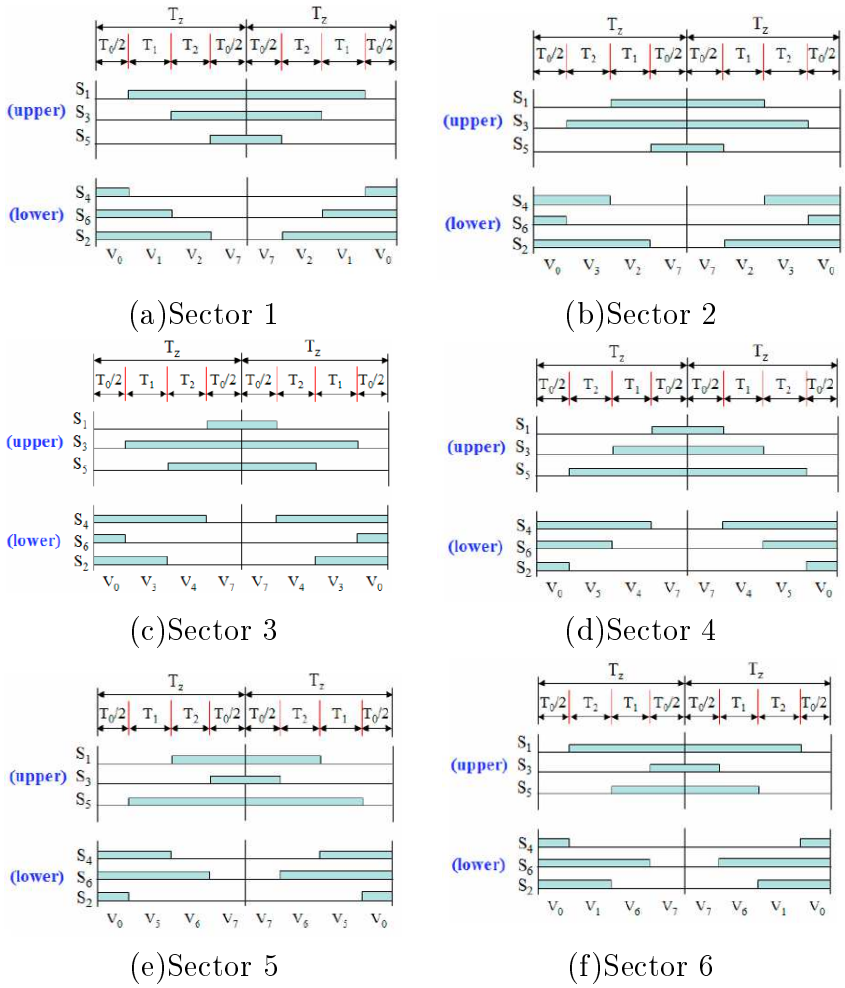


FIGURE 4.12 – Space Vector PWM switching patterns at each sector

#### 4.4.3.3 Determine the switching time of each transistor (S1 to S6)

Fig 4.12 illustrates space vector PWM switching patterns at each sector.Based on Fig 4.12, the switching time at each sector is summarized in Table 4.2.

| Sector | Upper Switches($S_1, S_3, S_5$) | Lower Switches($S_4, S_6, S_2$) |
|---|---|---|
| 1 | $S_1 = T_1 + T_2 + \frac{T_0}{2}$<br>$S_3 = T_2 + \frac{T_0}{2}$<br>$S_5 = \frac{T_0}{2}$ | $S_4 = \frac{T_0}{2}$<br>$S_6 = T_1 + \frac{T_0}{2}$<br>$S_2 = T_1 + T_2 + \frac{T0}{2}$ |
| 2 | $S_1 = T_1 + \frac{T_0}{2}$<br>$S_3 = T_1 + T_2 + \frac{T_0}{2}$<br>$S_5 = \frac{T_0}{2}$ | $S_4 = T_2 + \frac{T_0}{2}$<br>$S_6 = \frac{T_0}{2}$<br>$S_2 = T_1 + T_2 + \frac{T0}{2}$ |
| 3 | $S_1 = \frac{T_0}{2}$<br>$S_3 = T_1 + T_2 + \frac{T_0}{2}$<br>$S_5 = T_2 + \frac{T_0}{2}$ | $S_4 = T_1 + T_2 + \frac{T_0}{2}$<br>$S_6 = \frac{T_0}{2}$<br>$S_2 = T_1 + \frac{T0}{2}$ |
| 4 | $S_1 = \frac{T_0}{2}$<br>$S_3 = T_1 + \frac{T_0}{2}$<br>$S_5 = T_1 + T_2 + \frac{T_0}{2}$ | $S_4 = T_1 + T_2 + \frac{T_0}{2}$<br>$S_6 = T_2 + \frac{T_0}{2}$<br>$S_2 = \frac{T0}{2}$ |
| 5 | $S_1 = T_2 + \frac{T_0}{2}$<br>$S_3 = \frac{T_0}{2}$<br>$S_5 = T_1 + T_2 + \frac{T_0}{2}$ | $S_4 = T_1 + \frac{T_0}{2}$<br>$S_6 = T_1 + T_2 + \frac{T_0}{2}$<br>$S_2 = \frac{T0}{2}$ |
| 6 | $S_1 = T_1 + T_2 + \frac{T_0}{2}$<br>$S_3 = \frac{T_0}{2}$<br>$S_5 = T_1 + \frac{T_0}{2}$ | $S_4 = \frac{T_0}{2}$<br>$S_6 = T_1 + T_2 + \frac{T_0}{2}$<br>$S_2 = T_2 + \frac{T0}{2}$ |

TABLE 4.2 – Switching Time Calculation at Each Sector

## 4.5 Proposed technique

Based on the centrifugal pump theory, the quantity of the pumped water is increased with mechanical power at the pump shaft. Hence, the improvement of the pumped water is achieved by the maximization of the mechanical power as the insolation varies. The goal is obtained by the improvement of the motor efficiency which is expressed by eq (4.31) for every operating point.

$$\eta = 1 - \frac{P_{loss}}{P_{in}} = 1 - \frac{P_{loss}}{V_{ds}ids + V_{qs}i_{qs}} \tag{4.31}$$

Where : $P_loss = P_{in} - P_{out}$ and $P_{out} = w_m T_{em}$

Most of induction Motor control techniques use the rated value of flux as reference the command to ensure high dynamic performance. However, the high flux level produces additional core losses which leads to coming down efficiency. In that context, the proposed technique aims to determine the optimal reference flux which leads to increase the effectiveness of the PV water pumping system and reduces the motor losses. The proposed control strategy is based on the calculation of the copper losses (iron losses are neglected). The copper losses can be computed in(d,q) reference frame using direct stator current$i_{ds}$ and quadratic stator current $i_{qs}$ as follows :

The stator copper losses :

$$P_{cus} = R_s(i_{ds}^2 + i_{qs}^2) \tag{4.32}$$

The rotor copper losses :

$$P_{cur} = R_r(i_{dr}^2 + i_{qr}^2) \tag{4.33}$$

Therefore, the total copper losses can be expressed by :

$$P_{cu} = R_s(i_{ds}^2 + i_{qs}^2) + R_r(i_{dr}^2 + i_{qr}^2) \tag{4.34}$$

The rotor copper losses can be written in terms of $i_{qs}$ :

$$P_{cur} = R_r(\frac{M}{L_r})^2 i_{qs}^2 \tag{4.35}$$

Using Eq. (4.34) and (4.35), we obtain :

$$P_{cu} = R_s(i_{ds}^2 + i_{qs}^2) + R_r(\frac{M}{L_r})^2 i_{qs}^2 \tag{4.36}$$

Thus, the stator currents rotor in terms of flux and electromagnetic torque can be

written as :

$$i_{ds} = \frac{\phi_r}{M} \tag{4.37}$$

$$i_{qs}^{*} = T_{em}^{*} \frac{L_r}{Mp\phi_r^{*}} \tag{4.38}$$

Replacing Eq. (4.38) into (4.36), the total losses expression can be written in terms of direct stator current $i_{ds}$ as follows :

$$P_{cu} = R_s i_{ds}^2 + (R_r(\frac{M}{L_r})^2 + R_s)(T_{em}^{*} \frac{L_r}{pM^2 i_{ds}})^2 \tag{4.39}$$

From Eq (4.39), it's clear that the losses depend on the value of $i_{ds}$ which controlled the rotor flux $\phi_r^{*}$. This involves the motor losses that can be controlled when the internal parameters of the induction motor remain unchanged under the constant load torque. Hence, the derivative of Eq (4.39) allows providing the optimal reference flux which ensures the minimum losses without degrading the performance of IM.

$$\frac{dP_{cu}}{di_{ds}} = 0 \tag{4.40}$$

Therefore, the direct stator current $I_{ds_{opt}}$ in field-oriented (d,q) system ensuring the optimal reference value of the rotor flux is given by :

$$I_{ds_{opt}} = K_{opt} i_{qs}^{*} \tag{4.41}$$

Where : $K_{opt} = \sqrt{1 + (\frac{M}{L_r})^2 \frac{R_r}{R_s}}$

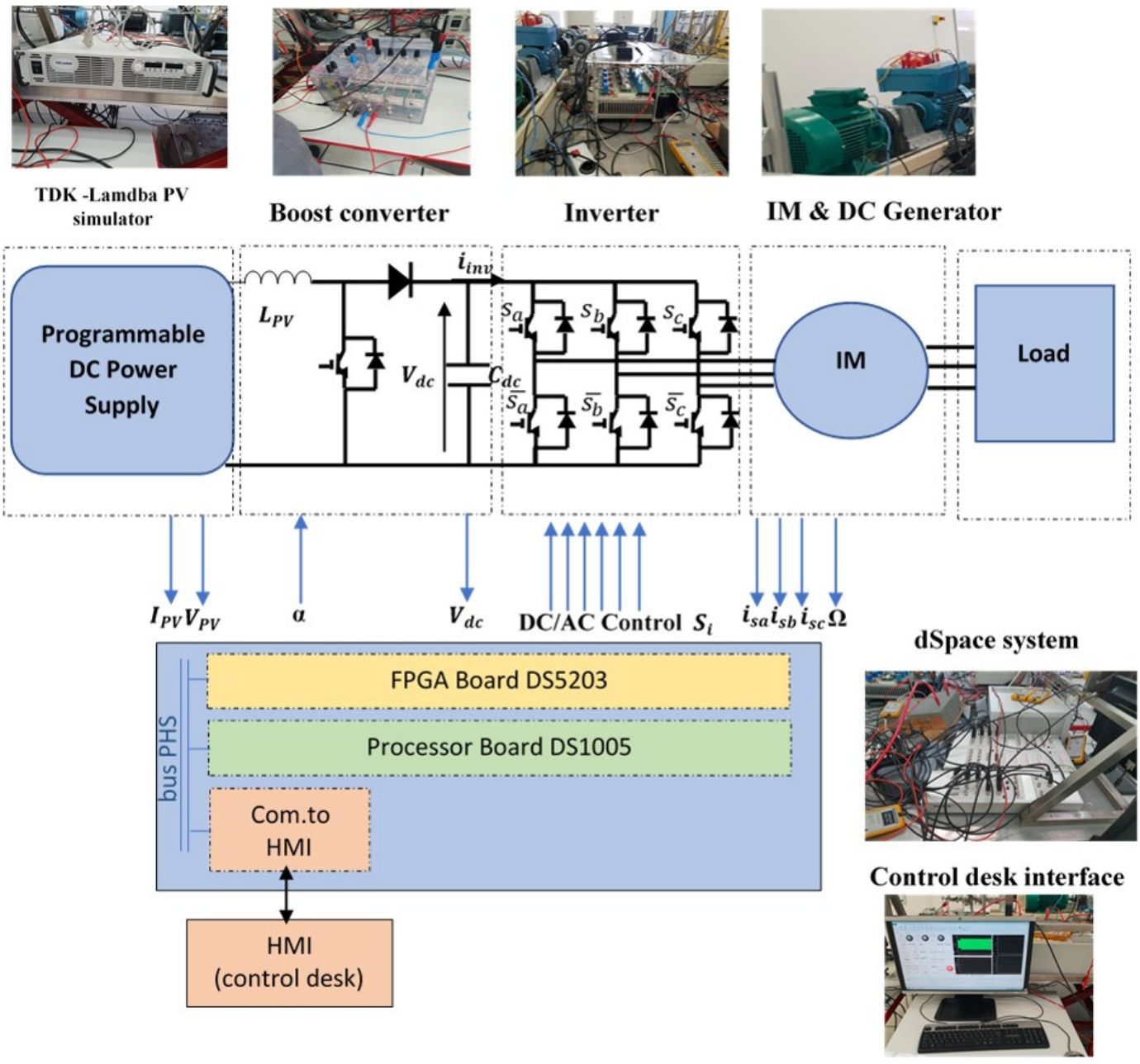


FIGURE 4.13 – The overview of the developed experimental prototype system

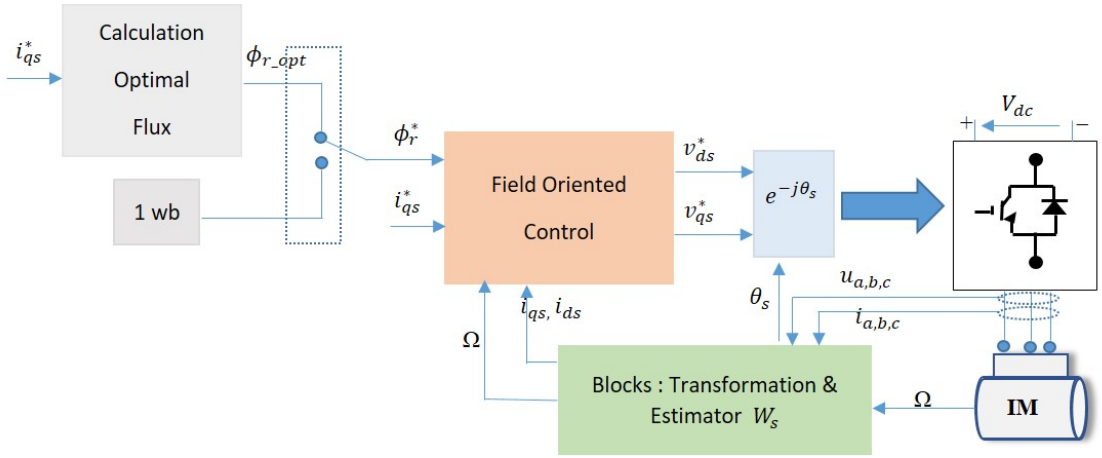


FIGURE 4.14 – Model block with total losses

## 4.6 Results and discussions

Experimental tests are developed in order to validate the control of proposed topology. The developed experimental prototype system is shown in Fig 4.13. The developed test bench consists of a solar panel simulator (TDK-Lambda), boost converter, voltage source inverter (VSI), induction motor which is characterized by the parameters presented in Table A.2, voltage sensors (P5205A) and a current sensors (TCP312A). A volumetric pump is realized using DC generator fed resistive load. The values of the proposed system components are summarized in table 4.3.

The test script has been effectuated using rapid control prototyping dSpace which is constituted of DS5203 FPGA board, DS1005 processor board, DS4003 digital I/O board, DS814 link board that allows us the connection with dSpace system and PHS bus for data exchange. The control functions under Matlab/Simulink include the Real Time Workshop (RTW) that generates a C-code using Simulink interface, the graphical object-oriented package (the Control Desk) and the Real Time Interface (RTI) that represents the interface between various dSpace platforms and Simulink.

With the aim of testing and evaluating the proposed control strategy, different tests are carried out using the real data of solar radiation from (Fes, Maroc) and various conditions. The proposed method is compared to conventional indirect field-

oriented control under the same conditions. The study will be as follows : for the same extracted power from the PV panels and the same electric motor speed, the performances of both systems are been compared.

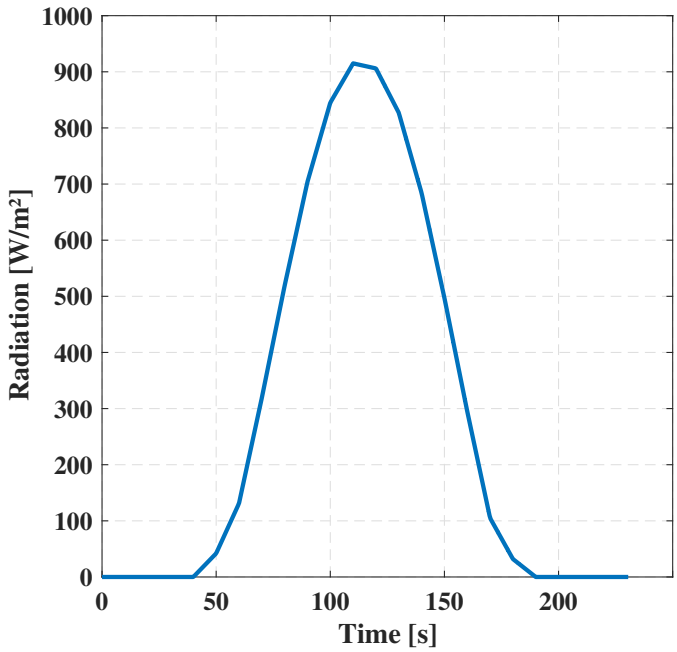


FIGURE 4.15 – irradiation Profile

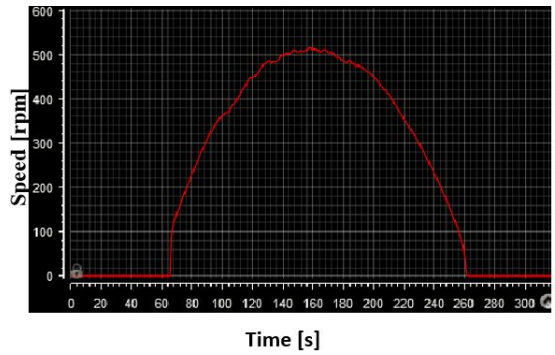


(a)Electric speed

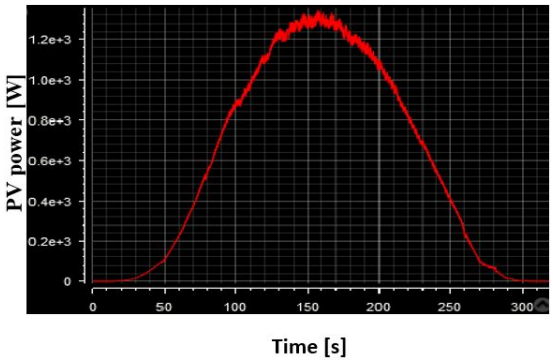


(b)Photovoltaic power

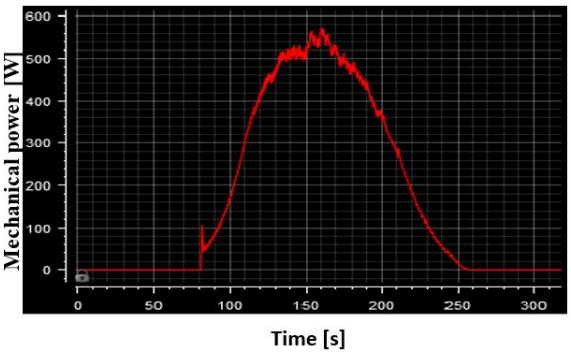


(c)Mechanical power using IFOC

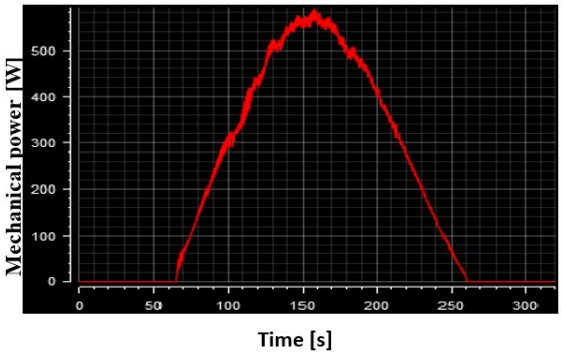


(d)Mechanical power using proposed method

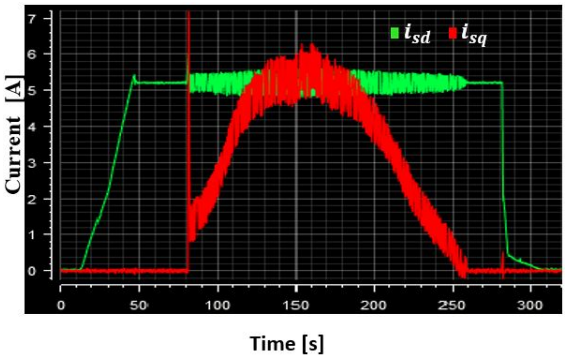


(e)Current responses using IFOC

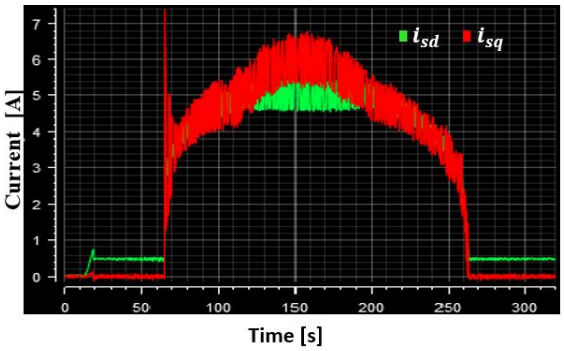


(f)Current responses using proposed method

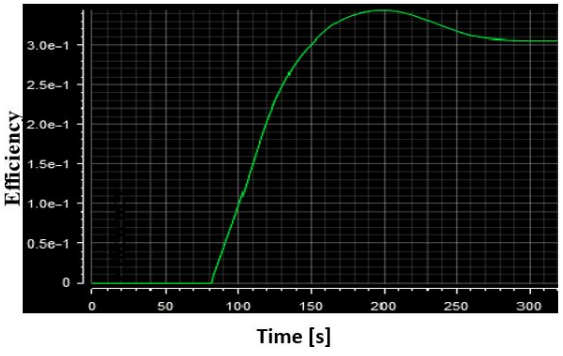


(g)System efficiency with IFOC

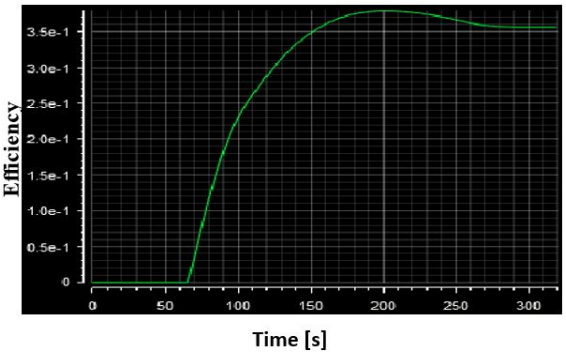


(h)System efficiency with proposed method

FIGURE 4.16 – Performances of PVWPS under a reduced daily profile

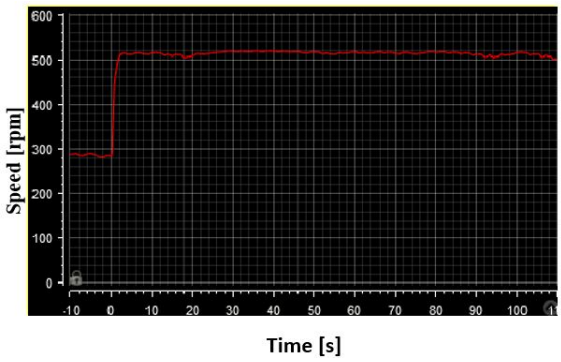


(a)Electric speed

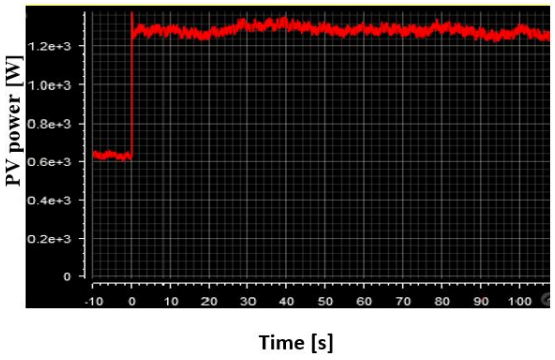


(b)Photovoltaic power

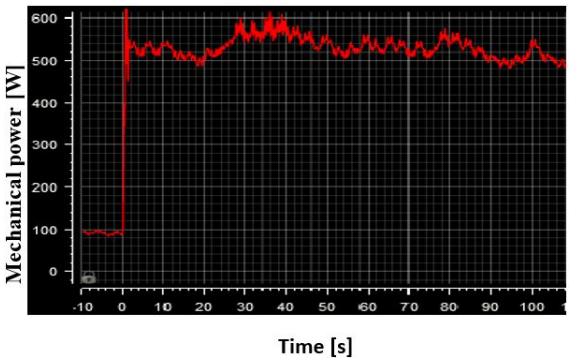


(c)Mechanical power using IFOC

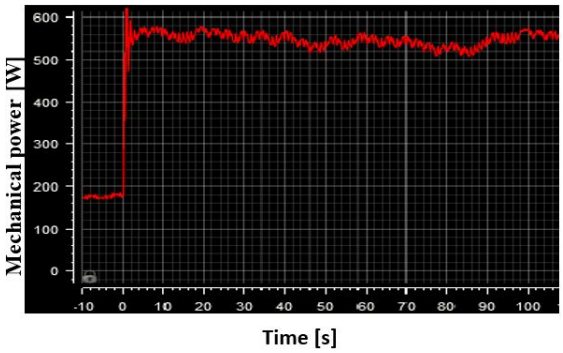


(d)Mechanical power using proposed method

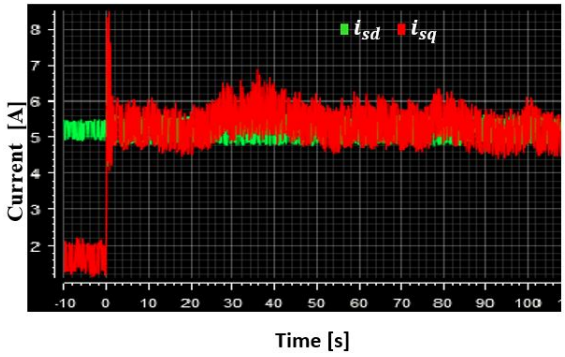


(e)Current responses using IFOC

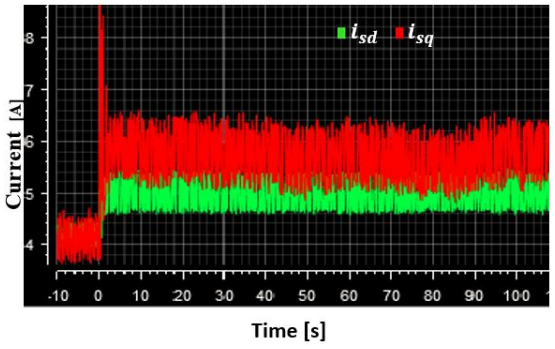


(f)Current responses using proposed method

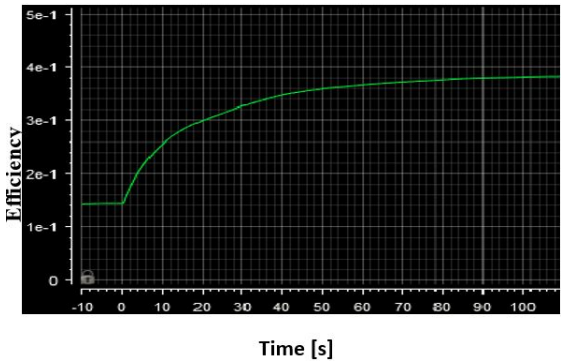


(g)System efficiency with IFOC

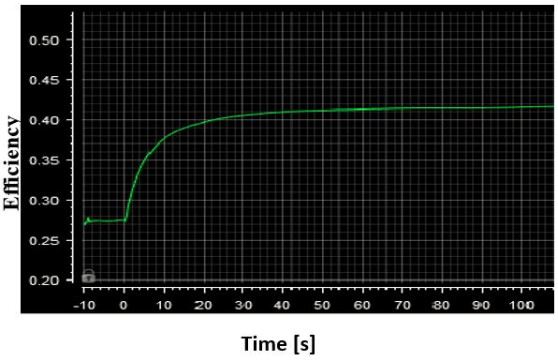


(h)System efficiency with proposed method

FIGURE 4.17 – Performances of PVWPS under sudden change in irradiance

| Component | Value |
|---|---|
| $V_{dc}^{*}$ | 400 V |
| $C_{dc}$ | 2000 $\mu F$ |
| $\alpha$ | 0.26 |
| $L_{pv}$ | 3 $mH$ |

TABLE 4.3 – Design of parameters of the system

### 4.6.1 Test under varying conditions

To evaluate the behavior of the PV pumping system, a sudden change in irradiance is applied which consists of changing the irradiance level from 375 $W/m^2$ to 750 $W/m^2$ at 0s. Figs 4.17 (a) and (b) show the evolution of the electric speed and the PV power using conventional IFOC and the proposed method.

Figs 4.17 (c) and (d) show the developed mechanical power of IM drive using the conventional and the proposed method. The results show that, under different levels of irradiation, the mechanical power of the proposed method is clearly higher than using the conventional method.

Figs 4.17 (e) and (f) show the direct current $i_{sd}$ and quadratic current $i_{sq}$ responses. By using the proposed method, the direct current is reduced compared with the conventional method. Figs 4.17 (g) and (h) prove that the efficiency of PV pumping systems using the proposed method is better.

### 4.6.2 Test under reduced daily profile

Another test was performed under a reduced daily profile of irradiance (Fig 4.15). Figs 4.16 (a) and (b) show the evolution of the electric speed and the PV power using conventional IFOC and the proposed method. It is clear in Figs 4.16(c) and (d) that the mechanical power of the proposed method is higher than using the conventional method and it starts to increase at 52s compared to IFOC which begin to rise at 57s. Figs 4.16 (e) and (f) present the direct current $i_{sd}$ and quadratic current $i_{sq}$ responses. Using IFOC conventional, the direct current increases rapidly

to 5.2 A at 10s and remains constant until 280s, contrarily to the proposed method, the direct current increases slowly to 0.8 A at 10s, then it converges to 5.2 A at 52s and it decreases at 255s, that means the current is reduced, therefore, by using the proposed method, joule losses are reduced compared with the conventional method. According to Figs 4.16 (g) and (h), we can see that the efficiency using the proposed method is better than the conventional method.

According to table 4.4, we notice the following summary :

The proposed method illustrates an apparent reduction in current amplitude which can reduce considerably the copper losses. In addition, this reduction allows to optimize energy. The efficiency of the proposed PV water pumping systems is also improved. It can be concluded that the proposed control strategy can be useful for PV water pumping.

| | Performance | | | | | |
|---|---|---|---|---|---|---|
| | Conventional IFOC | | | Proposed method | | |
| Irradiation $W/m^2$ | Mechanical Power (W) | Current $i_{sd}$ | Efficiency (%) | Mechanical Power(W) | Current (A) | Efficiency (%) |
| 375 | 100 | 5.2 | 15 | 185 | 4.2 | 27.5 |
| 750 | 510 | 5.2 | 39 | 570 | 5.2 | 41.5 |
| Daily profile | 550 | 5.1 | 30.5 | 580 | 0.8 | 36 |

TABLE 4.4 – Comparison between our proposal and conventional control strategy

## 4.7 Conclusion

A cost effective and simple PV water pumping systems driven by IM has been proposed here. An experimental validation of the control strategy is achieved by employing a dSpace 1005 board to validate the performance of proposed system. The effectiveness and performances of the proposed strategy which is based on the choosing of an optimal flux reference have been verified and compared with conventional technique which is based on constant flux reference. The experimental results

showed that the proposed control strategy admits a remarkable performance for rapidly changing climatic conditions and daily profile while reducing the stator current and losses and increasing the efficiency by 12 %, 2.5% and 5% under 375 $W/m^2$, 750 $W/m^2$ and daily profile respectively. The proposed PVWPS is reliable, simple, require less maintenance and is found suitable for drinking water supply and irrigation in remote areas.

# Conclusions and future work

## Conclusions

This dissertation deals with the performance improvement of a PV-powered induction-motor-driven water pumping system. DTC and FOC are the most used control strategies. DTC is a technique which provides a decoupled torque and flux control for the electrical drives. This control strategy is featured by simple structure, fast torque dynamic and less sensitivity to the machine parameters. However, it suffers from the high flux and torque ripples and the variable switching frequency. Therefore, they lead to an acoustical noise and more control difficulty in low speed regions which degrades the performance of the control algorithm. FOC allows independent control of the flux and torque during both the steady state and dynamic condition. it gives a good and faster response9, However, this control strategy is complex and influenced by the parameter variations. The main objective of this thesis is the improvement of the performance of an induction motor drive controlled by DTC and FOC using various control approaches. In this context, the research work has been addressed the following principal points regarding the direct torque control and indirect field-oriented techniques :

1. The reduction of the torque and flux ripples which caused by the variable switching frequency due to the use of hysteresis comparators.
2. The minimization of the total harmonic distortion, which means an improvement of the quality of current signals.
3. The increasing of pumping water flow

4. The association of losses minimization technique to improve the energy efficiency of the water pumping system

Furthermore, the aforementioned processes have been studied by simulation using MATLAB/Simulink software and hardware experimentation using the real-time interface linked to dSpace 1005 signal card.

Related to the water pumping systems, the first chapter has presented a state of the art about different configurations of the water pumping system based on renewable energy sources such as solar photovoltaic, solar thermal, wind, biomass and hybrid forms of energy. Depending on the components in the system, PV water pumping system has been classified by mentioning the relative advantages and disadvantages of each configuration. The choice of a suitable system for a particular application depends on several factors.

The second chapter has presented the modeling of the PV water pumping system components which are PV panel, boost converter, voltage source inverter (VSI), the induction motor and the centrifugal pump. Moreover, the missing parameters of the PV panel are determined using the tool provided by Mathworks. Moreover, it's demonstrated that the output of the PV panel is influenced by the shunt and series resistances, solar irradiation and temperature. Hence, in this chapter, the impact of these parameters on the behavior of the PV panel is investigated. Subsequently, the third chapter has presented a proposed robust control based on the artificial intelligence techniques. It consists of substituting the hysteresis controllers and the look-up table by fuzzy logic switching vector selection scheme. Different tests based on real climatic conditions have been carried out. a comparative study between the proposed method and the conventional DTC has been performed in Matlab/Simulink. The principal objectives were attained. It becomes clear that the proposed method based on fuzzy logic controller provides good performance in comparison with the conventional DTC, such as the perfect tracking of the references flux, the increasing of daily pumped water and the reduction of torque and flux ripples. Moreover, the

FFT analysis of the stator currents illustrated a lower total harmonic distortion, which means an improvement of the quality of current signals.

Finally, the fourth chapter has presented, a proposed approach associated with the indirect field-oriented control strategy which consists of determining the optimal flux level in order to improve the efficiency of PVWPS. The proposed technique uses the stator current as the objective function in the improvement process because it has been indicated that the stator current has more sensitivity to the flux variation. Consequently, an optimal control of direct axis (d- axis) stator current can result a reduction in flux level thus minimizing joules losses in IM. The optimal d-axis stator current is derived analytically using the loss equation of the IM and is employed in the dynamic model of the induction motor. The robustness of the proposed technique is approved by the reduction of the stator current, leading to a decrease in joule losses. As a result, the efficiency of the PVPWS is improved. Moreover, the proposed method is compared to conventional indirect field-oriented control and implemented using a dSpace system with DS1005 controller board under various operating conditions.

## Future work

For the continuity of research, the future work can be carried to develop other control strategies to improve the performance of the PV water pumping system as, for instance :

- Development of control strategies based on Artificial intelligent technique such as artificial neural network (ANN), and genetic algorithms.
- Elaborate the losses minimization strategies using intelligent optimizers such as Particle Swarm Optimization (PSO).
- Expanding the research to achieve other types of engines, such as permanent magnet assisted synchronous reluctance motors, permanent magnet motor and

synchronous reluctance motors, and elaborating a similar optimization technique based on their control structures and dynamic model

- Development of hybrid system of neuro-fuzzy and fuzzy-PSO in order to give better results.
- Introduce the Space Vector Modulation (SVM) to improve the performance.
- The use of Multilevel inverters structures.

# Publications arising from the Thesis

# Publications arising from the Thesis

The work developed in this thesis has been presented in several journal articles and conferences, which are cited now :

- **Articles in journals :**

  1. **M. Errouha**, A. Derouich, N. El Ouanjli, and S. Motahhir, “High-Per formance Standalone Photovoltaic Water Pumping System Using Induction Motor,” Int. J. Photoenergy, vol. 2020, 2020. (***Hindawi***)
  2. **M. Errouha**, A. Derouich, S. Motahhir, and O. Zamzoum, "Optimal Control of Induction Motor for Photovoltaic Water Pumping System", Technol. Econ. Smart Grids Sustain. Energy, vol. 5, no. 1, 2020, doi : 10.1007/s40866-020-0078-9.(***Springer nature***)
  3. **M. Errouha**, A. Derouich, B. Nahid-Mobarakeh, S. Motahhir, and A. El Ghzizal, "Improvement control of photovoltaic based water pumping system without energy storage", Sol. Energy, vol. 190, no. May, pp. 319–328, 2019, doi : 10.1016/j.solener.2019.08.024.(***Elsevier***)
  4. **M. Errouha**, A. Derouich, S. Motahhir, O. Zamzoum, N. El Ouanjli, and A. El Ghzizal, "Optimization and control of water pumping PV systems using fuzzy logic controller", Energy Reports, vol. 5, pp. 853–865, 2019, doi : 10.1016/j.egyr.2019.07.001. (***Elsevier***)
  5. **M. Errouha** and A. Derouich, "Study and comparison results of the

field oriented control for photovoltaic water pumping system applied on two cities in Morocco", Bull. Electr. Eng. Informatics, vol. 8, no. 4, pp. 1–7, 2019, doi : 10.11591/eei.v8i4.1301.

6. **M. Errouha**, Aziz Derouich, Saad Motahhir, Quentin Combe, ''Adaptive Fuzzy Logic Control of induction motor for photovoltaic water pumping system", Applied Solar Energy, (Major corrections), (***Springer nature***)
7. **M. Errouha**, Aziz Derouich, Saad Motahhir, Abdelaziz EL GHZIZAL, "Improved DTC strategy based on Fuzzy logic controller with losses minimization of induction motor for PV water pumping system" (Wiley), under review

- **IEEE conference publications (Indexed in Scopus and Web of Science) :**

1. **M. Errouha**, Saad Motahhir, Quentin Combe , Aziz Derouich, Abdelaziz El Ghzizal,"Fuzzy-PI controller for photovoltaic water pumping systems", 7th international in Renewable and Sustainable Energy Conference (IRSEC),Nov.27-30,2019- Agadir, Morocco.
2. **M. Errouha**, Saad Motahhir, Quentin Combe, Aziz Derouich, "Parameters extraction of single diode PV model and application in solar pumping", International Conference of Integrated Design and Production(CPI) , Oct 14-16,2019- Fez, Morocco.
3. **M. Errouha**, Saad Motahhir, Aziz Derouich, Abdelaziz El Ghzizal, " Experimental validation of the model of a photovoltaic panel and application in solar pumping : Case of the pumping station of the Higher School of Technology of Fez", 2éme Conférence internationale en Science et Technologies Electriques au Maghreb (CISTEM), 26, 27 et 28 Octobre 2017- Marrakech, Maroc.

- **Papers in conferences :**

1. **M. Errouha**, Aziz. DEROUICH, "Contrôle d'un système de pompage

photovoltaïque sans batterie de stockage ", Deuxième Journée Nationale sur les énergies renouvelables", 29 Décembre 2018- Fès, Maroc

2. **M.Errouha**, Aziz. DEROUICH, "Etude, dimensionnement et optimisation technico-économique d'un prototype d'une station de pompage solaire photovoltaïque dédiée à l'irrigation", 2ème Colloque Franco-Marocain sur les Energies Renouvelables et leur intégration aux réseaux de transport et de distribution (COFMER'02) , 11, 12 et 13 Avril 2017 –Fès, Maroc.

3. **M. Errouha**, Aziz. DEROUICH, "Etude et comparaison de la commande DTC pour un système de pompage photovoltaïque", International Congress On Energy and Environment (CI2E), 28 et 29 Mars 2017 –Fès, Maroc.

4. **M. Errouha**, Saad MOTAHHIR , Aziz DEROUICH et Abdelaziz El GHZIZAL , "Modélisation sur Matlab/Simulink d'une chaine de pompage photovoltaïque", 3ème Colloque International sur la Modélisation et analyse en mécanique Energétique (CIMANE), 28-29 avril 2016 – TAZA, Maroc.

5. **M. Errouha**, Aziz. DEROUICH, "Etude et commande d'un système de pompage photovoltaïque" 2ème Congrès international Environnement et développement durable (E2D), 20-21 avril 2016- Salé, Maroc.

# References


[1] H. Drissi, J. Khediri, W. Zaafrane, and E. B. Braiek, "Critical factors affecting the photovoltaic characteristic and comparative study between two maximum power point tracking algorithms," *International Journal of Hydrogen Energy*, vol. 42, no. 13, pp. 8689–8702, 2017. [Online]. Available : http://dx.doi.org/10.1016/j.ijhydene.2016.09.193

[2] M. Matam, V. R. Barry, and A. R. Govind, "Optimized Reconfigurable PV array based Photovoltaic water-pumping system," *Solar Energy*, vol. 170, no. November 2017, pp. 1063–1073, 2018. [Online]. Available : https://doi.org/10.1016/j.solener.2018.05.046

[3] S. S. Chandel, M. N. Naik, and R. Chandel, "Review of performance studies of direct coupled photovoltaic water pumping systems and case study," *Renewable and Sustainable Energy Reviews*, vol. 76, no. March, pp. 163–175, 2017. [Online]. Available : http://dx.doi.org/10.1016/j.rser.2017.03.019

[4] K. Yadav, A. Kumar, O. S. Sastry, and R. Wandhare, "Solar photovoltaics pumps operating head selection for the optimum efficiency," *Renewable Energy*, vol. 134, pp. 169–177, 2019.

[5] A. Chihi, H. Ben Azza, M. Jemli, and A. Sellami, "Nonlinear integral sliding mode control design of photovoltaic pumping system : Real time implementation," *ISA Transactions*, vol. 70, pp. 475–485, 2017. [Online]. Available : http://dx.doi.org/10.1016/j.isatra.2017.06.023

[6] T. Poompavai and M. Kowsalya, "Control and energy management

strategies applied for solar photovoltaic and wind energy fed water pumping system : A review," *Renewable and Sustainable Energy Reviews*, vol. 107, no. November 2018, pp. 108–122, 2019. [Online]. Available : https://doi.org/10.1016/j.rser.2019.02.023

[7] C. M. Reza, M. D. Islam, and S. Mekhilef, "A review of reliable and energy efficient direct torque controlled induction motor drives," *Renewable and Sustainable Energy Reviews*, vol. 37, pp. 919–932, 2014.

[8] C. Gopal, M. Mohanraj, P. Chandramohan, and P. Chandrasekar, "Renewable energy source water pumping systems - A literature review," *Renewable and Sustainable Energy Reviews*, vol. 25, pp. 351–370, 2013. [Online]. Available : http://dx.doi.org/10.1016/j.rser.2013.04.012

[9] B. Talbi, F. Krim, T. Rekioua, S. Mekhilef, A. Laib, and A. Belaout, "A high-performance control scheme for photovoltaic pumping system under sudden irradiance and load changes," *Solar Energy*, vol. 159, no. June 2017, pp. 353–368, 2018.

[10] R. Kumari and R. Dahiya, "Speed control of solar water pumping with indirect vector control technique," *Proceedings of the 2nd International Conference on Inventive Systems and Control, ICISC 2018*, no. Icisc, pp. 1401–1406, 2018.

[11] I. Yahyaoui and A. Serna Cantero, *Scalar and Vector Control of Induction Motor for Online Photovoltaic Pumping*. Elsevier Inc., 2018, vol. 1. [Online]. Available : http://dx.doi.org/10.1016/B978-0-12-812959-3.00010-1

[12] A. M. Delgado-Torres, "Solar thermal heat engines for water pumping : An update," *Renewable and Sustainable Energy Reviews*, vol. 13, no. 2, pp. 462–472, 2009.

[13] Y. W. Wong and K. Sumathy, "Solar thermal water pumping systems : a review," *Renewable & sustainable energy reviews*, vol. 3, no. 2, pp. 185–217, 1999.

[14] P. Camocardi, P. Battaiotto, and R. Mantz, "Autonomous BDFIG-wind generator with torque and pitch control for maximum efficiency in a water pumping system," *International Journal of Hydrogen Energy*, vol. 35, no. 11, pp. 5778–5785, 2010. [Online]. Available : http://dx.doi.org/10.1016/j.ijhydene.2010.02.099

[15] A. d. O. Ferreira, A. U. Brito, M. A. B. Galhardo, L. Ferreira, and W. N. Macêdo, "Modeling, control and simulation of a small photovoltaic-wind water pumping system without battery bank," *Computers and Electrical Engineering*, vol. 84, 2020.

[16] B. Xu, D. Chen, M. Venkateshkumar, Y. Xiao, Y. Yue, Y. Xing, and P. Li, "Modeling a pumped storage hydropower integrated to a hybrid power system with solar-wind power and its stability analysis," *Applied Energy*, vol. 248, no. May, pp. 446–462, 2019. [Online]. Available : https://doi.org/10.1016/j.apenergy.2019.04.125

[17] M. Das and R. Mandal, "A comparative performance analysis of direct, with battery, supercapacitor, and battery-supercapacitor enabled photovoltaic water pumping systems using centrifugal pump," *Solar Energy*, vol. 171, no. June, pp. 302–309, 2018. [Online]. Available : https://doi.org/10.1016/j.solener.2018.06.069

[18] M. Errouha, A. Derouich, S. Motahhir, and O. Zamzoum, "Optimal Control of Induction Motor for Photovoltaic Water Pumping System," *Technology and Economics of Smart Grids and Sustainable Energy*, vol. 5, no. 1, 2020.

[19] C. Ben Salah, M. F. Mimouni, and M. Ouali, "A real-time control of photovoltaic water-pumping network," *Computers and Electrical Engineering*, vol. 46, pp. 14–28, 2015. [Online]. Available : http://dx.doi.org/10.1016/j.compeleceng.2015.06.026

[20] D. H. Muhsen, T. Khatib, and F. Nagi, "A review of photovoltaic water pumping system designing methods, control strategies and field performance,"

*Renewable and Sustainable Energy Reviews*, vol. 68, no. August 2016, pp. 70–86, 2017. [Online]. Available : http://dx.doi.org/10.1016/j.rser.2016.09.129

[21] S. S. Chandel, M. Nagaraju Naik, and R. Chandel, "Review of solar photovoltaic water pumping system technology for irrigation and community drinking water supplies," *Renewable and Sustainable Energy Reviews*, vol. 49, pp. 1084–1099, 2015.

[22] P. Periasamy, N. K. Jain, and I. P. Singh, "A review on development of photovoltaic water pumping system," *Renewable and Sustainable Energy Reviews*, vol. 43, pp. 918–925, 2015.

[23] G. Li, Y. Jin, M. W. Akram, and X. Chen, "Research and current status of the solar photovoltaic water pumping system – A review," *Renewable and Sustainable Energy Reviews*, vol. 79, no. December 2016, pp. 440–458, 2017. [Online]. Available : http://dx.doi.org/10.1016/j.rser.2017.05.055

[24] Solarmarket, "Types of Solar Inverters." [Online]. Available : https://www.solarmarket.com.au/tips/types-of-solar-inverters/

[25] Kenbrooksolar, "Solar Inverter." [Online]. Available : https://kenbrooksolar.com/solar-inverter

[26] U. Global, "Types Of Solar Inverters." [Online]. Available : http://urjaglobal.in/5-types-of-solar-inverters.php

[27] LEONICS, "Inverter for Solar electric system." [Online]. Available : http://www.leonics.com/product/renewable/inverter/inverter_en.php

[28] V. C. Sontake and V. R. Kalamkar, "Solar photovoltaic water pumping system - A comprehensive review," *Renewable and Sustainable Energy Reviews*, vol. 59, pp. 1038–1067, 2016.

[29] A. Bahrami, C. O. Okoye, and U. Atikol, "Technical and economic assessment of fixed, single and dual-axis tracking PV panels in low latitude countries," *Renewable Energy*, vol. 113, pp. 563–579, 2017.

[30] S. Motahhir, A. EL Hammoumi, A. EL Ghzizal, and A. Derouich, "Open hardware/software test bench for solar tracker with virtual instrumentation," *Sustainable Energy Technologies and Assessments*, vol. 31, no. November 2018, pp. 9–16, 2019. [Online]. Available : https://doi.org/10.1016/j.seta.2018.11.003

[31] S. M. Alghuwainem, "Steady-State Performance of Dc Motors Supplied From Photovoltaic Generators with Step-Up Converter," *IEEE Transactions on Energy Conversion*, vol. 7, no. 2, pp. 267–272, 1992.

[32] S. K. Gupta, M. R. Khan, and K. Jahan, "Modeling , Analysis and Control of Solar Water Pumping System," pp. 356–363, 2015.

[33] R. Kumar and S. Member, "BLDC Motor Driven Solar PV Array Fed Water Pumping System Employing Zeta Converter," 2014.

[34] S. Iyappan and R. Ramaprabha, "Design and Implementation of Brushless DC Motor based Solar Water Pumping System for Agriculture using Arduino UNO," vol. 9, no. 1, pp. 224–232, 2017.

[35] G. Shokri and E. Naderi, "DTC based BLDC Motor Controlled Centrifugal Pump Fed by PI-BFO Tuning Strategy for Buck-Boost Converter in Solar PV Array Water Pumping System," *2019 10th International Power Electronics, Drive Systems and Technologies Conference (PEDSTC)*, pp. 769–774, 2019.

[36] R. Kumar and B. Singh, "Single Stage Solar PV Fed Brushless DC Motor Driven Water Pump," vol. 6777, no. c, 2017.

[37] R. Akkaya, "DSP implementation of a PV system with GA-MLP-NN based MPPT controller supplying BLDC motor drive," vol. 48, pp. 210–218, 2007.

[38] M. M.-s. Essam E. Aboul Zahab, Aziza M.Zaki, "Design and control of a standalone PV water pumping system."

[39] A. Terki, A. Moussi, A. Betka, and N. Terki, "An improved efficiency of fuzzy logic control of PMBLDC for PV pumping system," *Applied*

*Mathematical Modelling*, vol. 36, no. 3, pp. 934–944, 2012. [Online]. Available : http://dx.doi.org/10.1016/j.apm.2011.07.042

[40] A. M. Kassem, "Electrical Power and Energy Systems MPPT control design and performance improvements of a PV generator powered DC motor-pump system based on artificial neural networks," *International Journal of Electrical Power and Energy Systems*, vol. 43, no. 1, pp. 90–98, 2012. [Online]. Available : http://dx.doi.org/10.1016/j.ijepes.2012.04.047

[41] D. Halboot, A. Bakar, T. Khatib, I. Ahmed, and E. M. Natsheh, "Sizing of a standalone photovoltaic water pumping system using a multi-objective evolutionary algorithm," *Energy*, vol. 109, pp. 961–973, 2016. [Online]. Available : http://dx.doi.org/10.1016/j.energy.2016.05.070

[42] S. Sashidhar, V. G. P. Reddy, B. G. Fernandes, and S. Member, "A Single-Stage Sensorless Control of a PV based Bore-Well Submersible BLDC Motor," vol. 6777, no. c, pp. 1–8, 2018.

[43] A. A. S. Mohamed, A. Berzoy, and O. Mohammed, "Optimized-Fuzzy MPPT Controller Using GA for Stand-alone Photovoltaic Water Pumping System."

[44] S. Krim, S. Gdaim, A. Mtibaa, and M. F. Mimouni, "FPGA Contribution in Photovoltaic Pumping Systems : Models of MPPT and DTC-SVM Algorithms," vol. 6, no. 3, 2016.

[45] S. Jain, A. K. T, R. Karampuri, V. T. Somasekhar, and M. Ieee, "A Single-Stage PhotoVoltaic System for a Dual- Inverter fed Open-End Winding Induction Motor Drive for Pumping Applications," vol. 8993, no. IM, pp. 1–9, 2014.

[46] S. Jain, C. Ramulu, S. Padmanaban, J. Olorunfemi, and A. H. Ertas, "Engineering Science and Technology , an International Journal Dual MPPT algorithm for dual PV source fed Open-End Winding Induction Motor Drive for pumping application," *Engineering Science*

*and Technology, an International Journal*, 2016. [Online]. Available : http://dx.doi.org/10.1016/j.jestch.2016.07.008

[47] K. Khan, S. Shukla, and B. Singh, "Performance-Based Design of Induction Motor Drive for Single-Stage PV Array Fed Water Pumping," *IEEE Transactions on Industry Applications*, vol. 55, no. 4, pp. 4286–4297, 2019.

[48] J. Victor, M. Caracas, S. Member, G. D. C. Freitas, S. Member, and L. Felipe, "Implementation of a High Efficiency , High Lifetime , and Low Cost Converter for an Autonomous Photovoltaic Water Pumping System," no. c, 2013.

[49] R. Rai, S. Shukla, and B. Singh, "Sensorless Field Oriented SMCC Based Integral Sliding Mode for Solar PV Based Induction Motor Drive for Water Pumping," vol. 9994, no. c, 2020.

[50] B. Singh, U. Sharma, and S. Kumar, "Standalone Photovoltaic Water Pumping System Using Induction Motor Drive with Reduced Sensors," *IEEE Transactions on Industry Applications*, vol. 54, no. 4, pp. 3645–3655, 2018.

[51] M. Errouha and A. Derouich, "Study and comparison results of the field oriented control for photovoltaic water pumping system applied on two cities in Morocco," *Bulletin of Electrical Engineering and Informatics*, vol. 8, no. 4, pp. 1–7, 2019.

[52] R. V.-P. J. Linares-Flores, J.F. Guerrero-Castellanos, R. Lescas-Hernández, A. Hernández- Méndez, "Angular speed control of an induction motor via a solar powered boost converter-voltage source inverter combination," *Energy*, 2018. [Online]. Available : https://doi.org/10.1016/j.energy.2018.10.024

[53] M. Errouha, A. Derouich, S. Motahhir, O. Zamzoum, N. E. Ouanjli, and A. E. Ghzizal, "Optimization and control of water pumping PV systems using fuzzy logic controller," *Energy Reports*, vol. 5, pp. 853–865, 2019. [Online]. Available : https://doi.org/10.1016/j.egyr.2019.07.001

[54] A. Khiareddine, C. Ben, and M. Faouzi, "ScienceDirect Power management of a photovoltaic / battery pumping system in agricultural experiment station," *SOLAR ENERGY*, vol. 112, pp. 319–338, 2015. [Online]. Available : http://dx.doi.org/10.1016/j.solener.2014.11.020

[55] N. Karami, N. Moubayed, and R. Outbib, "General review and classification of different MPPT Techniques," *Renewable and Sustainable Energy Reviews*, vol. 68, no. September 2016, pp. 1–18, 2017.

[56] S. Motahhir, A. El Hammoumi, and A. El Ghzizal, "The most used MPPT algorithms : Review and the suitable low-cost embedded board for each algorithm," *Journal of Cleaner Production*, vol. 246, no. October, p. 118983, 2020. [Online]. Available : https://doi.org/10.1016/j.jclepro.2019.118983

[57] A. Gupta, Y. K. Chauhan, and R. K. Pachauri, "A comparative investigation of maximum power point tracking methods for solar PV system," *Solar Energy*, vol. 136, pp. 236–253, 2016. [Online]. Available : http://dx.doi.org/10.1016/j.solener.2016.07.001

[58] A. Farayola, A. Hasan, and A. Ali, "Implementation of modified incremental conductance and fuzzy logic MPPT techniques using MCUK converter under various environmental conditions," *Applied Solar Energy (English translation of Geliotekhnika)*, vol. 53, no. 2, pp. 173–174, 2017.

[59] I. Yahyaoui, M. Chaabene, and F. Tadeo, "Evaluation of Maximum Power Point Tracking algorithm for off-grid photovoltaic pumping," *Sustainable Cities and Society*, vol. 25, pp. 65–73, 2016. [Online]. Available : http://dx.doi.org/10.1016/j.scs.2015.11.005

[60] Y. Nezihe and E. Tacer, "Identification of photovoltaic cell single diode discrete model parameters based on datasheet values," vol. 127, pp. 175–183, 2016.

[61] N. Barth, R. Jovanovic, S. Ahzi, and M. A. Khaleel, "PV panel single and double diode models : Optimization of the parameters and temperature

dependence," *Solar Energy Materials and Solar Cells*, vol. 148, pp. 87–98, 2016. [Online]. Available : http://dx.doi.org/10.1016/j.solmat.2015.09.003

[62] K. Ishaque, Z. Salam, and Syafaruddin, "A comprehensive MATLAB Simulink PV system simulator with partial shading capability based on two-diode model," *Solar Energy*, vol. 85, no. 9, pp. 2217–2227, 2011. [Online]. Available : http://dx.doi.org/10.1016/j.solener.2011.06.008

[63] T. Ma, H. Yang, and L. Lu, "Solar photovoltaic system modeling and performance prediction," *Renewable and Sustainable Energy Reviews*, vol. 36, pp. 304–315, 2014. [Online]. Available : http://dx.doi.org/10.1016/j.rser.2014.04.057

[64] A. Bouraiou, M. Hamouda, A. Chaker, M. Sadok, M. Mostefaoui, and S. Lachtar, "Modeling and Simulation of Photovoltaic Module and Array Based on One and Two Diode Model Using Matlab/Simulink," *Energy Procedia*, vol. 74, pp. 864–877, 2015. [Online]. Available : http://dx.doi.org/10.1016/j.egypro.2015.07.822

[65] R. Khezzar, M. Zereg, and A. Khezzar, "Modeling improvement of the four parameter model for photovoltaic modules," *Solar Energy*, vol. 110, pp. 452–462, 2014. [Online]. Available : http://dx.doi.org/10.1016/j.solener.2014.09.039

[66] V. J. Chin, Z. Salam, and K. Ishaque, "Cell modelling and model parameters estimation techniques for photovoltaic simulator application : A review," *Applied Energy*, vol. 154, pp. 500–519, 2015. [Online]. Available : http://dx.doi.org/10.1016/j.apenergy.2015.05.035

[67] C. W. Hansen, "Parameter estimation for single diode models of photovoltaic modules," *Sandia Report*, no. SAND2015-2065, pp. 1–68, 2015.

[68] S. Motahhir, A. El Ghzizal, S. Sebti, and A. Derouich, "Shading effect to energy withdrawn from the photovoltaic panel and implementation of DMPPT using

C language," *International Review of Automatic Control*, vol. 9, no. 2, pp. 88–94, 2016.

[69] S. Motahhir, A. E. Hammoumi, and A. E. Ghzizal, "Photovoltaic system with quantitative comparative between an improved MPPT and existing INC and P & O methods under fast varying of solar irradiation," *Energy Reports*, vol. 4, pp. 341–351, 2018. [Online]. Available : https://doi.org/10.1016/j.egyr.2018.04.003

[70] S. Dahbi, R. Aboutni, A. Aziz, N. Benazzi, M. Elhafyani, and K. Kassmi, "Optimised hydrogen production by a photovoltaic-electrolysis system DC/DC converter and water flow controller," *International Journal of Hydrogen Energy*, vol. 41, no. 45, pp. 20 858–20 866, 2016. [Online]. Available : http://dx.doi.org/10.1016/j.ijhydene.2016.05.111

[71] S. Motahhir, A. E. Ghzizal, S. Sebti, and A. Derouich, "Modeling of Photovoltaic System with modified Incremental Conductance Algorithm for fast changes of irradiance."

[72] R. Rawat, S. C. Kaushik, and R. Lamba, "A review on modeling, design methodology and size optimization of photovoltaic based water pumping, standalone and grid connected system," *Renewable and Sustainable Energy Reviews*, vol. 57, pp. 1506–1519, 2016. [Online]. Available : http://dx.doi.org/10.1016/j.rser.2015.12.228

[73] M. F. AlHajri, K. M. El-Naggar, M. R. AlRashidi, and A. K. Al-Othman, "Optimal extraction of solar cell parameters using pattern search," *Renewable Energy*, vol. 44, pp. 238–245, 2012. [Online]. Available : http://dx.doi.org/10.1016/j.renene.2012.01.082

[74] F. Zaouche, D. Rekioua, J. P. Gaubert, and Z. Mokrani, "Supervision and control strategy for photovoltaic generators with battery storage," *International Journal of Hydrogen Energy*, vol. 42, no. 30, pp. 19 536–19 555, 2017.

[75] M. H. Taghvaee, M. A. Radzi, S. M. Moosavain, H. Hizam, and M. Hamiruce Marhaban, "A current and future study on non-isolated DC-DC converters for photovoltaic applications," *Renewable and Sustainable Energy Reviews*, vol. 17, pp. 216–227, 2013. [Online]. Available : http://dx.doi.org/10.1016/j.rser.2012.09.023

[76] I. Yahyaoui, *SPECIFICATIONS OF PHOTOVOLTAIC PUMPING SYSTEMS Sizing , Fuzzy Energy Management*, 2016.

[77] M. Jannati, S. A. Anbaran, S. H. Asgari, W. Y. Goh, A. Monadi, M. J. A. Aziz, and N. R. N. Idris, "A review on Variable Speed Control techniques for efficient control of Single-Phase Induction Motors : Evolution, classification, comparison," *Renewable and Sustainable Energy Reviews*, vol. 75, no. November, pp. 1306–1319, 2017.

[78] Z. Guo, J. Zhang, Z. Sun, and C. Zheng, "Indirect Field Oriented Control of Three-phase Induction Motor Based on Current-source Inverter," *Procedia Engineering*, vol. 174, pp. 588–594, 2017. [Online]. Available : http://dx.doi.org/10.1016/j.proeng.2017.01.192

[79] C. N. Bhende and S. G. Malla, "Novel control of photovoltaic based water pumping system without energy storage," *International Journal of Emerging Electric Power Systems*, vol. 13, no. 5, 2012.

[80] M. Azab, "Identification of one-diode model parameters of PV devices from nameplate information using particle swarm and least square methods," *2015 1st Workshop on Smart Grid and Renewable Energy, SGRE 2015*, 2015.

[81] P. Vas, *Vector Control of AC Machines*, ser. Monographs in electrical and electronic engineering. Oxford University Press, 1994. [Online]. Available : https://books.google.co.ma/books?id=feHXtAEACAAJ

[82] M. A. Hannan, J. A. Ali, A. Mohamed, and A. Hussain, "Optimization techniques to enhance the performance of induction motor drives : A review,"

*Renewable and Sustainable Energy Reviews*, vol. 81, no. April, pp. 1611–1626, 2018. [Online]. Available : http://dx.doi.org/10.1016/j.rser.2017.05.240

[83] M. Sreejeth, M. Singh, and P. Kumar, "Efficiency optimization of vector controlled induction motor drive," *IECON Proceedings (Industrial Electronics Conference)*, pp. 1758–1763, 2012.

[84] S. Rafa, A. Larabi, L. Barazane, M. Manceur, N. Essounbouli, and A. Hamzaoui, "Implementation of a new fuzzy vector control of induction motor," *ISA Transactions*, vol. 53, no. 3, pp. 744–754, 2014. [Online]. Available : http://dx.doi.org/10.1016/j.isatra.2014.02.005

[85] I. M. Alsofyani and N. R. Idris, "A review on sensorless techniques for sustainable reliablity and efficient variable frequency drives of induction motors," *Renewable and Sustainable Energy Reviews*, vol. 24, pp. 111–121, 2013. [Online]. Available : http://dx.doi.org/10.1016/j.rser.2013.03.051

[86] S. Allirani and V. Jagannathan, "Direct torque control technique in induction motor drives-A review," *Journal of Theoretical and Applied Information Technology*, vol. 60, no. 3, pp. 452–475, 2014.

[87] L. Amezquita-brooks, J. Liceaga-castro, and E. L.-c. Member, "Speed and Position Controllers Using Indirect Field Oriented Control : A Classical Control Approach," no. c, pp. 1–16, 2013.

[88] L. Harnefors, S. Member, S. E. Saarakkala, and M. Hinkkanen, "Speed Control of Electrical Drives Using Classical Control Methods," no. 1, pp. 1–10, 2013.

[89] R. Hedjar, P. Boucher, and D. Dumur, "Robust nonlinear receding-horizon control of induction motors," *International Journal of Electrical Power and Energy Systems*, vol. 46, no. 1, pp. 353–365, 2013. [Online]. Available : http://dx.doi.org/10.1016/j.ijepes.2012.10.007

[90] S. Lekhchine, T. Bahi, and Y. Soufi, "Indirect rotor field oriented control based on fuzzy logic controlled double star induction machine," *International*

*Journal of Electrical Power and Energy Systems*, vol. 57, pp. 206–211, 2014. [Online]. Available : http://dx.doi.org/10.1016/j.ijepes.2013.11.053

[91] A. Achour, D. Rekioua, A. Mohammedi, Z. Mokrani, T. Rekioua, and S. Bacha, "Application of direct torque control to a photovoltaic pumping system with sliding-mode control optimization," *Electric Power Components and Systems*, vol. 44, no. 2, pp. 172–184, 2016.

[92] D. Mohan, S. Member, X. Zhang, and G. Foo, "Generalized DTC Strategy for Multilevel Inverter fed IPMSMs with Constant Inverter Switching Frequency and Reduced Torque Ripples," vol. 8969, no. c, pp. 1–10, 2017.

[93] D. Islam, C. M. F. S. Reza, and S. Mekhilef, "Modeling and Experimental Validation of 5-level Hybrid H-bridge Multilevel Inverter Fed DTC-IM Drive," vol. 10, 2015.

[94] U. Mahanta and D. Patnaik, "Dynamic Modeling and Simulation of SVM-DTC of Five Phase Induction Motor," pp. 3–8, 2015.

[95] M. Hayette, "Commande DTC Prédictive D ' une Machine Synchrone à Aimants Permanents."

[96] A. Benamor, M. T. Benchouia, K. Srairi, and M. E. Benbouzid, "A novel rooted tree optimization apply in the high order sliding mode control using super-twisting algorithm based on DTC scheme for DFIG," *International Journal of Electrical Power and Energy Systems*, vol. 108, no. November 2018, pp. 293–302, 2019. [Online]. Available : https://doi.org/10.1016/j.ijepes.2019.01.009

[97] T. Sutikno, N. Rumzi, N. Idris, and A. Jidin, "A review of direct torque control of induction motors for sustainable reliability and energy ef fi cient drives," *Renewable and Sustainable Energy Reviews*, vol. 32, pp. 548–558, 2014. [Online]. Available : http://dx.doi.org/10.1016/j.rser.2014.01.040

[98] O. Castillo, L. Amador-Angulo, J. R. Castro, and M. Garcia-Valdez, "A comparative study of type-1 fuzzy logic systems, interval type-2 fuzzy logic systems and generalized type-2 fuzzy logic systems in control problems," *Information Sciences*, vol. 354, pp. 257–274, 2016. [Online]. Available : http://dx.doi.org/10.1016/j.ins.2016.03.026

[99] L. Cervantes and O. Castillo, "Type-2 fuzzy logic aggregation of multiple fuzzy controllers for airplane flight control," *Information Sciences*, vol. 324, pp. 247–256, 2015. [Online]. Available : http://dx.doi.org/10.1016/j.ins.2015.06.047

[100] M. A. Sanchez, O. Castillo, and J. R. Castro, "Generalized Type-2 Fuzzy Systems for controlling a mobile robot and a performance comparison with Interval Type-2 and Type-1 Fuzzy Systems," *Expert Systems with Applications*, vol. 42, no. 14, pp. 5904–5914, 2015. [Online]. Available : http://dx.doi.org/10.1016/j.eswa.2015.03.024

[101] A. A. El-samahy and M. A. Shamseldin, "Brushless DC motor tracking control using self-tuning fuzzy PID control and model reference adaptive control," *Ain Shams Engineering Journal*, vol. 9, no. 3, pp. 341–352, 2018. [Online]. Available : http://dx.doi.org/10.1016/j.asej.2016.02.004

[102] N. El Ouanjli, S. Motahhir, A. Derouich, A. El Ghzizal, A. Chebabhi, and M. Taoussi, "Improved DTC strategy of doubly fed induction motor using fuzzy logic controller," *Energy Reports*, vol. 5, no. February, pp. 271–279, 2019. [Online]. Available : https://doi.org/10.1016/j.egyr.2019.02.001

[103] C. D. Yahia and Miloud, "Direct Torque Control Strategies of Induction Machine : Comparative Studies," Ph.D. dissertation, 2012. [Online]. Available : http://dx.doi.org/10.1039/C7RA00172J{%}0Ahttps://www.intechopen.com/books/advanced-biometric-technologies/liveness-detection-in-biometrics{%}0Ahttp://dx.doi.org/10.1016/j.colsurfa.2011.12.014

[104] R. K. Bindal and I. Kaur, "Torque ripple reduction of Induction Motor using Dynamic Fuzzy Prediction Direct Torque Control," *ISA Transactions*, 2019. [Online]. Available : https://doi.org/10.1016/j.isatra.2019.09.012

[105] N. Gol, "DESIGN AND IMPLEMENTATION OF DTC BASED ON AFLC AND PSO OF A PMSM," *Mathematics and Computers in Simulation*, 2018. [Online]. Available : https://doi.org/10.1016/j.matcom.2018.04.010

[106] S. Gdaim, "Commande directe de couple d'un moteur asynchrone à base de techniques intelligente," 2017.

[107] A. Ammar, "Amélioration des Performances de la Commande Directe de Couple ( DTC ) de La Machine Asynchrone par des Techniques Non-Linéaires," Ph.D. dissertation, 2017.

[108] E. Ontiveros-Robles, P. Melin, and O. Castillo, "Comparative analysis of noise robustness of type 2 fuzzy logic controllers," *Kybernetika*, vol. 54, no. 1, pp. 175–201, 2018.

[109] M. H. Ali, "Parameters Estimation for Sensorless Induction Motor Drives Using Parameters Estimation for Sensorless Induction Motor Drives Using Intelligent Techniques," Ph.D. dissertation, 2018.

[110] S. Gdaim, A. Mtibaa, and M. F. Mimouni, "Design and Experimental Implementation of DTC of Induction Machine based on Fuzzy Logic Control on FPGA," vol. 6706, no. c, 2014.

[111] R. Rai, S. Shukla, and B. Singh, "Sensorless Field Oriented ISMCC for Solar PV Based Induction Motor Drive for Water Pumping," *Proceedings - 2019 IEEE International Conference on Environment and Electrical Engineering and 2019 IEEE Industrial and Commercial Power Systems Europe, EEEIC/I and CPS Europe 2019*, 2019.

[112] A. Ghosh, S. Ganesh Malla, and C. Narayan Bhende, "Small-signal modelling and control of photovoltaic based water pumping system,"

*ISA Transactions*, vol. 57, pp. 382–389, 2015. [Online]. Available : http://dx.doi.org/10.1016/j.isatra.2015.01.008

[113] S. Shukla and B. Singh, "Single-Stage PV Array Fed Speed Sensorless Vector Control of Induction Motor Drive for Water Pumping," *IEEE Transactions on Industry Applications*, vol. 54, no. 4, pp. 3575–3585, 2018.

[114] K. Yadav, O. S. Sastry, R. Wandhare, N. Sheth, M. Kumar, B. Bora, R. Singh, Renu, and A. Kumar, "Performance comparison of controllers for solar PV water pumping applications," *Solar Energy*, vol. 119, pp. 195–202, 2015. [Online]. Available : http://dx.doi.org/10.1016/j.solener.2015.06.050

[115] W. Sun, S. Shao, R. Zhao, R. Yan, X. Zhang, and X. Chen, "A Sparse Auto-encoder-Based Deep Neural Network Approach for Induction Motor Faults Classification," *MEASUREMENT*, 2016. [Online]. Available : http://dx.doi.org/10.1016/j.measurement.2016.04.007

[116] S. H., K. S.F., and S. B., "Improvements in direct torque control of induction motor for wide range of speed operation using fuzzy logic," *Journal of Electrical Systems and Information Technology*, vol. 5, no. 3, pp. 813–828, 2018. [Online]. Available : http://dx.doi.org/10.1016/j.jesit.2016.12.015

[117] K. Wang, Y. Li, Q. Ge, and L. Shi, "An Improved Indirect Field-Oriented Control Scheme for Linear Induction Motor Traction Drives," *IEEE Transactions on Industrial Electronics*, vol. 65, no. 12, pp. 9928–9937, 2018.

[118] R. Ortega, A. Pyrkin, A. Bobtsov, D. Efimov, and S. Aranovskiy, "A Globally Convergent Adaptive Indirect Field-Oriented Torque Controller for Induction Motors," *Asian Journal of Control*, vol. 22, no. 1, pp. 11–24, 2020.

[119] N. Rezaei, C. Cossar, and K. Mehran, "Modelling and Analysis of Indirect Field-Oriented Control of SVPWM-Driven Induction Motor Drive Based on a Voltage Source Inverter," *Canadian Conference on Electrical and Computer Engineering*, vol. 2018-May, 2018.

[120] Q. Xu, "Precision Motion Control of Piezoelectric Nanopositioning Stage With Chattering-Free Adaptive Sliding Mode Control," pp. 1–11, 2016.

[121] K. Zeb, Z. Ali, K. Saleem, W. Uddin, M. A. Javed, and N. Christofides, "Indirect field-oriented control of induction motor drive based on adaptive fuzzy logic controller," *Electrical Engineering*, vol. 99, no. 3, pp. 803–815, 2017.

[122] B. Karanayil and M. F. Rahman, *Artificial Neural Network Applications in Power Electronics and Electric Drives*, 4th ed. Elsevier Inc., 2018. [Online]. Available : http://dx.doi.org/10.1016/B978-0-12-811407-0.00041-6

[123] S. Masumpoor, H. Yaghobi, and M. Ahmadieh Khanesar, "Adaptive sliding-mode type-2 neuro-fuzzy control of an induction motor," *Expert Systems with Applications*, vol. 42, no. 19, pp. 6635–6647, 2015. [Online]. Available : http://dx.doi.org/10.1016/j.eswa.2015.04.046

[124] K. Bouhoune, K. Yazid, M. S. Boucherit, and A. Chériti, "Hybrid control of the three phase induction machine using artificial neural networks and fuzzy logic," *Applied Soft Computing Journal*, vol. 55, pp. 289–301, 2017. [Online]. Available : http://dx.doi.org/10.1016/j.asoc.2017.01.048

[125] N. Kiran, "Indirect Vector Control of Three Phase Induction Motor using PSIM," *Bulletin of Electrical Engineering and Informatics*, vol. 3, no. 1, 2014.

[126] Z. Tir, O. P. Malik, and A. M. Eltamaly, "Fuzzy logic based speed control of indirect field oriented controlled Double Star Induction Motors connected in parallel to a single six-phase inverter supply," *Electric Power Systems Research*, vol. 134, pp. 126–133, 2016. [Online]. Available : http://dx.doi.org/10.1016/j.epsr.2016.01.013

[127] H. Abu-rub and A. Iqbal, "Field Oriented Control," no. Im, pp. 16–44.

[128] D. L. Mon-Nzongo, T. Jin, G. Ekemb, and L. Bitjoka, "Decoupling Network of Field-Oriented Control in Variable-Frequency Drives," *IEEE Transactions on Industrial Electronics*, vol. 64, no. 7, pp. 5746–5750, 2017.

[129] J. Jin-Woo, "space vector PWM inverter," Tech. Rep. 614, 2005.

# Appendices

## A.1 Dynamic modeling of Induction machine

As mentioned above, the induction machine is easy to maintain, cheap to construct and robust. We can distinguish two categories of induction motors which are the wound induction motor and the squirrel cage induction motor and they are composed of two principal parts, a stationary stator and a rotating rotor. In this thesis, a three-phase squirrel cage induction motor is used which is composed of bars which are short circuited by connecting them to two end rings so that rotor produces the induction current and magnetic field by itself.

### A.1.1 Hypotheses

Generally, the modeling of the induction machine depends on several hypotheses. The principal hypotheses are :

- The magnetomotive forces created by stator and rotor phases are distributed in a sinusoidal way in the air gap, when those windings are crossed by a constant current.
- The machine air gap is also supposed to have a uniform thickness.
- The notching effects which generate space harmonic are ignored.
- Linear magnetic characteristic (no saturation).
- The skin effect is not taken into account.
- Temperature effect, hysteresis phenomenon, and eddy currents are neglected.

The machine can be represented in space by three identical windings for the stator and the rotor as shown in fig below : The application of the electromagnetic laws

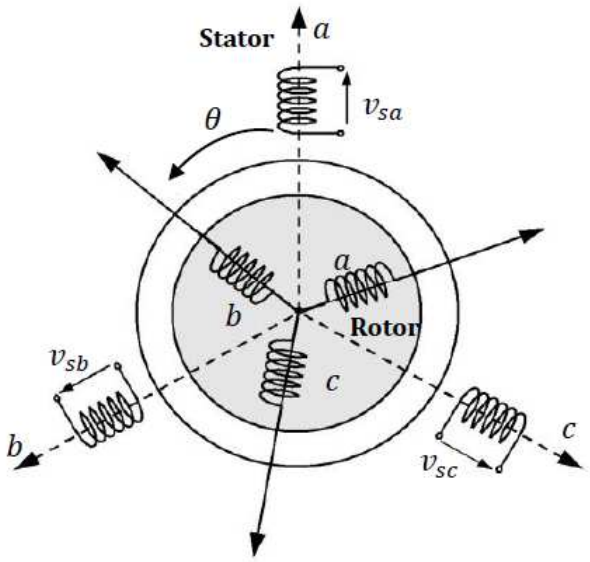


FIGURE A.1 – Induction motor equivalent structure

allows to obtain the equations describing the behavior of the machine.

### A.1.1.1 Voltage equations

$$\begin{aligned}[V_{sabc}] &= [R_s][i_{sabc}] + \tfrac{d}{dt}[\phi_{sabc}] \\ [V_{rabc}] &= 0 = [R_r][i_{rabc}] + \tfrac{d}{dt}[\phi_{rabc}]\end{aligned} \tag{A.1}$$

### A.1.1.2 Flux equations

$$\begin{aligned}[\phi_{sabc}] &= [l_s][i_{sabc}] + [M][i_{rabc}] \\ [\phi_{rabc}] &= [l_r][i_{sabc}] + [M][i_{sabc}]\end{aligned} \tag{A.2}$$

Where :

$$[V_{sabc}] = \begin{bmatrix} V_{sa} \\ V_{sb} \\ V_{sc} \end{bmatrix} ; [i_{sabc}] = \begin{bmatrix} i_{sa} \\ i_{sb} \\ i_{sc} \end{bmatrix} ; [\phi_{sabc}] = \begin{bmatrix} \phi_{sa} \\ \phi_{sb} \\ \phi_{sc} \end{bmatrix} \tag{A.3}$$

$$[V_{rabc}] = \begin{bmatrix} V_{ra} \\ V_{rb} \\ V_{rc} \end{bmatrix} ; [i_{rabc}] = \begin{bmatrix} i_{ra} \\ i_{rb} \\ i_{rc} \end{bmatrix} ; [\phi_{rabc}] = \begin{bmatrix} \phi_{ra} \\ \phi_{rb} \\ \phi_{rc} \end{bmatrix} \tag{A.4}$$

$$[R_s] = \begin{bmatrix} R_s & 0 & 0 \\ 0 & R_s & 0 \\ 0 & 0 & R_s \end{bmatrix} ; [R_r] = \begin{bmatrix} R_r & 0 & 0 \\ 0 & R_r & 0 \\ 0 & 0 & R_r \end{bmatrix} \tag{A.5}$$

$$[l_s] = \begin{bmatrix} l_s & M_s & M_s \\ M_s & l_s & M_s \\ M_s & M_s & l_s \end{bmatrix} ; [l_r] = \begin{bmatrix} l_r & M_r & M_r \\ M_r & l_r & M_r \\ M_r & M_r & l_r \end{bmatrix} \tag{A.6}$$

Where :

s : refer to stator

r : refer to rotor

$l_s$ and $l_r$ : the self-inductances

$M_s$ and $M_r$ : the mutual inductance between two stator and rotor phases

#### A.1.1 3 Mechanical equation

Eq A.3 describes the rotor motion :

$$J\frac{d}{dt}\Omega = T_{em} - T_r - f\Omega \tag{A.7}$$

### A.1.2 Matrix Transformations

This technique has been utilized to facilitate the study of AC machines by transforming the three phase variables from fixed reference frame (stationary) to a rotating frame (synchronous) defined by the Concordia/Clarke and Park transformations in order to reduce the complexity of the differential equations describing the behavior of the AC machines by eliminating time varying terms.

### A.1.2.1 Park transformation

Park transformation allows the transformation from a three-phase stationary frame to a two-phase direct quadrature (d, q, o) which leads to reduce three AC variables to two DC variables The representation of the Park transformation can be expressed as :

$$\begin{bmatrix} x_d \\ x_q \\ x_0 \end{bmatrix} = P(\theta) \begin{bmatrix} x_a \\ x_b \\ x_c \end{bmatrix} \tag{A.8}$$

$$P(\theta) = n \begin{bmatrix} \cos\theta & \cos(\theta - \frac{2\pi}{3}) & \cos(\theta + \frac{2\pi}{3}) \\ \sin\theta & \sin(\theta - \frac{2\pi}{3}) & \sin(\theta + \frac{2\pi}{3}) \\ K & K & K \end{bmatrix} \tag{A.9}$$

where : $\theta$ : The angle between the axis-a of the three-phase frame and the axis-d of the rotating reference frame.

$\eta$ : The ratio between the amplitude of the three-phase system variables $(x_a, x_b, x_c)$ with the amplitude of the corresponding two-phase system variables $(x_d, x_q, x_0)$.

### A.1.2.2 The Clarke/Concordia Transformation

Clarke or Concordia transformations are the transformation from a fixed three-phase system to a fixed two-phase system. Clarke transformation is represented by the matrix C and it aims to convert the three-phase quantities into two-phase orthogonal quantities by keeping the amplitude of the variables and the power is not kept, while Concordia transformation is represented by the matrix Co and it consists of preserving the power.

$$C = n \begin{bmatrix} 1 & -\frac{1}{2} & -\frac{1}{2} \\ 0 & \frac{sqrt3}{2} & -\frac{sqrt3}{2} \\ K & K & K \end{bmatrix}; C_0 = n \begin{bmatrix} 1 & -\frac{1}{2} & -\frac{1}{2} \\ 0 & \frac{sqrt3}{2} & -\frac{sqrt3}{2} \\ K & K & K \end{bmatrix} \tag{A.10}$$

#### A.1.2.3 Amplitude and power preserving transformations

Park transformations can preserve the amplitude or the power.

- The transformation preserving amplitude is obtained by selecting :

$$n = \frac{2}{3} \; ; \; k = \frac{1}{2}$$

- The transformation preserving power is obtained by selecting :

$$n = \sqrt{\frac{2}{3}} \; ; \; k = \frac{1}{\sqrt{2}}$$

### A.1.3 Two-phase models of induction machine

Different two-coordinate frames exist according to the select of $\theta$. The two most used in the literature are the rotating reference frame (d, q) and the fixed reference frame ($\alpha$,$\beta$) (i.e. stationary frame connected to the stator).

#### A.1.3.1 Equations of the induction machine in (d, q) frame

The transformation from the three-phase frame (a, b, c) to the rotating frame (d, q) is established by setting the angle $\theta = \theta_s$.By applying the Park transformations, the equations of IM in frame (d,q) can expressed as follows :

$$\begin{bmatrix} V_{ds} \\ V_{qs} \end{bmatrix} = [P(\theta_s)][V_{sabc}]; \begin{bmatrix} i_{ds} \\ i_{qs} \end{bmatrix} = [P(\theta_s)][i_{sabc}]; \begin{bmatrix} \phi_{ds} \\ \phi_{qs} \end{bmatrix} = [P(\theta_s)][\phi_{sabc}]; \tag{A.11}$$

$$\begin{bmatrix} V_{dr} \\ V_{qr} \end{bmatrix} = [P(\theta_s)][V_{rabc}]; \begin{bmatrix} i_{dr} \\ i_{qr} \end{bmatrix} = [P(\theta_s)][i_{rabc}]; \begin{bmatrix} \phi_{dr} \\ \phi_{qr} \end{bmatrix} = [P(\theta_s)][\phi_{rabc}]; \tag{A.12}$$

Therefore, the voltage equations are expressed by :

$$\begin{aligned} V_{ds} &= R_s i_{ds} + \tfrac{d}{dt}\phi_{ds} - w_s \phi_{qs} \\ V_{qs} &= R_s i_{qs} + \tfrac{d}{dt}\phi_{qs} + w_s \phi_{qs} \\ V_{dr} &= R_r i_{dr} + \tfrac{d}{dt}\phi_{rs} - (w_s - p w_r)\phi_{qr} \\ V_{qr} &= R_r i_{qr} + \tfrac{d}{dt}\phi_{rq} - (w_s - p w_r)\phi_{qr} \end{aligned} \tag{A.13}$$

Where $\theta_s$ is the stator field angle $w_s = \frac{d}{dt}\theta_s$ ; $w_r = \frac{d}{dt}\theta_r$ The equations of the flux are expressed by :

$$\begin{aligned}[\phi_{sdq}] &= [l_s][i_{sdq}] + M[i_{rdq}] \\ [\phi_{rdq}] &= [l_r][i_{rdq}] + M[i_{sdq}]\end{aligned} \tag{A.14}$$

The electromagnetic torque can be written in frame (d,q) as follows :

$$T_{em} = \frac{PM}{l_r}(\phi_{ds}I_{qs} - \phi_{qs}I_{ds}) \tag{A.15}$$

### A.1.3.2 Equations of the induction machine in $(\alpha, \beta)$ frame

The transformation from the three-phase frame (a, b, c) to the fixed $(\alpha, \beta)$ frame is established by setting angle $\theta$=0. the state model of induction machine whose the stator current and stator flux components are considered as state variables can be expressed in the stationary axes reference frame as follows :

$$\dot{X} = AX + BU \tag{A.16}$$

Where :$X = [i_{\alpha s} \quad i_{\beta s} \quad \phi_{\alpha s} \quad \phi_{\beta s}]^T$ ; $\quad U = [V_{\alpha_s} \quad V_{\beta_s}]^T$

$$A = \begin{bmatrix} -\frac{1}{\sigma}(\frac{1}{\tau_s} + \frac{1}{\tau_r}) & w_r & \frac{1}{\sigma L_s \tau_r} & \frac{w_r}{\sigma L_s} \\ -w_r & -\frac{1}{\sigma}(\frac{1}{\tau_s} + \frac{1}{\tau_r}) & -\frac{w_r}{\sigma L_s} & \frac{1}{\sigma L_s \tau_r} \\ -R_s & 0 & 0 & 0 \\ 0 & -R_s & 0 & 0 \end{bmatrix}; A = \begin{bmatrix} \frac{1}{\sigma L_s} & 0 \\ 0 & \frac{1}{\sigma L_s} \\ 1 & 0 \\ 0 & 1 \end{bmatrix} \tag{A.17}$$

$\sigma = 1 - \frac{M^2}{L_s L_r}; \tau_s = \frac{R_s}{L_s}; \tau_r = \frac{R_r}{L_r}$

# A.2 PI controller's gains calculation

## A.2.1 PI speed controller design

The transfer function and the dynamic equation using Laplace transform of the speed loop can be expressed by :

$$\frac{d}{dt}\Omega = -\frac{f}{J}\Omega + \frac{T_{em}}{J} - \frac{1}{J}T_L \tag{A.18}$$

$$G_\Omega(s) = \frac{\Omega(s)}{T_{em}(s) - T_L} = \frac{1}{J_s - f} \tag{A.19}$$

The transfer function of the PI controller is given by : $PI = K_p s + \frac{K_i}{s}$ Where :

$K_p$ : Proportional gain

$K_i$ : Integral gain

s : Laplace operator

Figure A.2 illustrates the block scheme of the speed control loop. The load torque

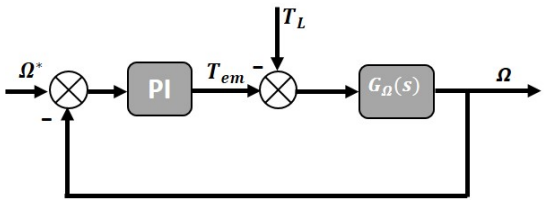


FIGURE A.2 – block scheme of the speed control loop

$T_L$ is considered as a disturbance. The global transfer function of the speed control in open loop is expressed by :

$$G_{wr}(s) = \frac{\Omega(s)}{\Omega^*(s)} = \frac{1}{J_s - f}(K_p s + \frac{K_i}{s}) \tag{A.20}$$

In closed loop, the transfer function is given by :

$$G_{wr}(s) = \frac{K_p s + K_i}{Js^2 + (K_p + f)s + K_i} \tag{A.21}$$

By identification member to member, the denominator of the equations (A.21) with the canonical form of second order system given in (A.22) :

$$G(s) = \frac{1}{s^2 + 2\xi w_n s + w_n^2} \tag{A.22}$$

Where : $w_n$ : The natural frequency, $\xi$ : The damping coefficient we get :

$$\begin{aligned} \frac{J}{K_i} &= \frac{1}{w_n^2} \\ \frac{K_p + f}{J} &= 2\xi w_n \end{aligned} \tag{A.23}$$

### A.2.2 Design of PI current controller

The block scheme of the current control loop is shown in Fig A.3. The transfer

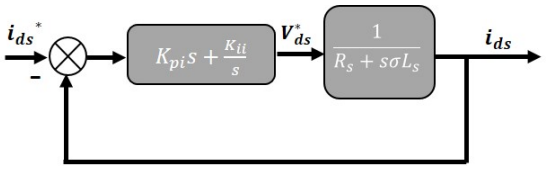


FIGURE A.3 – block scheme of the current control loop

function of the PI controller is given by : $PI = K_{pi}s + \frac{K_{ii}}{s}$ The transfer function of the current control in open loop is expressed by :

$$G_i(s) = K_{pi}(s + \frac{K_{ii}}{K_{pi}})\frac{1}{s}\frac{\frac{1}{\sigma L_s}}{s + \frac{R_s}{\sigma L_s}} \tag{A.24}$$

Then $\frac{K_{ii}}{K_{pi}} = \frac{R_s}{\sigma L_s}$ Thus, we obtain : $G_i(s) = \frac{K_{pi}}{s}\frac{1}{\sigma L_s}$ In closed loop, the TF becomes :

$$G_i(s) = \frac{\frac{K_{pi}}{s\sigma L_s}}{1 + \frac{K_{pi}}{s\sigma L_s}} = \frac{1}{1 + \tau s} \tag{A.25}$$

Where : $\tau = \frac{\sigma L_s}{K_{pi}}$

## A.3 Induction motor characteristics

Pairs poles number 2

| | | | |
|---|---|---|---|
| Stator resistance [Ω] | 4.85 | Mutual inductance [H] | 0.258 |
| Rotor resistance [Ω] | 3.805 | Inertia moment [$Kg.m^2$] | 0.031 |
| Stator inductance[H] | 0.274 | Nominal power [KW] | 1.5 |
| Rotor inductance [H] | 0.274 | Viscous Friction [N.m.s/rad] | 0.00114 |

TABLE A.1 – Parameters of induction machine

Pairs poles number 4

| | | | |
|---|---|---|---|
| Stator resistance [Ω] | 1.8 | Mutual inductance [H] | 0.0959 |
| Rotor resistance [Ω] | 2.227 | Inertia moment [$Kg.m^2$] | 0.0588 |
| Stator inductance[H] | 0.104 | Nominal power [KW] | 1.5 |
| Rotor inductance [H] | 0.104 | Viscous Friction [N.m.s/rad] | 0.1352 |

TABLE A.2 – Parameters of induction machine